This is a preprint, the final version is subject to change, of the American Mineralogist (MSA)
Cite as Authors (Year) Title. American Mineralogist, in press.
DOI: https://doi.org/10.2138/am-2019-6772

Composition, paragenesis and alteration of the chevkinite group of minerals

REVISION 1

RAY MACDONALD[1,2], BOGUSŁAW BAGIŃSKI[1], HARVEY E. BELKIN[3] AND MARCIN STACHOWICZ[1]

[1]Institute of Geochemistry, Mineralogy and Petrology, University of Warsaw, 02-089 Warszawa, Poland

[2]Environment Centre, Lancaster University, Lancaster LA1 4YQ, UK

[3]11142 Forest Edge Drive, Reston, VA 20190-4026, USA

ABSTRACT

The chevkinite-group minerals (CGM) are dominantly monoclinic REE-Ti-Fe sorosilicates [$(REE,Ca)_4Fe^{2+}(Fe^{2+},Fe^{3+},Ti)_2Ti_2(Si_2O_7)_2O_8$)], with REE_2O_3 contents up to ~50 wt%, but members with predominant Mg, Al, Mn, Cr, Sr or Zr in one of the cation sites are also known. Twelve members have been approved by the Commission of New Minerals, Nomenclature and Classification – International Mineralogical Association (CNMNC IMA) but more will undoubtedly be identified. Minerals of the group are known from hundreds of terrestrial localities and have also been recorded in lunar and Martian rocks. The main occurrences are in igneous rocks ranging from diamond in kimberlites through mafic and intermediate lithologies to metaluminous and peralkaline felsic rocks. They also occur in metamorphic rocks, including granulites, metacarbonates and jadeitites, and in metasomatic rocks, such as skarns and fenites, and in rare-metal deposits. Chevkinite-group minerals may form over the pressure range 50 - <10 kbar, and over a wide temperature range. Their formation appears to be relatively insensitive to pH_2O and fO_2.

The stability of CGM *vis-à-vis* other REE-Ti-bearing accessories is poorly understood. They are often the major carriers of REE and actinides and they have a high potential for fractionating the light lanthanides and Th from U. Very little systematic work has been done in

determining CGM-melt partition coefficients, yet such data are critical in, *inter alia*, geochemical modelling. Similarly, CGM are amenable to geochronology due to their high Th abundances, commonly at the several percent level. In common with other REE-bearing accessories, CGM are prone to alteration by hydrothermal fluids. The nature and extent of the alteration is primarily determined by the composition of the fluids. Fluids poor in ligands tend to generate a Ti-enriched phase whose nature is unknown but is probably amorphous. With increasing F + CO_2 levels, complex replacement assemblages are formed, usually in more than one step. Although observational evidence of the effects of alteration and element mobility is accumulating and chemical equations can be constructed to approximate the reactions, there is still no firm geochemical basis for understanding element redistribution during these processes.

Keywords: Chevkinite-group, structure, composition, occurrence, alteration, petrogenetic significance

INTRODUCTION

The minerals of the chevkinite group are commonly regarded as rare accessory phases. Why, then, do they merit a review?

(1) Chevkinite-group minerals (CGM) occur in a very wide range of crustal environments, including igneous lithologies ranging from mafic to felsic, granulites and gneisses, hydrothermal and pegmatitic rocks, skarns and ore deposits. Members of the group are known from hundreds of localities worldwide and hundreds more undoubtedly remain to be documented. Occurrences in mantle rocks have been reported and the group has also gone extra-terrestrial: a CGM has been found in lunar basalts (Muhling et al. 2014) and Liu and Ma (2015) and Liu et al. (2015, 2016) reported two chevkinite group members in a benmoreite/trachyandesite clast in a Martian breccia meteorite.

While CGM are, in many cases, a minor component of their host rocks, in other cases they are relatively abundant. For example, Vlach and Gualda (2007) found CGM to be the dominant rare earth element (REE)-bearing phase in several A-type granite intrusions of the Graciosa Province, Brazil, and Macdonald et al. (2013) reported CGM as the most important REE-bearing phases in many Paleogene granites of the Scottish and Northern Irish sections of the North Atlantic Igneous Superprovince. Padilla and Gualda (2016) recorded that of the accessory minerals in the rhyolitic Peach Spring Tuff, southwest USA (titanite, chevkinite, zircon and apatite), chevkinite played the dominant role in the partitioning of the light rare-earth elements (LREE: La-Sm). In contrast to those examples, CGM are apparently not present in the numerous major REE-deposits of Australia, according to the compilation of Hoatson et al. (2011).

(2) A total of 55 elements have been recorded in CGM, in amounts ranging from ppm to tens of weight percent; for comparison, the total is slightly more than the 52 recorded in the apatite supergroup by Hughes and Rakovan (2015). There is, therefore, considerable compositional diversity, resulting in many substitution schemes and structural varieties.

(3) The range of host lithologies attests to the remarkable range of temperature and pressure conditions under which the CGM may form. A CGM found as inclusions in diamond in a kimberlite at Ranch River, Zimbabwe, grew under mantle P-T conditions (Kopylova et al. 1997a, 1997b). No robust estimates of the lower temperature conditions of natural CGM crystallization have been made but their occurrence in amygdales in lavas and miarolitic cavities in intrusions points to temperatures perhaps as low as 350 °C at very low pressures.

(4) Like many REE-bearing accessory minerals, CGM are prone to metasomatic alteration, that is the introduction and/or removal of chemical components through interaction of the host rock with fluids. With REE_2O_3 contents up to ~50 wt% and lesser, but significant, abundances of the high-

field strength elements (HFSE) and actinides, they can contribute to significant element mobility during metasomatism and ultimately to the origin of rare-metal ore deposits.

(5) As a result of their high Th concentrations, there is considerable potential for the CGM to be used in geochronology. Vasquez (2008) showed that for young chevkinite (<350 ka), the compositional variations in single crystals could be linked to absolute age through ^{238}U- ^{230}Th dating via ion microprobe analysis. An advantage is the slow diffusion rates for Th and U in comparison with other large cations, estimated as 10^{-27} and 10^{-28} m^2/s, respectively (Vasquez et al. 2014), which means that CGM dates derived from ^{238}U-^{230}Th disequilbrium are likely to be crystallization rather than cooling ages.

(6) Where CGM occur as phenocrysts in volcanic rocks or as early crystallizing phases in plutonic rocks, they can have an important influence on trace element partitioning between melt and crystals and thus on melt fractionation paths (Green and Pearson 1988). As noted below, a few studies have determined melt/crystal partition coefficients but little is yet known about how the partitioning varies with bulk-rock composition, P, T and fluid composition. Chevkinite-group minerals may also act as refractory phases during partial melting of crustal rocks and retain the REE, HFSE and actinides which might otherwise be removed in a melt or fluid phase (Green and Pearson 1988).

(7) The last three decades have seen an exponential increase in the use of REE in diverse aspects of modern technology, such as in permanent magnets for vehicle motors and wind generation, high-density batteries, phosphors for screens and lighting, and medical image contrast media (e.g., Haque et al. 2014; Dickson 2015). This greatly increased use, coupled with the near monopoly on REE production held by the People's Republic of China, has led to much REE exploration worldwide. For example, Canada wanted to have 20% of the global REE market by 2018 (Els 2014). Although CGM have not been described as the main REE carrier in any deposit,

they may be present in the REE ore (e.g., Li and Zhou 2017). Thus, knowledge of CGM chemistry and petrogenesis will be important for beneficiation and exploration.

The specific aims of the review are to: (i) heighten awareness of the CGM (cf. Bagiński and Macdonald 2013); (ii) describe progress in establishing their compositional range; (iii) describe the crystal structure and how it varies with chemical composition; (iv) outline the range of lithologies and P-T-X conditions in which CGM form; (v) describe compositional changes during hydrothermal alteration; (vi) explore selected aspects of their petrogenetic significance; and (vii) make suggestions about fruitful future lines of research on the group.

Members and structural formulae of the chevkinite group

The most widely used formula for the CGM is $A_4BC_2D_2(Si_2O_7)_2O_8$, where the common cations in each site are: A, REE, Y, Ca, Sr; B, Fe^{2+}; C, Fe^{2+}, Fe^{3+}, Mn, Ti, Al, Zr, Mg; and D, Ti (Ito and Arem 1971). Other formulations have, however, been used, e.g. $A_2B_2M_5(Si_2O_7)_2O_8$ (Chukanov et al. 2012a, 2012b) and work on new species has commonly shown that the standard formula and site allocations are not always applicable. Some workers, e.g. Sokolova et al. (2004) and Chukanov et al. (2012a), have preferred a more rigorous approach to classification, using cation allocations to specific sites on the basis of site properties, such as size and coordination number. In these approaches, up to four M sites replace the B, C, D site terminology. Here the traditional names for sites from the simplified formula are used. The A site is occupied mainly by large REE, Ca and Sr ions, and B, C and D by cations of octahedral MO_6 coordination. In the asymmetric unit of the perrierite-type structure, there are two A sites, A1 and A2, one B site, one C site and one D site. In chevkinite, the D site splits into D1 and D2. The unique sites B, C, D1 and D2 correspond to sites M1-M4 (Popov et al. 2001; Sokolova et al. 2004: Holtstam et al. 2017) and to B, C1, C2A and C2B (Yang et al. 2002, 2007; Li et al. 2005; Xu et al. 2008).

The two most abundant members of the group are chevkinite and perrierite, which are structurally different. Haggerty and Mariano (1983) reported a robust method to discriminate between the two phases by measuring the monoclinic β angle (chevkinite ~100°, perrierite ~113°). The CGM could then be divided into the chevkinite and perrierite subgroups (Sokolova et al. 2004). We appreciate that the use of subgroups is not recommended by the CNMNC-IMA but is has proved immensely useful in descriptive studies of the CGM and will continue to do so until a committee is set up to formulate a set of nomenclature rules for the group.

The majority of chevkinites and perrierites are completely metamict and cannot, therefore, be distinguished by crystal structure. Macdonald and Belkin (2002) and Macdonald et al. (2009) found that a simple compositional feature, the relative proportions of FeO* (total Fe as Fe^{2+}) and (CaO+SrO), matched the division based on the β angle almost perfectly: Subsequently, the type perrierite-(La) was found to plot just above their suggested boundary line but could be accommodated by a slight shift of the line (Fig. 1a). Whilst empirical, the classification scheme has proved useful in electron microprobe studies where crystal size and/or the metamict nature have precluded structural determinations. However, it will be shown below that there are ways of crossing the empirical boundary, almost certainly without structural modification.

Twelve members of the CGM have been approved to date by the CNMNC-IMA, six in the chevkinite subgroup and six in the perrierite subgroup, their formulae pointing to variable cation occupancy of the "standard" sites (Table 1). The chemical compositions of the type minerals are listed in Table 2. Given the wide range of potential host rocks and P-T environments, and the flexibility of the CGM structure, it is likely that further new phases will be documented, such as Sc-dominant chevkinite, Th-dominant chevkinite and Mg-dominant perrierite.

Certain issues concerning the nomenclature of the CGM need to be addressed at this stage. First, which sites should be used to distinguish species within the group? For example,

conventional usage has been that the dominant cation in the C site in chevkinite and perrierite can be Fe or Ti. However, Xu et al. (2008) proposed that minerals with the ideal end-member composition $Ce_4Fe^{2+}Ti_2Ti_2(Si_2O_7)_2O_8$ be named dingdaohengite-(Ce), a proposal accepted by the CNMNC-IMA. Should all chevkinite with Ti dominant in the C site be renamed dingdaohengite? In the type perrierite-(Ce), from Nettuno, Italy, Al is dominant in the C site (Macdonald et al. 2009), which might preclude all perrierites with Fe or Ti dominance in the site being termed perrierite. If it is assumed that A = Ca, Sr, Y, La, Ce, Nd, Th; B = Mg, Mn, Fe^{2+}; C = Al, Ti, Cr, Fe^{2+}, Fe^{3+}, Zr, Nb; D= Ti, Nb; 294 potential combinations of site dominance could possibly be used in classification, probably not a desirable situation.

Second, knowledge of the Fe^{2+}/Fe^{3+} ratios in a phase may be important in classification. Determination by instrumental methods, such as Mössbauer spectroscopy, or by wet-chemical methods is seldom possible because of small crystal size. The ratio is often calculated from stoichiometry but such methods are influenced by the presence of non-determined elements and by analytical imprecision for elements in low abundance: Macdonald and Belkin (2002) found poor agreement in CGM between ratios calculated from stoichiometry and those determined by wet chemical methods or Mössbauer spectroscopy. As a further example, an electron microprobe analysis by Macdonald et al. (2009) of the type perrierite-(Ce) from Nettuno gave the formula $A_{4.1}BC_{1.9}D_{2.0}(Si_2O_7)_2O_8$, where all Fe was presented as Fe^{2+} and the sum of cations was 13.0. The formula is close to stoichiometric and there is apparently no need for Fe^{3+} in the phase. However, our unpublished Mössbauer spectroscopic data for the analyzed material indicates an oxidation ratio $[Fe^{3+}/(Fe^{3+}+Fe^{2+})]$ of 0.39.

The issue of an accurate knowledge of oxidation ratio is particularly important where Fe^{3+} proves to be the dominant cation in a particular site and could thus have an influence on mineral classification. Cation entry into the B site of an Fe-rich chevkinite-(Ce) from Mianning County,

169 Sichuan, China, was given by Yang et al. (2002) as $(Fe^{3+}_{0.29}Ti_{0.21}Fe^{2+}_{0.18}Mn^{2+}_{0.13}Mg_{0.08}\square_{0.11})_{\Sigma 1.00}$.

170 Analytical totals were low (92.84-94.23 wt%) and structural water was invoked to achieve charge
171 balance. Unusually in the CGM, vacancies in the structure were also invoked. The phase has
172 clearly been affected by secondary hydration, with an increase in the oxidation ratio, as noted by
173 Vlach and Gualda (2007).

174 In the face of these complications, formulae have been calculated here on the basis of 22
175 oxygens and, given the small number (13) of available Mössbauer determinations
176 (Supplementary Table 1), and uncertainties in recalculation schemes, all Fe has been taken to be
177 Fe^{2+}. For species approved by the CNMNC-IMA the formal names are used here (Table 1). All
178 other analyses have been classified using the empirical scheme of Macdonald et al. (2009).

179

180 **STRUCTURE OF CHEVKINITE-GROUP MINERALS**

181 Part of the difficulties in determining the structure of CGM lies in the multivalent nature of
182 cations in certain crystallographic sites, e.g. Fe^{2+}, Al^{3+}, Ti^{4+} and Nb^{5+} in the C site. A further
183 complication is that certain cations, importantly Fe, may exist in more than one valency state:
184 Stachowicz et al. (in revision), for example, have argued that Ti occurs as Ti^{4+}, Ti^{3+} and possibly
185 Ti^{2+} in Nb-rich chevkinite-(Ce) from the Biraya deposit, Mongolia. Another difficulty in
186 comparing CGM structures is due to the use of different choices for the origin of the unit cell in
187 part of the stuctures (a shift by vector [0, 0, ½]); see below. To clarify which site in the crystal
188 structure corresponds to a site from the empirical formula, the published data for CGM are
189 summarized based on the nomenclature scheme used here (Table 3).

190 There can also be discrepancies in the assignment of cations to particular B, C and D sites
191 because CGM occur in different polymorphic forms, the C2/m and $P2_1/a$ space groups.
192 Stachowicz et al. (in revision) noted that annealing of metamict CGM can lead to a slightly

different crystal structure from the initial structure and to migration of cations to different crystallographic sites.

It was noted earlier that chevkinite and perrierite are distinguished by different monoclinic β angles (~100° and ~113°, respectively). These are associated with a different stacking order of sheets consisting of REE cations (Stachowicz et al. 2014). The arrangement of the remaining cations for both subgroups is essentially the same, consisting of sheets of MO_6 (C and D sites) octahedra interleaved with layers of n[$B(Si_2O_7)$] hetero-polyhedra (Calvo and Faggiano 1974). CO_6 edge-sharing octahedra form chains that share a corner with chains of DO_6 edge-sharing octahedra. Each Si_2O_7 group is joined to six BO_6 octahedra (Fig. 2). A-cations fill large cavities within the framework and are arranged in planar hexagonal arrays, with a Si-centred tetrahedron (Figs. 2, 3) inside each array.

The green planes were plotted on two adjacent REE surfaces in both structure types to emphasize the differences in the mutual organization of REE atoms which are the source of the different β angles of the unit cells in the two structures. Stachowicz et al. (2014) proposed that a characteristic feature of the perrierite-type structure, a D/M(3) cation displacement parallel to the tetrad axis of the coordination octahedron, is an effect of the REE stacking arrangement. A trigonal distortion of BO_6 octahedra is present in both structure types; four B-O bonds are elongated with a length of 2.2 Å and the remaining two are 2.0 Å. The C-O and D-O bond lengths in chevkinite and D-O bond lengths in perrierite are similar and within 1.9-2.0 Å.

Assuming a value of 3 Å as a limit for the A site coordination sphere, its number varies with the space group. A-coordination polyhedra in the C2/m space group have the following numbers: $^{VIII}A(1)$ and $^{X}A(2)$ in perrierite (Miyajima et al. 2002; Yang et al. 2012) and chevkinite (Popov et al. 2001; Yang et al. 2002, 2007; Sokolova et al. 2004). In the $P2_1/a$ space group the numbers are $^{IX}A(1)$ and $^{IX}A(2)$ in perrierite (Calvo and Faggiani 1974; Miyawaki et al. 2002; Chukanov et al.

2012a) and chevkinite (Calvo and Faggiani 1974; Xu et al. 2008). Stachowicz et al. (in revision a, b) found these trends in natural Nb-rich chevkinite-(Ce), one with a C2/m space group and the other with $P2_1/a$. Moreover, with transformation due to annealing from C → P of a particular crystal a change in coordination numbers $^{XIII}A(1) \rightarrow {}^{IX}A(1)$ and $^{X}A(2) \rightarrow {}^{IX}A(2)$ was also observed, which is associated with a bending of the Si-O-Si angle in sorosilicate groups. The exceptions are perrierite-(Ce) with C2/m and $^{IX}A(1)$ and $^{IX}A(2)$ (Gottardi 1960) and delhuyarite-(Ce) with C2/m and $^{VIII}A(1)$ and $^{XII}A(2)$ (Holtstam et al. 2017). The only CGM member with the $P2_1/m$ space group, christofschäferite-(Ce), has four independent A sites in the asymmetric unit, $^{VIII}A(1)$, $^{X}A(2)$, $^{VIII}A(3)$ and $^{X}A(4)$ (Chukanov et al. 2012b).

Status of dingdaohengite-(Ce) and maoniupingite-(Ce)

The status of the Fe-Ti-dominant phases maoniupingite-(Ce) (Shen et al. 2005) and dingdaohengite-(Ce) (Xu et al. 2008; Kasatkin et al. 2015) is unclear, in particular their relationship to chevkinite-(Ce) (Belkin et al. 2009). Xu et al. (2008) assigned Fe^{2+} to the B/M(1) and C/M(2) sites; however, the corresponding deposited crystal structure cif file contains different information. Xu et al. (2008) placed the origin of the unit cell in their crystal structure in a different position relative to their reference structure determined by Sokolova et al. (2004). Xu et al. (2008) also exchanged the B/M(1) and D2/M(4) sites in their crystal structure. The error came from a comparison of identical fractional coordinates to those of Sokolova et al. (2004), despite their different Wyckoff positions. Moreover, although the C/M(2) site is assigned correctly there are two crystal information files (cif) available, one in the American Mineralogist database and one in the Inorganic Crystal Structure Database (ICSD). The occupancies for the C sites are different in the two files, 23.3 and 21.4 assigned electron counts, yet the anisotropic displacement parameters are identical. The same applies to the D2/M(4) site. In the ICSD cif the

241 occupancy is 0.84 Fe, in the American Mineralogist cif there is a full occupancy of Fe (21.8 *v.* 26
242 electrons) and the anisotropic displacement parameters are again identical. We recommend that
243 the crystal structure of dingdaohengite-(Ce) be revisited, with Fe^{2+} and Mg^{2+} being assigned to
244 the B site, which will result in electron counts close to the experimentally refined value.
245 Maoniupingite-(Ce) (Shen et al. 2005), first referred to as Fe-rich chevkinite-(Ce) by Yang et
246 al. (2002), is acknowledged as a mineral species due to the dominance of Fe^{3+} in the B site. Yang
247 et al. (2002) allocated to this site the following components:
248 $Fe^{3+}_{0.29}Th_{0.21}Fe^{2+}_{0.18}Mn^{2+}_{0.13}Mg_{0.09}\square_{0.11}$. The ratio of $Fe^{3+}/\Sigma Fe = 0.61$ was based only on charge
249 distribution calculations (Nespolo et al. 1999). In later structural studies of chevkinite-(Ce) from
250 the same locality and based on the same average of 24 electron microprobe analyses (Li et al.
251 2005; Yang et al. 2007) the total $Fe^{3+}/(Fe^{3+} + Fe^{2+})$ ratio, based on Mössbauer spectroscopy, was
252 given as 0.39, which contradicted the earlier assumption from charge distribution calculations.
253 The B site was considered to be occupied by the following cations: $Fe^{2+}_{0.61}Mn_{0.13}Ti_{0.12}Mg_{0.08}$. The
254 experimental evidence apparently shows that maoniupingite-(Ce) should be discredited as a
255 mineral species, rather it is chevkinite-(Ce), as suggested by Belkin et al. (2009).
256 Given these uncertainities, dingdaohengite-(Ce) snd maoniupingite-(Ce) have not been
257 included in the following discussion of compositional variation in chevkinite and perrierite.
258

259 **COMPOSITION OF CHEVKINITE-GROUP MINERALS**

260 Chemical compositions of CGM were collected from the literature and our unpublished data
261 (Supplementary Table 2). In our experience, an oxide total ≥96 wt% is acceptable for CGM, in
262 that few analyses present the full range of elements, especially all the REE, Nb, Th and Zr, and
263 some Fe is commonly present as Fe^{3+} although all Fe is normally presented as Fe^{2+}. After
264 application of the 96 wt% filter, the number of analyses compiled was 266, with 164 in the

chevkinite subgroup and 102 in the perrierite subgroup. The nature of the data set is variable: some are averages, others are multiple point analyses of several crystals in the same sample, especially where the compositional range in the sample was taken to be important. In places, reference is made in the text to specific analyses not included in the data set, e.g. the Th-chevkinite of Doelter (1931).

One caveat concerning the elemental composition of CGM, especially minor components, is that most published data are obtained with electron microprobe wavelength dispersive spectroscopy which limits, or precludes, detection of elements such as B, Be, and Li. Laser-ablation inductively-coupled mass spectroscopy analysis of CGM would be helpful in obtaining a more complete inventory of substituent elements.

Chevkinite and perrierite

The compositional ranges in chevkinite and perrierite (excluding Sr-rich varieties, polyakovite and delhuyarite, which are discussed separately) are given in Table 4. There are major overlaps between the subgroups for all elements. Given the nature of the compositional discriminant employed (Figs 1a, 1b), a main difference is in the (CaO+SrO) and FeO* contents. Perrierite has higher average abundances of Al_2O_3, MgO, CaO, SrO and ZrO_2, and lower average contents of FeO*, Nb_2O_5 and ΣREE_2O_3 than chevkinite. In the C site of chevkinite Fe > Ti > Al; in perrierite Ti > Al > Fe. Magnesium is required to fill the C site in many perrierite analyses but not in chevkinite. The main compositional variations are expressed in the general equation proposed by Vlach and Gualda (2007): $(Ca^{2+} + Sr^{2+})_A + (Ti^{4+} + Zr)_C \leftrightarrow [(REE,Y)^{3+}]_A + (M^{2+,3+})_C$ (Fig. 4).

Compositional evolution *within* the chevkinite and perrierite subgroups generally follows the trend shown in Fig. 4, the trend towards an increasingly "chevkinitic" character indicating an

increasingly felsic character of the host rocks. This tendency was shown in a $\Sigma(La_2O_3\text{-}Sm_2O_3)$ – FeO* - $(CaO+SrO+MgO+Al_2O_3)$ plot by Macdonald and Belkin (2002) (Fig. 5).

One consequence of the compositional trends is that some magmatic trends may cross the empirical boundary on the discriminant plot (Fig. 6). It is improbable that the structure changes (e.g., the β angle from ~113° to ~100°), especially within single crystals, as represented by the Azambre et al. (1987) example shown in Fig. 6. It is more likely that there is a zone around the boundary where phases can exist in either structural state, as predicted by Macdonald & Belkin (2002). As Muhling et al. (2014) stressed, structural study is required to determine precisely the nature of phases in the transitional zone. Nevertheless, the discriminant has proven to be a useful tool in CGM studies, allowing preliminary names to be given to phases where no structural study has been possible.

A site

The dominant cations in the A site are REE and Ca. Rare earth elements predominate, exceptions being two point analyses from kersantites of the Oroscocha volcano, Peru, where Ca > REE (Fig. 7), potentially making the phase perrierite-(Ca). A constraint on describing REE distribution is the scarcity of complete data sets. For example, Eu concentrations have been reported in only 45 analyses (including values given as below detection). The large compositional range is, therefore, demonstrated here on a plot of $[La/Nd]_{CN}$ (as a measure of fractionation within the LREE) against $[La/Y]_{CN}$ (fractionation of LREE from heavy rare-earth elements (HREE; Gd-Yb), with Y proxying for the HREE) (Fig. 8). The full data set has the following features.

(i) Ce is overwhelmingly the dominant REE in the site; La exceeds Ce in only seven cases. The type perrierite-(La) was described from the Eifel volcanic district, Germany, by Chukanov et al.

(2012a), although perrierite analyses with dominant La had earlier been reported, without structural data, from Bjørkedalen in the Oslo region, Norway (Segelstad and Larsen 1978), and Golden Lake in Ontario, Canada, and Rajasthan, India (Macdonald et al. 2009). Chevkinite with La exceeding Ce was reported from Sandefjord, Bjørkedalen and Stokkoya, Oslo region, by Segelstad and Larsen (1978), in trachyandesites from Moravia, Czech Republic (Macdonald et al. 2017a), granites from Zhitkovichi, Belarus, by Povarennykh and Ganzeeva (1972) and without presenting an analysis from a hornfels in the Khibiny massif, Kola Peninsula, Russia, by Yakovenchuk et al. (2005). However, the species has not yet been submitted to the CNMNC-IMA. Proshchenko (1967) presented three analyses of chevkinite in albitites from eastern Siberia, with La/Ce (atomic) ratios of 2.7, 1.21 and 1.16. It would be valuable to restudy this material, to determine whether the La dominance is a function of the paragenesis or the result of an analytical problem. A quite exceptional Y-dominant perrierite was described from a quartzofeldspathic gneiss of the Archean Napier Complex, Antarctica, by Belkin et al. (2009), the only record so far of a Y-dominant mineral in the CGM. Liu and Ma (2015) and Liu et al. (2015, 2016) reported a CGM with Nd dominant in the A site from Martian breccia meteorite NWA 7034, the first record of such Nd dominance.

(ii) Chevkinite has slightly higher ΣREE_2O_3 (37.4-53.2 wt%; average 44.5 wt%) than perrierite (26.5-51.0 wt%; average 40.7 wt%) (Table 4) but clearly REE contents alone are insufficient to distinguish the subgroups.

(iii) The great majority of analyses are LREE-enriched, with $[La/Y]_{CN}$ ranging from 2-5608 (Fig. 8). Chevkinite shows stronger LREE enrichment relative to HREE than perrierite (average $[La/Y]_{CN}$ 420 and 271, respectively). In both subgroups, there is no simple relationship between the degree of enrichment, the nature of the host rock or the paragenesis. Note, for example, the major overlaps on a La-Y plot between CGM from peralkaline rhyolites (comendites) and

tholeiitic intrusions, and between CGM from potassic volcanics and the A-type Woshui syenite in the Emeishan igneous province, SW China (Fig. 9).

(iii) Both subgroups show large ranges in $[La/Nd]_{CN}$, indicating significant fractionation within the LREE (Fig. 8). There is apparently no simple link between the value of the ratio and any other parameter, such as host lithology or mineral paragenesis.

(iv) Cerium anomalies are ubiquitous and can be positive or negative, although positive anomalies are dominant (85%). The magnitude of the anomalies is similar in chevkinite (Ce/Ce* 0.6-1.4; average 1.1) and perrierite (Ce/Ce* 0.7-1.3; average 1.1). The lowest values (0.6-0.7) in both cases are predictably from the La-dominant phases from Oslofjord noted above (Segelstad and Larsen 1978).

Europium anomalies (Eu/Eu*) have been calculated for only 16 samples. Shellnutt and Iizaka (2013) recorded unusually large positive anomalies (Eu/Eu* 2.3-23) in CGM from the metaluminous Woshui syenite, noting that the anomalies mirror those in the whole-rocks. Huraiová et al. (2007) reported, without comment, chevkinite-(Ce) in a syenite xenolith from the Pincina maar, Slovakia, with equally large positive anomalies (3-28). In an interesting approach, Troll et al. (2003) used an Onuma diagram to estimate the proportions of Eu^{3+} and Eu^{2+} (~33% Eu^{2+}) in chevkinite-(Ce) from Gran Canaria, Spain.

Strontium levels are very low (<0.2 apfu) in the great majority of chevkinite and perrierite analyses (Fig. 7), with the exception, *inter alia*, of perrierite-(Ce) from the Bearpaw Mountains, Montana, USA (0.35-1.18 apfu; Chakhmouradian and Mitchell 1999) and Sr-Zr-rich perrierite-(Ce) from the Burpala massif, Russia (0.88, 0.94 apfu; Portnov 1964; Macdonald et al. 2012). Thorium abundances reach a maximum of 8.4 wt% ThO_2 (0.40 apfu) in perrierite-(Ce) from the Joe Lott Tuff Member of the Belknap Volcanics, Utah (Budding et al. 1987), an exception being a Th-rich chevkinite-(Ce) from the Urals, Russia, which has 20.9 wt% ThO_2 (Doelter 1931).

Thorium abundances do not appear to be correlated with any other geochemical feature. Uranium abundances are low (≤0.30 wt% UO_2), with the exception of chevkinite-(Ce) from Samalpatti, India (2.53 wt%; Semenov et al. 1978), and Samchampi, India (0.69 wt%; Viladkar et al. 2009). Barium levels are also low, reaching 0.45-0.54 wt% BaO in chevkinite-(Ce) from syenite xenoliths in the Pinciná basaltic maar, Slovakia (Huraiová et al. 2007), although such high values may be an artefact arising from Ti uncorrected for peak interference.

B site

The B site is filled in 90% of analyses by Fe^{2+}. The deficit in the remaining analyses is made up by Mn ± Mg, with the exception of a low-Fe perrierite-(Ce) from the Khibiny massif (**Σ**B = 0.83 apfu; Yakovenchuk et al. 2005). The Fe-deficient rocks include perrierite from Italian potassic volcanoes (Van Bergen 1984; Parodi et al. 1994; Della Ventura et al. 2001; Macdonald et al. 2009), potassic volcanics from the Oroscocha volcano (Carlier and Lorand 2008), and Al-rich perrierites from Antarctica and India (Harley 1994; Hokada 2007; Belkin et al. 2009). The latter also contain the highest levels of Mg in the B site, up to 0.77 apfu (Harley 1994), making the phase the Mg-Al-dominant analogue of perrierite-(Ce).

In christofschäferite-(Ce) (Table 1) Mn fills the octahedral site B, Ti dominates the C and D2 sites, and D1 is occupied by Fe and Ti (Chukanov et al. 2012b). The phase contains 4.39 wt% MnO (0.76 Mn apfu). Povarennykh and Ganzeeva (1972) presented an analysis of chevkinite in albititized granites at Zhitkovichi, Belarus, with 5.0 wt% MnO (0.90 Mn apfu). The formula can be written as:
$(La_{1.87}Ce_{1.51}Ca_{0.49}Nd_{0.17})_{4.04}(Mn_{0.90}Fe^{2+}_{0.10})(Fe^{3+}_{1.02}Ti_{0.79}Fe^{2+}_{0.21})_{2.02}Ti_{2.00}(Si_2O_7)_2O_8$, which would potentially make it the La-dominant analogue of christofschäferite-(Ce).

C site

The only cations to achieve dominance in the C site are Ti, Fe^{2+} and Al, which occur in very variable proportions (Fig. 10). Macdonald et al. (2009) listed several perrierite occurrences in Antarctica and India where Al is dominant in the site; Al-dominance in chevkinite is uncommon but has been recorded in albitites from Siberia (Proschchenko 1967) and the Pyrenees (Monchoux et al. 2006). Iron- or Ti- dominance appears not to be specific to certain lithologies; indeed both forms can be found in the same sample.

All determinations of oxidation ratio [$Fe^{3+}/(Fe^{3+} + Fe^{2+})$] by Mössbauer spectroscopy of which we are aware are listed in Supplementary Table 1. The majority are for members of the chevkinite subgroup. Values range from 0.18 to 0.61 and have no simple relationship to mineral species or to the nature of the host rock.

In the majority of point analyses the Mg levels are low (<0.3 apfu; <1 wt% MgO). The maximum Mg value recorded is 0.90 apfu (2.99 wt% MgO) in perrierite-(La) from a metacarbonate at Golden Lake, Ontario (Macdonald et al. 2009). The most consistently Mg-rich phases are Al-rich perrierites from Antarctica and Anakpalle, India (0.21-0.77 apfu; 0.72-2.74 wt% MgO; Harley 1984; Hokada 2007; Belkin et al. 2009). The majority of Mn values are low (≤0.5 wt% MnO; <0.1 apfu Mn) but there is a continuum of compositions to 0.50 apfu; then there is an apparent compositional gap to christofschäferite (1 apfu Mn).

Chromium oxide levels in chevkinite and perrierite are extremely low (≤0.13 wt%), indicating a huge compositional gap between them and polyakovite-(Ce). Scandium abundances have been reported for only seven occurrences, in only one in significant amounts, perrierite-(Ce), from Bayan Obo in Inner Mongolia, China (3.26 wt% Sc_2O_3; 0.57 apfu Sc; Shimazaki et al. 2008a). Mention may be made here of the so-called Sc-perrierite, first recorded from quartz-fluorite pegmatites in Akzhaylau, southeastern Kazakhstan by Semenov et al. (1966). Its Sc content was

409 0.82 apfu (Sc_2O_3 4.14 wt%). Scandium was thought to have entered the structure through the
410 substitution $Sc^{3+} + Fe^{3+} = Fe^{2+} + Ti^{4+}$ and the formula given as $Ce_4ScFe^{3+}Fe^{2+}Ti_2Si_4O_{22}$. The
411 analysis as presented has 43.3 positive charges and plots in the chevkinite field of the empirical
412 discrimination scheme of Macdonald et al. (2009). A reinvestigation of this interesting material
413 would be welcome. Vanadium has been reported in three samples, the highest value being 0.49
414 wt% V_2O_3 in perrierite-(Ce) from alkaline silicate – carbonate assemblages of the
415 Vishnevogorsky complex, South Urals (Makagonov and Muftakhov 2016).
416 Niobium is commonly present in low to moderate concentrations (<5 wt% Nb_2O_5).
417 Makarochkin et al. (1959) described, from a fenitised granite in the Ilmen Mountains, southern
418 Urals, Russia, a phase which they named niobochevkinite. However, the phase contains only 7.4
419 wt% Nb_2O_5 (Nb 0.71 apfu) and is strictly Nb-rich chevkinite. Sample 10047-11 from the Moon
420 has ~3 wt% Nb_2O_5 (Muhling et al. 2014). The most Nb-rich CGM so far recorded is from the
421 Biraya carbonatite complex, Russia, with 11 wt% Nb_2O_5 (Stachowicz et al., in revision a, b).
422 Niobium is usually allocated to the C site, perhaps because in almost all chevkinites and
423 perrierites, the D site is taken to be filled by Ti. However, Popov et al. (2001) allocated Nb to the
424 D site in polyakovite and Stachowicz et al. (in revision, Part 2) found Nb to be allocated between
425 both C and D sites in their Nb-rich phase.
426 Taking 0.10 wt% as a reasonable limit of detection, 31 Ta determinations are available
427 (Supplementary Table 2), with a maximum Ta_2O_5 value of 0.50 wt% in chevkinite-(Ce)
428 from the Paleogene Meall Dearg granite, Isle of Skye, Scotland (Macdonald et al. 2013).
429 Zirconium shows a fairly continuous spread of values up to 7.0 wt% ZrO_2 (0-0.63 apfu Zr).
430 The highest values are in perrierite from the Oroscocha volcano (Carlier and Lorand 2008), in
431 mafic sills of Western Australia, and in lunar samples (Muhling et al. 2014). Taking 0.10 wt% as

a reasonable detection limit for HfO_2, 20 determinations of Hf are available, with a maximum value of 0.44 wt% in perrierite-(Ce) from the Woshui syenite.

D site

With two exceptions, the D site is filled with Ti. Belkin et al. (2009) described two samples of perrierite-(Ce) from Antarctica with Ti and Nb abundances unable to fill the site and suggested that some Al (0.21 apfu, 0.56 apfu) may enter the site. In their structural study of Nb-rich chevkinite from the Biraya complex, Stachowicz et al. (in revision a, b) allocated, in addition to Ti, Nb, Fe^{3+}, Fe^{2+} and Mg to the D site.

T site

In 87% of analyses, the tetrahedral site is filled by Si. Phosphorus is sometimes considered to be a minor constituent: CGM from tholeiitic sills of Western Australia have the highest values, up to 0.062 apfu (0.37 wt% P_2O_5; Muhling et al. 2014). Huraiová et al. (2007) allocated some Al to the site (up to 0.065 apfu). Carlier and Lorand (2008) also raised the possibility of Al entering the site in perrierite-(Ce) from Oroscocha.

Anion site

Water has been reported in analyses of CGM, in amounts up to 0.90 wt% (Supplementary Table 2). The question arises: did the water enter the mineral when it formed or was it added under subsolidus conditions, e.g., by hydrothermal fluids? In a study of chevkinite-(Ce) from an aegirine granite at Mianning, Yang et al. (2008) used single-crystal FTIR to detect OH in the structure, suggesting that it possibly replaced oxygen. However, their analysis gave only 42.24 positive charges; from charge balance, they calculated an OH content of 1.76 pfu (1.27 wt%

H_2O). Despite this addition, the analytical total was still low (95.22 wt%) and the structural role of the OH is uncertain. More recently, Holtstam et al. (2017) recorded structural water and vacancies in delhuyarite (see below).

Fluorine has also been reported in chevkinite and perrierite, at levels up to 1 wt% (Supplementary Table 2). It has been argued by Belkin et al. (2009) that the F values determined by electron microprobe represent interference between the F-*K*α (λ = 18.3199 Å) and Ce-*M*ξ (λ = 18.3499 Å) peaks. Chlorine has been recorded in four samples of chevkinite, at levels ≤0.03 wt%, possibly below a realistic detection level.

We know of no example of an absolutely pristine CGM, occurring, for example, as phenocrysts in young eruptive rocks, being shown to carry OH and F. Lacking positive evidence of these components being incorporated during crystallization, we suggest that pristine CGM are volatile–free.

Polyakovite-(Ce)

Polyakovite-(Ce) was first recorded in a carbonatite (dolomite) veinlet cross-cutting a phlogopite-olivine rock in the Ilmen Mountains (Popov et al. 2001). It is an unusual member of the chevkinite group, in that Cr is a species-forming element. The structural formula is $(Ce_{1.86}La_{1.23}Nd_{0.35}Pr_{0.15}Sm_{0.01}Y_{0.04}Ca_{0.24}Th_{0.12})_{4.00}(Mg_{0.80}Fe^{2+}_{0.20})_{1.00}\,(Cr_{1.28}Fe^{3+}_{0.72})_{2.00}$ $(Ti_{1.52}Nb_{0.32}\square_{0.16})_{2.00}Si_{4.00}O_{22.00}$. Magnesium is dominant at the B site (M(1) in the terminology of Popov et al. (2001)) and Cr is dominant at the C [M(3)) and M(4)] sites. Also unusual is the presence of vacancies in D (M(2)). A later analysis of a cotype from the same locality showed slightly higher Cr_2O_3 and Nb_2O_5 contents, and lower SiO_2, FeO*, MgO, CaO and La_2O_3 contents (Macdonald et al. 2012). Their structural formula did not include vacancies.

Earlier, Kopylova et al. (1997a, 1997b) had described a mineral which they termed Cr-chevkinite, occurring as inclusions in diamonds from the River Ranch kimberlite pipe in Zimbabwe. They gave the formula as $(Ce_{2.22}La_{0.96}Nd_{0.51}Pr_{0.18}Th_{0.06}Sr_{0.29})_{3.99}(Mg_{0.46}Fe^{2+}_{0.23}Ca_{0.13})_{0.83}Cr_{1.95}(Ti_{1.44}Nb_{0.26}Al_{0.32})_{2.02}Si_{4.02}O_{22}$. Despite some minor differences, there are clear similarities to polyakovite-(Ce), a particular point of interest being the much higher Cr content. The inclusions in the River Ranch kimberlite may have been formed during a K-metasomatic event and incorporated into diamonds outside the diamond stability field prior to, or during, kimberlite eruption (Kopylova et al. 1997b).

Delhuyarite-(Ce)

Delhuyarite-(Ce), the newest CGM, is known from only one locality, the Nya Bastnäs Fe-Cu-REE deposit in Sweden (Holtstam et al. 2017). Its ideal formula is given as $Ce_4Mg(Fe^{3+}_2W)\square(Si_2O_7)_2O_6(OH)_2$. The W content (0.89 apfu; 15.53 wt% WO_3) is quite unique in the CGM. Also notable are the dominance of Mg in the M1 site, the presence of H_2O, confirmed by IR-spectroscopy from a strong absorption band at 3495 cm^{-1}, and a 50% vacancy in the M2 site. Vacancies in the structure were invoked partly to explain the entry of W into the phase, *via* a charge-balanced exchange mechanism of the type: $2Ti^{4+} + 2O^{2-} \leftrightarrow W^{6+} + \square + 2(OH^-)$. The unusual nature of the phase may be related to its formation from hot (initially ≥400°C), originally juvenile magmatic fluids (Holtstam et al. 2017).

Sr-rich varieties

These are defined here as having Sr > Ca and include, therefore, the Sr-dominant species rengeite, matsubaraite, strontiochevkinite and hezuolinite (Table 1). Possible compositional relationships between the species are shown on Fig. 11.

Rengeite [$(Sr_4ZrTi_4(Si_2O_7)_2O_8)$] is compositionally variable. Two varieties, occurring in association with natrolite and analcime in jadeitites from the type area in the Itoigawa-Ohmi district, Japan (Miyajima et al. 2001; Goto et al. 2017), contain very different proportions of REE, Ca and Sr (Fig. 7). An orthorhombic polymorph, reported as microdomains in the rengeite, contains neither Ca nor REE (Mashima et al. 2008); however, the phase has not been submitted to the CNMNC-IMA and may not be valid. Rengeite is also known from Mount Kaskasnyunchorr, Khibiny massif, occurring in an albite-anorthoclase hornfels from a large xenolith in foyaite (Yakovenchuk et al. 2005; Mikhailova et al. 2007). It contains no REE and has the highest Ca/Sr ratio so far reported in the mineral (0.16). Matsubaraite [$(Sr_4Ti_5(Si_2O_7)_2O_8)$] is known only from its type locality, the same jadeitite locality as for rengeite. It can be considered as the Zr-free analogue of rengeite (Miyajima et al. 2002; Miyawaki et al. 2002).

The type locality of hezuolinite [$(Sr,REE)_4Zr(Ti,Fe^{3+},Fe^{2+})_2Ti_2O_8(Si_2O_7)_2$] is in sodic lujavrite of the Saima alkaline complex, northeastern China (Yang et al. 2012; Wu et al. 2016). It has not been recorded elsewhere but is in some respects similar to strontiochevkinite [$(Sr_2[La,Ce]_{1.5}Ca_{0.5})_4Fe^{2+}_{0.5}Fe^{3+}_{0.5}(Ti,Zr)_2Ti_2(Si_2O_7)_2O_8$] (Haggerty and Mariano 1983), except that Zr and Fe occupy different positions in the B and C sites. There is, however, a substantial compositional gap between strontiochevkinite and Sr-Zr perrierite, such that it is difficult to identify substitution schemes. A possible scheme connecting strontiochevkinite and Sr-rich perrierite-(Ce) from Pegmatite Peak in the Bearpaw Mountains, Montana (Chakhmouradian and Mitchell 1999) is $2REE^{3+} + Fe^{2+} = Ti^{4+} + Zr^{4+}$ (Fig. 11). Strontiochevkinite and Sr-Zr perrierite-(Ce) may be connected by the scheme $REE^{3+} + Fe^{2+} = Sr^{2+} + Fe^{3+}$ (Fig. 11).

OCCURRENCE OF CHEVKINITE AND PERRIERITE

527 **Igneous rocks**

528 Chevkinite and perrierite have been recorded in very diverse igneous lithologies, in a range
529 extending from ultramafic cumulates to granitic pegmatites. Mutanen (1997) reported perrierite
530 as an intercumulus phase in ultramafic cumulates of the Akanvaara and Koitelainen mafic layered
531 intrusions, northern Finland. It has long been recognised that CGM are common in mafic and
532 intermediate rocks of potassic affinity. However, it is being increasingly recognised that they also
533 occur in more sodic types; Muhling et al. (2014) described CGM in tholeiitic intrusive rocks from
534 Western Australia and Melluso et al. (2014) found CGM in low-Ti, low-Fe tholeiitic rocks from
535 Tasmania. In the tholeiitic types, the CGM commonly occur in late-stage granophyric patches,
536 indicating that they crystallized when the residual melts had felsic compositions.
537 There are some lithologies where CGM are scarce or absent, such as peraluminous granites
538 where the main REE-bearing phase tends to be monazite. Their absence from mid-ocean ridge
539 basalts possibly results from the low Ti and REE contents of such rocks. CGM are also relatively
540 uncommon in *strongly* peralkaline [(mol. $(Na_2O+K_2O)/Al_2O_3$ >1.3)] rhyolites and granites, where
541 aenigmatite and astrophyllite tend to be the stable Ti-bearing phases. However, Noble (1965)
542 recorded chevkinite in pantellerite of the Gold Flat Member of the Thirsty Canyon Tuff, Nevada;
543 although he did not present an analysis we have confirmed its presence *via* electron microprobe
544 analyses (unpublished data).
545
546 **Early magmatic**
547 Chevkinite-group minerals occur as (micro)phenocrysts in a wide range of lithologies, from
548 quartz latite (Warren et al. 1989), through trachyandesites-dacites (Van Bergen 1984) and
549 metaluminous rhyolites (Ewart 1981; Martz and Brown 1981; Cameron and Cameron 1986;
550 Macdonald and Belkin 2002; Miyawaki et al; 2012; Vasquez et al. 2014; Padilla and Gualda

2016) to peralkaline rhyolites (Jørgensen 1980; Novak and Mahood 1986; Sawyer and Sargent 1989; Macdonald et al. 2002, 2015a; Troll et al. 2003; Marshall et al. 2009; Vasquez et al. 2014; Peretyazhko et al. 2015) (Fig. 12a).

Estimates of the temperatures and pressures of equilibration and of fO_2 for various CGM phenocryst occurrences have been made by different methods, including coexisting oxides, QUILF (which assesses equilibrium among T-magnetite, ilmenite, augite, pigeonite, orthopyroxene, olivine and quartz, or subassemblages thereof), clinopyroxene-melt, $\Delta^{18}O$ (Quartz-Magnetite) and phase equilibrium studies, and are not strictly comparable. The temperature range is from >900 °C in quartz latites (e.g. Mills et al. 1997; Bindeman and Valley 2003) to ~700 °C in rhyolites (Mills et al. 1997; Scaillet and Macdonald 2001), with perrierite being the typical CGM at higher T and chevkinite at lower T. Pressure estimates are less well constrained but where the geological context is provided the phenocrysts can be inferred to have formed at P ≤5 kbar. Oxygen fugacities vary from ΔFMQ -1 to +2 and show no simple relationship to host lithology (Mills et al. 1997; Scaillet and Macdonald 2001; Bindeman and Valley 2003; Troll et al. 2003; Macdonald et al. 2015a).

Estimates of the water contents of CGM-phyric felsic magmas generally show that such magmas were water-rich, with H_2O contents in the range 4-5 wt% (Novak and Mahood 1986; Mills et al. 1997). This is consistent with experimental evidence that chevkinite crystallized from peralkaline rhyolites (comendites) under conditions of near H_2O saturation (Scaillet and Macdonald 2001).

Also considered to be of early magmatic crystallization are CGM found as inclusions in early phases in plutonic rocks, such as feldspar, pyroxene and amphibole (Van Bergen 1984; Ridolfi et al. 2003: Macdonald et al. 2013) (Fig. 12b). Estimates of the P-T-fO_2 conditions of CGM formation are broadly in line with those for phenocrysts. McDowell (1979) estimated that GGM

575 groundmass grains in the Little Chief granite porphyry stock, California, crystallized at 700-750
576 °C and 1.5 kbar, with fO_2 >NNO. Liquidus temperatures of between 800 and 900 °C at fO_2 close
577 to FMQ were estimated for A-type alkaline granitoid intrusions of the Graciosa Province, Brazil,
578 where CGM are the typical REE phase (Vlach and Gualda 2007). The Paleogene Western Granite
579 on the island of Rum, Scotland, gave the range 808-781 °C at fO_2 ~NNO, at pH_2O <1 kbar
580 (Macdonald et al. 2013).
581
582 **Late magmatic**
583 One form of late magmatic CGM is at grain boundaries between the major phases. Cellai et al.
584 (1993) recorded perrierite-(Ce) up to 30 μm long, generally occurring enclosed in the rims of K-
585 feldspars in an evolved minette from Montecatini Val di Cecina, Tuscany, Italy. Enclosure of
586 CGM within feldspar rims was also noted in weakly peralkaline syenites from the Agua de Pau
587 volcano, São Miguel, Azores Islands, by Ridolfi et al. (2003). Carlier and Lorand (2008) recorded
588 perrierite crystallizing alongside sanidine and tridymite as late-magmatic phases in kersantites of
589 the Oroscocha volcano; formation conditions were estimated at 950 °C and oxygen fugacity at
590 FMQ +5 log units. The chevkinite-(Ce) shown in Fig. 12c grew along boundaries between alkali
591 feldspar crystals in the Ełk syenite, NE Poland. Hezuolinite forms a late magmatic mineral, in
592 association with titanite, loparite-(Ce) and britholite-(Ce)? in lujavrite from Saima (Wu et al.
593 2016). A further form of late magmatic crystallization is in mesostases and interstices, for
594 example in tholeiitic intrusions (Melluso et al. 2014; Muhling et al. 2014). de Hoog and Van
595 Bergen (2000) described perrierite-(Ce) growing in the groundmass of a potassic trachyandesite
596 from the Lewotolo volcano, Indonesia. Chevkinite found as microlites in groundmass glass from
597 high-silica vitrophyres from the Yellowstone caldera, Wyoming, must also represent late
598 magmatic crystallization (Vasquez et al. 2009).

599

600 **Carbonatites and associated hydrothermal metasomatic rocks**

601 Chevkinite-group minerals are perhaps uncommon components of carbonatite bodies. For
602 example, Berger et al. (2009) recorded chevkinite as occurring in only four out of 58 Nb- and
603 REE-bearing carbonatite deposits. Chevkinite-(Ce) was reported in carbonatite of the Bayan Obo
604 Nb-REE-Fe deposit by Shimazaki et al. (2008b; Smith et al. 2016), associated with tremolite-
605 richterite, barite, monazite-(Ce), bastnäsite-(Ce), fluorbritholite-(Ce), gadolinite-(Ce), FeTi-
606 oxides and sulphides. Chevkinite also occurs in a sövite dyke in the Maoniuping REE deposit,
607 China (Wang et al. 2001; Xu et al. 2008). Shen et al. (2005, p. 216) suggested that the type
608 maoniupingite-(Ce), which occurs in carbonatitic veins and pegmatites at Maoniuping, "directly
609 crystallized from a type of F-, water- and REE-rich mineralizing fluids during the transitional
610 stages of magmatic-hydrothermal processes". Viladkar et al. (2009) reported that chevkinite-(Ce)
611 is the only REE-bearing accessory mineral in carbonatites of the Samchampi massif, suggesting
612 that it formed by hydrothermal alteration of ilmenite or magnetite in the late stages of carbonatite
613 formation. Perrierite-(Ce) occurs concentrated at the endocontact between a carbonatite dyke and
614 host melanephelinite in the Danadai alkaline complex, Rajasthan, India (Macdonald et al. 2009).
615 A Nb-rich chevkinite has been found in a carbonate vein in the Biraya Fe-REE deposit by Mills
616 et al. (2012) and Stachowicz et al. (in revision a, b). Makagonov and Muftakhov (2016) reported
617 perrierite-(Ce) in apatite-albite-phlogopite-calcite veins of the the Vishnevogorsky complex,
618 suggesting that they characterized the silicate-to-carbonatite transition in the complex. Strontium-
619 Zr-rich perrierite was found in apatite veins in the Mushgai-Khuduk carbonatite complex,
620 Mongolia, by Andreev and Ripp (1995).

The type strontiochevkinite, from a rheomorphic fenite associated with carbonatites at Cerro Sarambi, Paraguay, is estimated by Haggerty and Mariano (1983) to have formed at a depth of ~5 km at high fO_2 (much greater than MH) and at T ~500-550 °C.

Albitites occur in several forms, including large concordant bodies, discordant pegmatites and dykes, and albite breccias, and are formed by several mechanisms, such as Na-metasomatism of granitic rocks, partial melting of amphibolites, and liquid immiscibility from gabbroic magma. Proshchenko (1967) reported "chevkinite-(La)" in albitites from eastern Siberia. It would be valuable to restudy this material, to determine whether the La dominance is a function of the paragenesis. Monchoux et al. (2006) recorded chevkinite-(Ce) in igneous albitite dykes intruding lherzolite in the western Pyrenees, France, in association with albite, muscovite, biotite, chlorite, epidote, zircon, titanite, thorite, pyrochlore, aeschynite-(Ce), ferrocolumbite, rutile, ilmenite, magnetite, allanite-(Ce), apatite and monazite-(Ce). The albitites are thought to have been formed by very low-degree (<1%) partial melting of a shallow mantle, harzburgitic, source previously enriched by carbonate-related metasomatism (Pin et al. 2006).

Pegmatites, quartzolites and miarolitic cavities

Included in this category are parageneses where a significant fluid phase coexisted with melt.

Pegmatites. Pegmatites are a common host of CGM, with some impressive occurrences (Fig. 12d). Rajesh (2003), for example, noted CGM crystals up to 0.1 m long in pegmatites associated with the Puttetti syenite, India. CGM-bearing pegmatites are generally, but not invariably, associated with syenitic and granitic intrusions, and can be of both metaluminous (Semenov et al. 1966; Mitchell et al. 1976; Miyazaki and Santosh 2005; Prol-Ledesma et al. 2012) and alkaline or peralkaline (Segelstad and Larsen 1978; Čech et al. 1988; Chakhmouradian and Mitchell 1999; Macdonald et al. 2015b) affinity.

Miarolitic cavities. Parodi et al. (1994) described perrierite-Ce) occurring in association with titanite, zircon and baddeleyite on the walls of miarolitic cavities in an ejected syenite block in the Sabatini complex, Latium, Italy, linking its origin to the late pneumatolitic-pegmatitic stages of the regional volcanic activity (Fig. 12e). Della Ventura et al. (2001) reported perrierite-(Ce) in miarolitic cavities in a syenite block from the Roccamonfina volcano, Latium, which they related to late metasomatic stages. Chevkinite occurs in miarolitic cavities in the Kuiqi peralkaline granite, SE China, associated with *inter alia* apatite, allanite, zircon, titanite, xenotime and pyrochlore (Martin et al. 1994). The type perrierite-(La) occurs in miarolitic cavities in lava in the Eifel, in association with sanidine, phlogopite, pyrophanite, zirconolite, members of the jacobsite-magnetite series, zircon and fluorcalciopyrochlore (Chukanov et al. 2012a).

Quartzolites ("silexites" in the Russian literature) are rocks composed primarily of quartz (>60 vol%) and with quartz:feldspar ratios ≥9:1 (Bel'kov et al. 1988; Zozulya and Eby 2010; Macdonald et al. 2017b). They are transitional between higher-temperature orthomagmatic granites and fluid-magmatic rocks, such as pegmatites, and mesothermal hydrothermal rocks. Significant amounts of fluorite and other F- or OH-bearing minerals indicate the active involvement of fluids in their formation. In the Western Keivy massif quartzolites commonly host rare metals, such as the Purnach (Bel'kov and Batieva 1991), Pessarjok (Macdonald et al. 2012) and Rovozero (Macdonald et al. 2012; Lyalina et al. 2014) occurrences. In the Keivy quartzolites, zircon is the main mineral in the ore assemblages, accompanied by various combinations of aeschynite-(Y), chevkinite-(Ce), fergusonite-(Y), britholite-group minerals, yttrialite-(Y), thorite, monazite-(Ce), xenotime-(Y) and bastnäsite-(Ce) (Fig. 12f).

Metamorphic rocks

668 Chevkinite-group minerals have been recorded in several high-grade metamorphic occurrences
669 (gneisses and associated pegmatites), e.g. Archean charnockitic gneisses in the West Hoggar,
670 Algeria (Acef et al. 2001), from various localities in Antarctica (Atrashenok et al. 1967; Grew
671 and Manton 1979a, 1979b; De Paolo et al. 1982; Harley 1994; Hokada 2007; Belkin et al. 2009;
672 Fig.13a), and the Eastern Ghats Province, India (Grew and Manton 1986; Belkin et al. 2009;
673 Fig.13b). Čech et al. (1988) reported chevkinite-(Ce) in a pegmatite associated with a pre-Upper
674 Proterozoic peralkaline quartzo-feldspathic gneiss at Mbolwe Hill, Zambia. CGM-bearing
675 pegmatites are known from the largely granulitic gneiss terrain of the Purulia district, West
676 Bengal, India (Baidya 1992).
677 Temperatures and pressures of 1000-1180 °C and 3-4 kbar have been estimated for the
678 formation of perrierite in a partially melted sapphirine granulite xenolith from the Vestfold Hills,
679 Antarctica (Harley 1994; Harley and Christy 1995), and temperatures up to 1100 °C in granulites
680 of the Archean Napier Complex, Antarctica (Harley 2008). The high Al content of the perrierite
681 (≤9 wt%; Supplementary Table 2b) has been attributed to the high pressures of crystallization.
682 This is consistent with experimental evidence; in CGM crystallized from a series of REE-
683 enriched compositions ranging from basalt through andesite to rhyolite at pressures from 7.5 to
684 20 kbar and temperatures from 900-1050 °C, the Al content of the CGM increased with
685 increasing pressure (Green and Pearson 1988) (Fig. 10).
686 The type examples of the rare minerals, rengeite and matsubaraite (Fig. 13c), occur in jadeitite
687 in the high P/T type Renge belt, Itoigawa-Ohmi-district, Japan (Miyajima et al. 2001, 2002). The
688 belt (330-280 Ma) was metamorphosed under glaucophane-schist to epidote-amphibolite facies
689 conditions. Chevkinite-(Ce) and perrierite-(La) occur in different layers of Proterozoic
690 metacarbonate rocks at Golden Lake, Ontario (Macdonald et al. 2009) (Fig. 13d). No study has
691 yet examined the factors stabilising the different phases.

692 So far as we know, CGM has not yet been recorded in a low-grade metamorphic rock
693 although, given their occurrence in hydrothermal and ore deposits, such parageneses cannot be
694 precluded. Neither has a CGM been reported growing in a low-temperature sedimentary
695 environment.
696 A potentially rewarding study would be the role of CGM in influencing REE and HFSE
697 behaviour during partial melting of crustal rocks. Hokada (2007), for example, suggested that the
698 conditions for the formation of perrierite in an ultrahigh temperature (UHT) sapphirine-quartz
699 gneiss from East Antarctica might have been achieved by the generation of an anatectic melt,
700 leaving the LREE and Ti, incorporated into the perrierite, behind in the solid rock. Another
701 natural laboratory for such studies might be a migmatite suite where the products of partial
702 melting and their subsequent evolution can be recognised. For example, Johnson et al. (2003)
703 have inferred a genetic connection between migmatites, leucosomes, dykes and peraluminous
704 granites in the Proterozoic Dalradian rocks of NE Scotland, but no study has been made of the
705 accessory minerals from this rock suite, and how their assemblages and compositions varied as
706 the inferred melting proceeded.
707
708 **Skarns**
709 Chevkinite-group minerals occur in calc-skarns of eastern Tuva and eastern Siberia, where
710 they formed in fissures in association with pyrochlore, fergusonite, fluorite, phenakite,
711 meliphanite and zircon (Kudrin et al. 1967). Ontoyev (1993) described, from the Bayan Obo rare-
712 earth deposit, CGM in humite and humite-clinohumite skarns formed at or close to the contacts
713 between dolomites and syenitic rocks. Associated minerals are humite, clinohumite, spinel,
714 periclase, phlogopite, allanite, fluorite and titanomagnetite. The skarns are thought to have

715 formed at temperatures >500 °C. The type dingdaohengite-(Ce) was first recognised in
716 magnesian skarns at Bayan Obo (Xu et al. 2008).
717 Chevkinite-group minerals can also form by recrystallization of primary CGM by interaction
718 with metasomatic fluids. Macdonald et al. (2015d), for example, described, in a quartz-epidote
719 metasomatite from the Khaldzan Buregtey massif, Mongolian Altai, prismatic chevkinite-(Ce)
720 crystals up to 8 x 1.5 cm in size which had grown by recrystallization and enlargement of the
721 same mineral in the precursor pegmatite where it never exceeded 1 mm in size.
722 The range of occurrences testifies to the ability of CGM to form under very diverse, relatively
723 low temperature conditions, with different fluid compositions, and in a multitude of parageneses.
724 Quantifying the variables active during their formation will undoubtedly be difficult: REE-
725 bearing deposits can be formed in several stages, with changes in temperature and fluid
726 composition(s) and under disequilibrium conditions.
727

728 **HYDROTHERMAL ALTERATION OF CGM**

729 The presence of even moderate concentrations of actinides makes the CGM prone to
730 metamictization (e.g., <0.5 wt% ThO_2; Sokolova et al. 2004). The structural damage in turn
731 promotes entry of water into the structure; thus in common with other accessory minerals, such as
732 apatite, monazite and xenotime, CGM can be susceptible to alteration by magmatic and/or
733 hydrothermal fluids. Studies of the hydrothermal alteration of CGM go back at least as far as that
734 of Lacroix (1915), and were then pursued chiefly by Russian workers, such as Mineev et al.
735 (1962), Marchenko et al. (1968) and Rozanov et al. (1983). We discuss here only more recent
736 work where microanalytical techniques have allowed a more complete characterization of the
737 phases involved in the alteration.

738 Three general replacement schemes can be recognised: (1) compositional modification of the
739 CGM produced a zone of "altered chevkinite" (Jiang 2006; Vlach and Gualda 2007; Bagiński et
740 al. 2015); (2) formation of this zone was followed by the development of a new mineral
741 assemblage (Jiang 2006; Macdonald et al. 2015b, 2015c); and (3) alteration proceeded directly to
742 the formation of a new assemblage (Macdonald et al. 2015d; Bagiński et al. 2016). The examples
743 provided below were chosen to describe the three schemes and to show the effects of different
744 ligands on the alteration products.
745
746 **"Altered chevkinite"**
747 Bagiński et al. (2015) described the alteration of chevkinite-(Ce) in quartzolite from the Keivy
748 massif, where the mineral was replaced by a presumably amorphous phase which, lacking
749 structural information, they simply termed altered chevkinite, after the usage by Jiang (2006) and
750 Vlach and Gualda (2007). In places, the altered material is present as rims on the unaltered CGM,
751 or developed along fractures (Fig. 14a). Elsewhere, the alteration proceeded to a very complex
752 mixture of unidentified phases of different BSE brightness, occurring as amoeboid patches and
753 fibres (Bagiński et al. 2015). No structural data exist for these phases. The compositional
754 modification of the CGM during alteration is described below.
755
756 **Alteration of CGM with formation of new phases**
757 In some cases, the formation of altered chevkinite was followed by the formation of a different
758 phase assemblage. This progression presumably reflected the continuity of fluid input and the
759 aggressivity of the fluid (essentially its temperature and content of ligands).
760 In a study of hydrothermally altered chevkinite-(Ce) in syenites of the Shuiquangou intrusion,
761 China, Jiang (2006) found that the chevkinite was replaced by an allanite-ilmenite association in

762 the inner part of a corona texture, either directly or *via* a thin zone of altered chevkinite. This was
763 in turn mantled by a ring of allanite, titanite and ilmenite and then by a distal rim of epidote. A
764 detailed description of element redistribution during replacement was given. Jiang (2006) did not
765 specify the composition of the fluid but from the nature of the alteration assemblage it apparently
766 had low F and CO_2 contents. Hydrothermal alteration of CGM to allanite and titanite was also
767 recorded by Savel'eva and Karmanov (2008, 2010), Hirtopanu et al. (2013) and Papoutsa and Pe-
768 Piper (2013).

769 A broadly similar replacement sequence to that in Jiang (2006) was reported by Macdonald et
770 al. (2015c) in chevkinite-(Ce) from a quartz-epidote metasomatite from the Keivy massif. In this
771 case, the allanite zone comprises ferriallanite-(Ce) and davidite-(La), rimmed by a zone of
772 allanite-(Ce) richer than the ferriallanite-(Ce) in the epidote component, and there is no ilmenite
773 in the titanite-rutile mantle (Fig. 14b). Rare-earth carbonates, aeschynite-(Ce) and aeschynite-(Y)
774 were accessory minerals in all the alteration zones. The hydrothermal fluids were inferred to have
775 had high Ca activities and significant contents of F and CO_2. Li and Zhou (2017) have also
776 recorded replacement of chevkinite-(Ce) by allanite-(Ce) and aeschynite-(Ce) from the Sin
777 Quyen deposit.

778 A complex alteration sequence was described in a syenitic pegmatite from the Vishnevye
779 Mountains by Macdonald et al. (2015b). The chevkinite-(Ce) was altered, *via* a series of
780 texturally complex intermediate steps, to a bastnäsite-(Ce)-ilmenite-columbite-(Fe) assemblage
781 (Fig. 14c). The intermediate stages involved partial replacement and formation of symplectite
782 texture. An approach to equilibrium was achieved only during the final stages of alteration. The
783 hydrothermal fluids were inferred to have been F- and CO_2-rich, with variable levels of Ca
784 activity.

Ignoring the complexities of the intermediate stages, the *critical* reaction in the alteration of the chevkinite-(Ce) was given as:

$$2[Ce_{3.5}Ca_{0.5})_{\Sigma 4}Fe(Fe_{1.5}Ti_{0.5})_{\Sigma 2}Ti_2(Si_2O_7)_2O_8] + 8CO_2 + 7F^- = 7CeCO_3F + 5FeTiO_3 + 8SiO_2 + CaCO_3 + 5O^{2-}$$

chevkinite-(Ce) bastnäsite ilmenite quartz

Li and Zhou (2017) described replacement of chevkinite-(Ce) by allanite-(Ce) + aeschynite-(Ce) ± bastnäsite-(Ce) ± columbite-(Fe) ± ilmenite at Sin Quyen.

Alteration directly to new phases

A quartz-epidote metasomatite from the Khaldzan Buregtey massif is an example of alteration of a CGM proceeding directly to new phases (Fig. 14d) (Macdonald et al. 2015d). A peralkaline granite pegmatite was metasomatized by hydrothermal fluids, where minerals in the pegmatite, including chevkinite-(Ce), fergusonite-(Y) and epidote supergroup minerals, were recrystallized and texturally coarsened at temperatures in the range 318-446 °C. An influx of low-temperature fluids (156-160 °C) resulted, *inter alia*, in the replacement of chevkinite-(Ce) by titanite-cerite-(Ce)-REE carbonate assemblages. The hydrous fluids were interpreted to have been acidic and oxidizing, with significant amounts of CO_2 but poor in F and Cl.

Many other replacement schemes undoubtedly exist. Kartashov (1994; reaction 3), for example, proposed a reaction involving high Ca and CO_2 activities for altered chevkinite from the Khaldzan Buregtey massif:

$$Ce_4Fe(Fe,Ti)_2Ti_2Si_4O_{22} + Fe^{2+} + 4Ca^{2+} + 8CO_3^{2-} + 2H_2O \rightarrow 4CaCe(CO_3)_2(OH) + 3FeTiO_3 + 4SiO_2$$

chevkinite REE carbonate ilmenite quartz

As further examples, Mitchell et al. (1976) described perrierite with alteration crusts of halloysite, monazite and anatase in a granitic pegmatite from Bedford County, Virginia, and Prol-Ledesma et al. (2012) reported replacement of perrierite-(Ce) by a symplectitic intergrowth of allanite-(Ce) + titanite + thorite in the El Muerto granitic pegmatite. Vasyukova and Williams-

Jones (2016) reported, in an inclusion in granite from the Strange Lake pluton, chevkinite-(Ce) being locally replaced by karnasurtite-(Ce) [$(Ce,La,Th)(Ti,Nb)(Al,Fe^{3+})(Si,P)_2O_7(OH)_4.3H_2O$] or, in some cases, by an intergrowth of bastnäsite-(Ce), fluorite and a Na-deficient variety of gagarinite-(Y) [$Na(REE_xCa_{1-x})(REE_yCa_{1-y})F_6$].

Important studies remain to be made of the controls of the different replacement sequences. In considering the difference between columbite-bearing and columbite-free sequences, Macdonald et al. (2015b) suggested that columbite has low solubility in CO_2-rich fluids, resulting in two potential assemblages:

(i) ilmenite + titanite + rutile + (Nb,REE)-oxides = low $X(CO_2)$ and higher Ca

(ii) ilmenite + columbite + REE-carbonate = high $X(CO_2)$ and lower Ca

The examples above show that the alteration products of CGM are dependent on the compositions of the host rock and CGM, the pressure and temperature and the composition of the fluids, in particular, the activities of Ca, F and CO_2. Studies of the fluids are, however, hampered by their loss from the system and by the fact that they may change composition as alteration proceeds. In the case of the CGM, difficulties in interpreting the record of the passage of fluids through the rocks are exacerbated by the lack of any experimental information on CGM-fluid interactions, in contrast, for example, to monazite (Harlov and Hetherington 2010; Budzyń et al. 2011; Harlov et al. 2011; Harlov 2015).

Compositional modifications during hydrothermal alteration to altered chevkinite

Bagiński et al. (2015) outlined some of the compositional changes occurring in CGM during interaction with hydrothermal fluids. Initial alteration generally results in Ca enrichment, but with increasing degrees of alteration, Ca abundances fall, as do those of the REE, Fe and Si. Levels of Ti increase strongly, with less marked enrichment in Nb ± Th. Oxide totals of the altered phase

835 are very low (sometimes <90 wt%) and cation totals are not stoichiometric. As a measure of the
836 degree of alteration, the parameter Ti* was introduced by Bagiński et al. (2015), defined as (total
837 Ti apfu – 2), i.e. a measure of the Ti excess over that filling the D site. Figure 15 shows the
838 variation of Ti* and Ca in CGM from various suites. The data generally follow a looped
839 distribution, somewhat arbitrarily divided in the inset into unaltered, partly altered and strongly
840 altered segments.

841 The overall compositional variations during alteration in many ways mirror in the initial stages
842 those produced by magmatic crystallization and, as in that process, the trend may cross the
843 empirical boundary between the chevkinite and perrierite subgroups, but this time from
844 chevkinite to perrierite (Vlach and Gualda 2007) (Fig. 16). For comparison, perrierite from
845 apatite-albite-phlogopite-calcite veins in the Vishnevogorsky complex also became more calcic
846 with increasing hydration (Makagonov and Muftakhov 2016). Are there ways of telling whether
847 compositional zonation in a given CGM results from hydrothermal alteration rather than
848 crystallization? Using A-type syenites and granites of the Graciosa Province, Brazil, Vlach and
849 Gualda (2007) noted that magmatic chevkinites followed (quasi-)horizontal trends on a Th-Ti
850 plot, whereas altered CGM followed positive trends. Furthermore, as noted above progressive
851 alteration is almost always accompanied by a decrease in oxide totals and increasingly non-
852 stoichiometric structural formulae.

853 Payette and Martin (1988) gave a description of the alteration of chevkinite-(Ce) in alkali
854 granites of the Welsford igneous complex, New Brunswick, Canada. They reported altered
855 "chevkinite" with remarkable levels of Ti enrichment (up to 7.17 apfu; 50.6 wt% TiO_2).
856 Compared to other altered occurrences, the chevkinite shows strong Ca depletion starting from
857 Ti* values of 1 (Fig. 15). This occurrence would undoubtedly repay a detailed study of the
858 structural, textural and compositional changes during the alteration process(es).

PETROGENETIC SIGNIFICANCE

Geochemical modelling

Chevknite-group minerals occurring as phenocrysts or as inclusions in early-crystallised minerals in plutonic rocks may strongly influence trace element distribution during fractional crystallization of intermediate to felsic magmas. In several igneous rock suites, for example, CGM have been the dominant control over LREE distribution (Vlach and Gualda 2007; Hokada 2007; Viladkar et al. 2009; Macdonald et al. 2013; Padilla and Gualda 2016). As an indication of its fractionation potential, Troll et al. (2003) calculated that crystallization of 0.05 wt% chevkinite from a peralkaline rhyolite (comendite) magma with 300 ppm Ce would produce 207 ppm in the residual melt. The CGM may also play an important role in controlling trace element behaviour during partial melting of crustal rocks; where refractory, they could retain such elements in the restite (Green and Pearson 1988; Hokada 2007).

Testing of geochemical models requires a detailed knowledge of the partitioning of trace elements between CGM and host melts. The most complete information on the partitioning of REE between CGM and coexisting melts comes from high-silica rhyolites, including comendites from the Olkaria complex, Kenya (Macdonald et al. 2002; Marshall et al. 2009), Gran Canaria (Troll et al. 2003), and from the metaluminous Peach Spring Tuff (Padilla and Gualda 2016). All three data sets show strong partitioning of the LREE into chevkinite-(Ce), with apparent partition coefficients for La and Ce exceeding 1000 (Fig. 19; Table 5). Chevkinite-(Ce) also concentrates the HREE, although less strongly. In all cases, Ce/Ce* values in chevkinite-(Ce) microphenocrysts are closely similar to those in matrix glass, indicating that CGM crystallization does not significantly affect the size of the Ce anomaly. Similarly, Eu anomalies are fairly comparable in CGM and coexisting glasses and are not affected by CGM crystallization. There is a similar situation in the metaluminous Peach Springs Tuff rhyolite.

884 Although the partition coefficients are for chevkinite-(Ce) in a compositionally rather similar
885 set of rocks (high-silica rhyolites), there are some important inter-rock differences. For example,
886 two samples have steep decreases at Eu, two do not (Fig. 17). The apparent partition coefficient
887 for Sr in the Gran Canaria chevkinite-(Ce) (84) greatly exceeds those in Olkaria (≤27). Such
888 differences may be related in part to the crystallization of other accessory minerals, such as
889 allanite or titanite. In their study of chevkinite-(Ce) and titanite microphenocrysts in a Gran
890 Canaria ignimbrite, for example, Troll et al. (2003) found that (i) the chevkinite-(Ce) was
891 enriched in LREE by some three orders of magnitude above that of the glass matrix, whereas
892 titanite was enriched by only 1.5 orders of magnitude; (ii) the titanite, but not the chevkinite-(Ce),
893 showed minima at La and Eu on chondrite-normalised REE plots; and (iii) the titanite was more
894 sensitive to melt composition than the chevkinite-(Ce). They concluded that chevkinite, where
895 present, might be the controlling REE-bearing phase in peralkaline rhyolitic magmas. Padilla and
896 Gualda (2016) found, in the metaluminous Peach Spring Tuff, that whereas chevkinite-(Ce)
897 concentrated the LREE more efficiently than other minerals, titanite had a significant preference
898 for the REE between Sm and Ho.
899 These studies have clearly shown that, to be most valuable, partition coefficients should be
900 determined for individual suites and that any accessory cannot be treated in isolation from any
901 coexisting phases. A potentially rewarding way forward is *via* detailed examination of multi-
902 phase accessory assemblages in volcanic rocks (Padilla and Gualda 2016). For example, many
903 Cenozoic latite to rhyolite eruptive sequences of Nevada, USA, have microphenocryst
904 assemblages containing various proportions of titanite, allanite, perrierite, apatite, zircon and
905 monazite (Broxton et al. 1989; Warren et al. 1989). In the example shown in Fig. 18, from the
906 Devine Canyon Tuff, Oregon, four accessory phases (CGM, REE-Si-bearing apatite, zircon and
907 ilmenite) were incorporated into a growing clinopyroxene, with the enclosing glass acting as a

guide to the melt composition. By documenting specific textural relationships, such assemblages provide an excellent opportunity to distinguish the effects of melt composition, temperature and fO_2 on mineral stabilities and to track the partitioning of elements into the accessory phases.

The relationships between CGM and other REE-bearing accessory phases

It is important to understand as fully as possible the relationships between the CGM and other accessory minerals coexisting in the same rocks. During equilibrium or near-equilibrium crystallization, the first major REE phase to appear may preclude or have a tendency to limit the abundance of the other competing phase(s). Such relationships will determine *inter alia* trace element fractionation paths in residual melts and our ability to decipher P-T-fO_2 conditions during magma crystallization. Determining the stability relationships between CGM and coexisting accessory minerals may, however, be extremely difficult due to the textural complexities and ambiguities and to the non-equilibrium conditions under which the minerals often form. In this section, some aspects of the relationships between CGM and two REE-bearing phases, allanite and monazite, in igneous suites are described.

Reconnaissance experiments by Vasquez et al. (2004) showed that allanite saturation in high-silica rhyolites occurred at 760-770 °C, whereas at 780 °C, chevkinite replaced allanite. This is consistent with textural evidence of allanite mantling chevkinite in granites from the Aztec Wash Pluton, Nevada (Robinson and Miller 1999), UK Paleogene granites (Macdonald et al. 2013), and the Lucerne intrusion, Maine, USA (Fig. 19a). Prol-Ledemsa et al. (2012) reported perrierite-(Ce) inclusions up to 5 cm across occurring in allanite in the wall zone and first intermediate zone of the El Muerto granitic pegmatite. Vlach and Gualda (2007) showed that in the A-type granites of the Graciosa Province, Brazil,

chevkinite-(Ce) is the main REE phase in metaluminous syenites, alkali-feldspar syenites and peralkaline alkali-feldspar granites of the alkaline association, while allanite-(Ce) is the main REE phase in the aluminous association.

In cooling silicate liquids, monazite is the only common accessory phase with a REE abundance similar to CGM. Monazite solubility increases with increasing peralkalinity (Montel 1986, 1993) and decreases with increasing alumina saturation index (Rapp et aI. 1987). In contrast, we know of no record of a CGM in a peraluminous granite. This may suggest that CGM are favored in metaluminous and peralkaline melts *vs* peraluminous melts.

Monazite and CGM do seem to be able to coexist, apparently in, or close to, equilibrium. Hokada (2007) recorded perrierite and monazite in sapphirine-quartz gneiss from the Napier Complex, East Antarctica, noting that the perrierite is the dominant phase. Monazite and CGM coexist in the Boso and Noto volcanics (Miyawaki et al., 2012). Liu et al. (2015) reported subhedral monazite-(Ce) and chevkinite in a lithic clast in a Martian breccia meteorite. In a quartzolite from the Rova occurrence, Keivy massif, Macdonald et al. (2017b) found that chevkinite-(Ce) and monazite-(Ce) formed part of the primary crystallizing assemblage, in association with fergusonite-(Y) and zircon (Fig. 19b). Li and Zhou (2017, 2018) reported that monazite-(Ce) and chevkinite-(Ce) formed together from high-temperature fluids, and were subsequently mantled by allanite (Fig. 19c), in the early ore-forming stage at Sin Quyen. Monazite crystallization post-dating that of CGM is recorded in a perrierite-(Ce) in plagioclase, with late monazite-(Ce) on the CGM rims, Cañada Pinabete granite, Questa complex, New Mexico (Fig. 19d).

Thus, while it appears that the relationship between CGM and allanite is generally determined by melt composition and temperature, that between CGM and monazite is more complex, especially in the low-temperature regime where fluid composition and availability

become important factors.

Geochronology

Several studies have demonstrated the usefulness of CGM in geochronology in rocks ranging from Archean to Recent. Using U-Th-Pb elemental ratios, Hokada (2007) found a chemical age of 2460 ± 110 Ma for perrierite from a sapphirine gneiss of the Napier Complex. *In situ* SHRIMP (Sensitive High Resolution Ion Micro Probe) U-Pb methods were employed by Rasmussen et al. (2014) to date CGM from a tholeiitic sill of the Eel Creek Formation, Western Australia (~1.07 Ga), but high common Pb contents resulted in an unreliable date. Min et al. (2006) used the (U-Th)/He method to date (1.62 ± 0.11 Ma) volcanic phenocrysts with chevkinite and britholite inclusions, in the Jemez Volcanic Field, New Mexico. Vasquez et al. (2014) reported ^{238}U-^{230}Th dating of chevkinite in rhyolites from La Primavera, Mexico (125-85 ka) and Yellowstone (110-250 ka) calderas. A potentially useful project would be to use CGM altered by interaction with hydrothermal fluids to date the alteration event but, so far as we know, no such study has yet been published.

CGM and magma mixing

Given the ubiquity of magma mixing in the evolution of igneous suites, an interesting question is whether the CGM have been used to identify the process. The accessory mineral assemblage titanite, perrierite, zirconolite and baddeleyite was reported as late magmatic phases in kersantites of the Oroscocha volcano by Carlier and Lorand (2008). The assemblage formed under low water pressure and high fO_2 (FMQ+5), the strongly oxidizing conditions having been promoted by magma mixing between lamprophyric and felsic end-members. Macdonald et al. (2013a) ascribed reverse zoning and resorbed textures in chevkinite-(Ce) to possible magma mixing in A-type

granites of the UK Paleogene province but did not present robust evidence as to the nature of the mixing components.

Implications

The review has attempted to show that the CGM are a widespread and important group of accessory minerals, capable of incorporating a wide range of elements over a considerable P-T range. Much progress has been made in recent years in understanding critical aspects of the group's formation and post-formation histories but much remains to be done. We have noted throughout the text topics which we feel would be particularly valuable areas of research, such as gaining further insights into the allocation of cations between structural sites, quantifying by experiment the stability relationships between CGM and other REE-bearing accessory minerals, studies of hydrothermal alteration processes and the remobilization and transport of rare-metals, and understanding the role(s) of CGM in crystal fractionation and crustal anatexis.

ACKNOWLEDGMENTS

We thank Fernando Camara, Pavel Kartashov, Silvio Vlach, Mark Welch and Dmitry Zozulya for educating us in many aspects of CGM: we gratefully acknowledge their insights and expertise. Anton Chakhmouradian and Janet Muhling provided very detailed and helpful reviews of the manuscript. We also thank Dan Harlov for editorial handling and him and Keith Putirka for encouraging us to prepare this review.

REFERENCES CITED

Acef, K., Ouzegane, K., and Kienast, J.R. (2001) Archean alkaline charnockitic gneisses in the In Ouzzal granulitic unit, West Hoggar, Algeria. Special Abstract Issue, EUG XI. Strasbourg, France, 571.

Andreev, G.V. and Ripp, G.S. (1995) About perrierite found in apatite ore. Proceedings of the Russian Mineralogical Society, 124, 83-84 (in Russian).

Atrashenok, L.Ya., Avdzeyko, G.V., Klimov, A.V., Krylov, A.Ya., and Silin, Yu.I. (1967) Comparative data on absolute ages of Antarctic rocks (lead and argon methods). Pp. 227-229 in: Questions of the dating of the most ancient (Katarchean) geological formations and of basic rocks. Izdatelstvo Nauka, Moscow (in Russian).

Azambre, B., Rossy, M., and Lago, M. (1987) Caractéristiques pétrologiques des dolérites tholéiitiques d'âge triasique (ophites) du domaine pyrénéen. Bulletin de Minéralogie, 110, 379-396.

Bagiński, B. and Macdonald, R. (2013) The chevkinite group: underestimated accessory phase from a wide range of parageneses. Mineralogia, 44 (2-3). Doi: 10.2478/mipo-2013-0006.

Bagiński, B., Macdonald, R., Dzierżanowski, P., Zozulya, D., and Kartashov, P.M. (2015) Hydrothermal alteration of chevkinite-group minerals: products and mechanisms. Part 1. Hydration of chevkinite-(Ce). Mineralogical Magazine, 79, 1019-1037.

Bagiński, B., Zozulya, D., Macdonald, R., Kartashov, P.M., and Dzierżanowski, P. (2016) Low-temperature hydrothermal alteration of a rare-metal rich quartz-epidote metasomatite from the El'ozero deposit, Kola Peninsula, Russia. European Journal of Mineralogy, 28, 789-810.

Baidya, T.K. (1992) A note on some uranium-thorium bearing pegmatoids of Nawahatu area, Purulia district, West Bengal. Indian Minerals, 46, 175-176.

Belkin, H.E., Macdonald, R., and Grew, E.S. (2009) Chevkinite-group minerals from granulite-facies metamorphic rocks and associated pegmatites of East Antarctica and South India. Mineralogical Magazine, 73, 149-164.

Bel'kov, I.V., and Batieva, I.D. (1991) New data on rare-metal mineralogy of silexites

1029 stock within the Purnach alkali granite pluton. In: New Data on Mineralogy of Rare
1030 Elements in Kola Peninsula. Apatity: Kola Science Center, USSR Academy of
1031 Sciences, pp. 15-19 (in Russian).
1032 Bel'kov, I.V., Batieva, I.D.,Vinogradova, G.V. and Vinogradov, A.N. (1988) Mineralization and
1033 fluid regime in the contact zones of alkali granite intrusions. Kola Branch, USSR, Academy of
1034 Sciences, Apatity, pp. 110 (in Russian).
1035 Berger, V.I., Singer, D.A., and Orris, G.J. (2009) Carbonatites of the world, explored
1036 deposits of Nb and REE – database and grade and tonnage models. U.S. Geological
1037 Survey Open-File Report 2009-1139, 17 pp.
1038 Bindeman, I.N., and Valley, J.W. (2003) Rapid generation of both high- and low-$\delta^{18}O$,
1039 large-volume silicic magmas at the Timber Mountain/Oasis Valley caldera complex,
1040 Nevada. Geological Society of America Bulletin, 115, 581-595.
1041 Broxton, D.E., Warren, R.G., Byers, F.M., and Scott, R.B. (1989) Chemical and
1042 mineralogical trends within the Timber Mountain-Oasis Valley caldera complex,
1043 Nevada: evidence for multiple cycles of chemical evolution in a long-lived silicic
1044 magma system. Journal of Geophysical Research, 94, 5961-5985.
1045 Budding, K.E., Cunningham, C.G., Zielinski, R.A., Steven, T.A., and Stern, C.R. (1987)
1046 Petrology and chemistry of the Joe Lott Tuff Member of the Mount Belknap volcanics,
1047 Marysvale volcanic field, west-central Utah. U.S. Geological Survey Professional Paper,
1048 1354, 47 pp.
1049 Budzyń, B., Harlov, D.E., Williams, M.L., and Jercinovic, M.J. (2011) Experimental
1050 determination of stability relations between monazite, fluorapatite, allanite, and REE-
1051 epidote as a function of pressure, temperature, and fluid composition. American
1052 Mineralogist, 96, 1547-1567.

Calvo, C., and Faggiani, R. (1974) A re-investigation of the crystal structures of chevkinite and perrierite. American Mineralogist, 59, 1277-1285.

Cameron, K.L., and Cameron, M. (1986) Whole-rock/groundmass differentiation trends of rare earth elements in high-silica rhyolites. Geochimica et Cosmochimica Acta, 50, 759-769.

Carlier, G., and Lorand, J.-P. (2008) Zr-rich accessory minerals (titanite, perrierite, zirconolite, baddeleyite) record strong oxidation associated with magma mixing in the south Peruvian potassic province. Lithos, 104, 54-70.

Čech, F., Povondra, P., and Vrána, S. (1988) Crystal chemistry of chevkinite from Zambia. Acta Universitatis Carolinae: Geologica, No. 2, 181-193.

Cellai, D., Conticelli, S., and Diella, V. (1993) Perrierite-chevkinite in igneous ultrapotassic rocks from Central Italy: chemical data and their petrological significance. Periodico di Mineralogia, 62, 57-66.

Chakhmouradian, A.R., and Mitchell, R.H. (1999). Primary, agpaitic and deuteric stages in the evolution of accessory Sr, REE, Ba and Nb-mineralization in nepheline-syenite pegmatites at Pegmatite Peak, Bearpaw Mountains, Montana. Mineralogy and Petrology, 67, 85-110.

Chukanov, N.V., Blass, G., Pekov, I.V., Belakovskiy, D.I., Van, K.V., Rastsvetaeva, R.K., and Aksenov, S.M. (2012a) Perrierite-(La), $(La,Ce,Ca)_4(Fe^{2+},Mn)(Ti, Fe^{3+},Al)_4(Si_2O_7)_2O_8$, a new mineral species from the Eifel volcanic district, Germany. Geology of Ore Deposits, 54, 647-655.

Chukanov, N.V., Aksenov, S.M., Rastsvelaeva, R.K., Belakovskiy, D.I., Göttlicher, J., Britvin, S.N., and Möckel, S. (2012b) Christofschäferite-(Ce), $(Ce.La,Ca)_4Mn^{2+}(Ti,Fe^{3+})_3(Fe^{3+},Fe^{2+},Ti)(Si_2O_7)_2O_8$ – a new chevkinite-group mineral from the Eifel area, Germany. Novye Dannye o Mineralakh, 47, 33-42.

de Hoog, J.C.M., and van Bergen, M.J. (2000) Volatile-induced transport of HFSE, REE, Th and U in arc magmas: evidence from zirconolite-bearing vesicles in potassic lavas of Lewotolo volcano (Indonesia). Contributions to Mineralogy and Petrology, 139, 485-502.

Della Ventura, G., Williams, C.T., Raudsepp, M., Bellatreccia, F., Caprilli, E., and Giordano, G. (2001) Perrierite-(Ce) and zirconolite from syenitic ejectum of the Roccamonfina volcano (Latium, Italy): implications for the mobility of Zr, Ti and REE in volcanic environments. Neues Jahrbuch für Mineralogie Monatshefte, 2001, 385-402.

De Paolo, D.J., Manton, W.I., Grew, E.S., and Halpern, M. (1982) Sm-Nd, Rb-Sr and U-Th-Pb systematics of granulite facies rocks from Fyfe Hills, Enderby Land, Antarctica. Nature, 298, 614-618.

Dickson, J.S. (2015) Rare earth elements: Global market overview. In: Simandl, G.J. and Neetz, M., (Eds.), Symposium on Strategic and Critical Materials Proceedings, November 13-14, 2015, Victoria, British Columbia. British Columbia Ministry of Energy and Mines, British Columbia Geological Survey Paper, 2015-3, 5-11.

Doelter, C. (1931) Handbuch der Mineralchemie. Volume 3. Steinkopff; Dresden.

Els, F. (2014) Canada wants 20% of global rare earth market by 2018. www.mining.com, Jan. 8, 2014 (http://www.mining.com/canada-wants-20-of-global-rare-earth-market-by-2018-27834/ accessed 10 February 2017).

Ewart, A. (1981) The mineralogy and chemistry of the anorogenic Tertiary silicic volcanics of S.E. Queensland and N.E. New South Wales, Australia. Journal of Geophysical Research, 86, 10242-10256.

Goto, A., Kunugiza, K., and Miyajima, H. (2017) Phase relations in the $NaAlSiO_4$ – SiO_2

– H_2O system for the hydrothermal precipitation of jadeite, albite, natrolite, and analcime in jadeitite of the Itoigawa-Omi area, Japan. Journal of the Mineralogical and Petrological Sciences, 112, 271-280.

Gottardi, G. (1960) The crystal structure of perrierite. American Mineralogist, 45, 1-14.

Green, T.H., and Pearson, N.J. (1988) Experimental crystallization of chevkinite/ perrierite from REE-enriched silicate liquids at high pressure and temperature. Mineralogical Magazine, 52, 113-120.

Grew, E.S., and Manton, W.I. (1979a) Archean rocks in Antarctica: 2.5-billion-year uranium-lead ages of pegmatites in Enderby Land. Science, 206, 443-445.

Grew, E.S., and Manton, W.I. (1979b) Geochronologic studies in East Antarctica; age of a pegmatite in Mawson charnockite. Antarctic Journal of the United States, 14, 2-3.

Grew, E.S., and Manton, W.I. (1986) A new correlation of sapphirine granulites in the Indo-Antarctic metamorphic terrain; late Proterozoic dates from the Eastern Ghats province of India. Precambrian Research, 33, 123-137.

Haggerty, S.E., and Mariano, A.N. (1983) Strontian-loparite and strontio-chevkinite: Two new minerals in rheomorphic fenites from the Parana Basin carbonatites, South America. Contributions to Mineralogy and Petrology, 84, 365-381.

Haque, N., Hughes, A., Lim, S., and Vernon, C. (2014) Rare earth elements: Overview of mining, mineralogy, uses, sustainability and environmental impact. Resources, 3, 614-635.

1124 Harley, S.L. (1994) Mg-Al yttrian zirconolite in a partially melted sapphirine granulite,
1125 Vestfold Hills, East Antarctica. Mineralogical Magazine, 58, 259-269.
1126 Harley, S.L. (2008) Refining the P-T records of UHT crustal metamorphism. Journal of
1127 Metamorphic Geology, 26, 125-154.
1128 Harley, S.L., and Christy, A.G. (1995) Titanium-bearing sapphirine in a partially melted
1129 aluminous granulite xenolith, Vestfold Hills, Antarctica. European Journal of
1130 Mineralogy, 7, 637-653.
1131 Harlov, D.E. (2015) Apatite: a fingerprint for metasomatic processes. Elements, 11, 171-
1132 176.
1133 Harlov, D.E., and Hetherington, C.J. (2010) Partial high-grade alteration of monazite
1134 using alkali-bearing fluids: Experiment and nature. American Mineralogist, 95, 1105-
1135 1108.
1136 Harlov, D.E., Wirth, R., and Hetherington, C.J. (2011) Fluid-mediated partial alteration
1137 in monazite: the role of coupled dissolution-reprecipitation in element redistribution
1138 and mass transfer. Contributions to Mineralogy and Petrology, 162, 329-348.
1139 Hirtopanu, P., Andersen, J.C., Fairhurst, R.J., and Jakab, G. (2013) Allanite-(Ce) and its
1140 associations, from the Ditrau intrusive massif, East Carpathians, Romania. Proceedings
1141 of the Romanian Academy, Series B, 2013, 59-74.
1142 Hoatson, D.M., Jaireth, S., and Miezitis, Y. (2011) The major rare-earth-element deposits
1143 of Australia.: geological setting, exploration, and resources. Geoscience Australia, 204
1144 pp.
1145 Hokada, T. (2007) Perrierite in sapphirine-quartz gneiss: geochemical and
1146 geochronological features and implications for accessory-phase paragenesis of UHT
1147 metamorphism. Journal of Mineralogical and Petrological Sciences, 102, 44-49.

Holtstam, D., Bindi, L., Hålenius, U., and Andersson, U.B. (2017) Delhuyarite-(Ce) – $Ce_4Mg(Fe^{3+}{}_2W)\square(Si_2O_7)_2O_6(OH)_2$ – a new mineral of the chevkinite group, from the Nya Bastnäs Fe-Cu-REE deposit, Sweden. European Journal of Mineralogy, 29, 897-905.

Hughes, J.M., and Rakovan, J.F. (2015) Structurally robust, chemically diverse: apatite and apatite supergroup minerals. Elements, 11, 165-170.

Huraiová, M., Konečný, P., and Hurai, V. (2007) Chevkinite-(Ce) – REE-Ti silicate from syenite xenoliths in the Pinciná basaltic maar near Lučenec (Southern Slovakia). Mineralia Slovaca, 39, 255-268. (in Slovak, with English summary)

Imaoka, T., and Nakashima, K. (1994) Chevkinite in syenites from Cape Ashizuri, Shikoku Island, Japan. Neues Jahrbuch für Mineralogie Monatshefte, 1994 (8), 358-366.

Ito, J., and Arem, J.E. (1971) Chevkinite and perrierite: synthesis, crystal growth, and polymorphism. American Mineralogist, 56, 307-319.

Jaffe, H.W., Evans, H.T., and Chapman, R.W. (1956) Occurrence and age of chevkinite from the Devil's Slide fayalite-quartz syenite near Stark, New Hampshire. American Mineralogist, 41, 474-487.

Jiang, N. (2006) Hydrothermal alteration of chevkinite-(Ce) in the Shuiquangou syenitic intrusion, northern China. Chemical Geology**,** 227, 100-112.

Johnson, T.E., Hudson, N.F.C., and Droop, G.T.R. (2003) Evidence for a genetic granite-migmatite link in the Dalradian of NE Scotland. Journal of the Geological Society, London, 160, 447-457.

Jørgensen, K.A. (1980) The Thorsmörk ignimbrite: an unusual comenditic pyroclastic flow in southern Iceland. Journal of Volcanology and Geothermal Research, 8, 7-22.

1172 Kartashov, P.M. (1994) Zr- and Nb-bearing varieties of chevkinite-(Ce) and their
1173 alteration products, first occurrence in Mongolia. Ninth IAGOD Symposium (Beijing),
1174 2, 696-697 (abstr.).
1175 Kasatkin, A.W., Epanczincev, S.G., and Niestola, F. (2015) Dingdaohengite-(Ce) from
1176 Obuhovskovo Uwala, south Urals – first find in Russia. Mineralogy, Yiming Urb RAS.,
1177 No. 3, 3-7 (in Russian).
1178 Kopylova, M.G., Gurney, J.J., and Daniels, L.R.M. (1997a) Mineral inclusions in
1179 diamonds from the River Ranch kimberlite, Zimbabwe. Contributions to Mineralogy
1180 and Petrology, 129, 366-384.
1181 Kopylova, M.G., Rickard, R.S., Kleyenstucher, A., Taylor, W.R., Gurney, J.J., and
1182 Daniels, L.R.M. (1997b) First occurrence of strontian K-Cr loparite and Cr-chevkinite
1183 in diamonds. Russian Geology and Geophysics, 38, 405-420.
1184 Kudrin, V.S., Kudrina, M.A., and Moreyeva, N.V. (1967) Tantalum-niobium
1185 mineralisation in lime skarns. Doklady Akademii Nauk SSSR, 177, 430-432 (in
1186 Russian).
1187 Lacroix, A. (1915) La bastnaésite et la tscheffkinite de Madagascar. Bulletin de la
1188 Société Française de Minéralogie, 38, 106-114.
1189 Li, G., Yang, G., Ma, Z., Shi, N., Xiong, M., Fan, H., and Sheng, G. (2005) Crystal
1190 structure of natural non-metamict Ti- and Fe^{2+}-rich chevkinite-(Ce). Acta Geologica
1191 Sinica, 79, 325-331.
1192 Li, X.-C., and Zhou, M.-F. (2017) Hydrothermal alteration of monazite-(Ce) and
1193 chevkinite-(Ce) from the Sin Quyen Fe-Cu-LREE-Au deposit, northwestern Vietnam.
1194 American Mineralogist, 102, 1525-1541.
1195 Li, X.-C., and Zhou, M.-F. (2018) The nature and origin of hydrothermal REE

1196 mineralization in the Sin Quyen deposit, northwestern Vietnam. Economic Geology,
1197 113, 645-673.
1198 Liu, Y., and Ma, C. (2015) Monazite, chevkinite-perrierite and xenotime in Martian
1199 breccia meteorite NWA 7034. 46th Lunar and Planetary Science Conference, 2015,
1200 #1287. www.hou.usra.edu/meetings
1201 Liu, Y., Ma, C., Beckett, J., and Guan, Y. (2015) Rare-earth minerals in Martian
1202 meteorite NWA 7034/7533: evidence for fluid-rock interaction in the Martian crust.
1203 78th Annual Meeting of the Meteoritical Society, 2015, 5051.
1204 Liu, Y., Ma, C., Beckett, J.R., Chen, Y., and Guan, Y. (2016) Rare-earth-element
1205 minerals in martian breccia meteorites NWA 7034 and 7533: Implications for fluid-
1206 rock interaction in the martian crust. Earth and Planetary Science Letters, 451, 252-262.
1207 Lyalina, L.M., Zozulya, D.R., Savchenko, Ye.E., Tarasov, M.P., Selivanova, E.A., and
1208 Tarasova, E. (2014). Fluorbritholite-(Y) and yttrialite-(Y) from silexites of the Keivy
1209 alkali granites, Kola Peninsula. Geology of Ore Deposits, 56, 589-602.
1210 Macdonald, R. and Belkin, H.E. (2002) Compositional variation in minerals of the
1211 chevkinite group. Mineralogical Magazine, 66, 1075-1098.
1212 Macdonald, R., Marshall, A.S., Dawson, J.B., Hinton, R.W., and Hill, P.G. (2002)
1213 Chevkinite-group minerals from salic volcanic rocks of the East African Rift.
1214 Mineralogical Magazine, 66, 287-299.
1215 Macdonald, R., Belkin, H.E., Wall, F., and Bagiński, B. (2009) Compositional variation
1216 in the chevkinite group: new data from igneous and metamorphic rocks. Mineralogical
1217 Magazine, 73, 777-796.
1218 Macdonald, R., Bagiński, B., Kartashov, P., Zozulya, D., and Dzierżanowski, P. (2012)
1219 Chevkinite-group minerals from Russia and Mongolia: new compositional data from

fenites, metasomatites and ore deposits. Mineralogical Magazine, 76, 535-549.

Macdonald, R., Bagiński, B, Dzierżanowski, P., Fettes, D.J., and Upton, B.G.J. (2013) Chevkinite-group minerals in UK Palaeogene granites: underestimated REE-bearing accessory phases. The Canadian Mineralogist, 51, 333-347.

Macdonald, R., Sumita, M., Schmincke, H.-U., Bagiński, B., White, J.C., and Ilnicki, S.S. (2015a) Peralkaline felsic magmatism at the Nemrut volcano, Turkey: impact of volcanism on the evolution of Lake Van (Anatolia) IV. Contributions to Mineralogy and Petrology, 169:34.

Macdonald, R., Bagiński, B., Kartashov, P.M., Zozulya, D., Dzierżanowski, P., and Jokubauskas, P. (2015b) Hydrothermal alteration of a chevkinite-group mineral to a bastnäsite-(Ce)-ilmenite-columbite-(Fe) assemblage: interaction with a F-, CO_2-rich fluid. Mineralogy and Petrology, 109, 659-678.

Macdonald, R., Bagiński, B., Kartashov, P.M., Zozulya, D., and Dzierżanowski, P. (2015c) Hydrothermal alteration of chevkinite-group minerals. Part 2. Metasomatite from the Keivy massif, Kola Peninsula, Russia. Mineralogical Magazine, 79, 1039-1059.

Macdonald, R., Bagiński, B., Kartashov, P.M., Zozulya, D., and Dzierżanowski, P. (2015d) Interaction of rare-metal minerals with hydrothermal fluids: evidence from quartz-epidote metasomatites of the Haldzan Buragtag massif, Mongolian Altai. The Canadian Mineralogist, 55, 1015-1034.

Macdonald, R., Nejbert, K., Bagiński, B., and Jurewicz, E. (2017a) Ti-Zr-Nb-bearing accessory minerals in high-K trachyandesitic rocks from the Western Outer Carpathians, Moravia, Czech Republic. European Journal of Mineralogy, 30, 135-147.

Macdonald, R., Bagiński, B., and Zozulya, D. (2017b) Differing responses of zircon, chevkinite-(Ce), monazite-(Ce) and fergusonite-(Y) to hydrothermal alteration:

1244 Evidence from the Keivy alkaline province, Kola Peninsula, Russia. Mineralogy and
1245 Petrology, 111, 523-545.
1246 Makagonov, E.P., and Muftakhov, V.A. (2016) REE and Sr mineralization with
1247 perrierite-(Ce) in alkaline silicate – carbonate assemblage of the contact zone of the
1248 Vishnevogorsk Block (South Urals). Mineralogy, No. 4, 19-30 (in Russian).
1249 Makarochkin, B.A., Gonibesova, K.A. and Makarochkina, M.S. (1959) Chevkinite from
1250 the Ilmen Mountains. Zapiski Vserossiiskogo Mineralogicheskogo Obshchestva USSR,
1251 88, 547-553 (in Russian).
1252 Marchenko, Ye.-Ya., Chashka, A.I., and Gurova, Ye. P. (1968) The substitution of
1253 chevkinite by bastnesite under the conditions of a carbonate-halide hydrothermal
1254 process. Dopovidi Akademiyi Nauk Ukrayins'koyi RSR, Seriya B: Geologichni,
1255 Khimichni ta Biologichni Nauki, 1, 69-72 (in Ukrainian).
1256 Marshall, A.S., Macdonald, R., Rogers, N.W., Fitton, J.G., Tindle, A.G., Nejbert, K.,
1257 and Hinton, R.W. (2009) Fractionation of peralkaline silicic magmas: the Greater
1258 Olkaria Volcanic Complex, Kenya Rift Valley. Journal of Petrology, 50, 323-359.
1259 Martin, H., Bonin, B., Capdevila, R., Jahn, B.M., Lameyre, J., and Wang, Y. (1994)
1260 The Kuiqi peralkaline granitic complex (SE China): petrology and geochemistry.
1261 Journal of Petrology, 35, 983-1015.
1262 Martz, A.M., and Brown, F.H. (1981) Chemistry and mineralogy of some Plio-
1263 Pleistocene tuffs from the Shungura Formation, southwest Ethiopia. Quaternary
1264 Research, 16, 240-257.
1265 Mashima, H., Akai, J., Nakamuta, Y., and Matsubara, S. (2008) Orthorhombic
1266 polymorph of rengeite from Ohmi region, central Japan. American Mineralogist,
1267 93, 1153-1157.

1268 McDowell, S.D. (1979) Chevkinite from the Little Chief Granite porphyry stock,
1269 California. American Mineralogist, 64, 721-727.
1270 Melluso, L., Hergt, J.M., and Zanetti, A. (2014) The late crystallization stages of low-Ti,
1271 low-Fe tholeiitic magmas: Insights from evolved Antarctic and Tasmanian rocks.
1272 Lithos, 188, 72-83.
1273 Mikhailova, Yu. A., Konopleva, N.G., Yakovenchuk, V.N., Ivanyuk, G.Yu.,
1274 Men'shikov, Yu.P. and Pakhomovsky, Ya.A. (2007) Corundum-group minerals in
1275 rocks of the Khibiny alkaline pluton, Kola Peninsula. Geology of Ore Deposits, 49,
1276 590-598.
1277 Mills, J.G., Saltoun, B.W., and Vogel, T.A. (1997) Magma batches in the Timber
1278 Mountain magmatic system, Southwestern Nevada Volcanic Field, Nevada, USA.
1279 Journal of Volcanology and Geothermal Research, 78, 185-208.
1280 Mills, S.J., Kartashov, P.M., Kampf, A.R., Konev, A.A., Koneva, A.A., and Raudsepp,
1281 M. (2012) Cordylite-(La), a new mineral species in fenite from the Biraya Fe-REE
1282 deposit, Irkutsk, Russia. The Canadian Mineralogist, 50, 1281-1290.
1283 Min, K., Reiners, P.W., Wolff, J.A., Mundil, R., and Winters, R.L. (2006) (U-Th)/He
1284 dating of volcanic phenocrysts with high-U-Th inclusions, Jemez Volcanic Field,
1285 New Mexico. Chemical Geology, 227, 223-235.
1286 Mineev, D.A., Makarochkin, B.A., and Zhabin, A.G. (1962) The study of lanthanide
1287 behaviour in alteration processes of rare-earth minerals. Geokhimiya, 7, 590-597
1288 (in Russian).
1289 Mitchell, R.S., Swanson, S.M., and Crowley, J.K. (1976) Mineralogy of a deeply
1290 weathered pegmatite, Bedford County, Virginia. Southeastern Geology, 18, 37-47.
1291 Miyajima, H., Matsubara, S., Miyawaki, R., Yokoyama, K., and Hirokawa, K. (2001)

Rengeite, $Sr_4ZrTi_4Si_4O_{22}$, a new mineral, the Sr-Zr analogue of perrierite from the Itoigawa-Ohmi district, Niigata prefecture, central Japan. Mineralogical Magazine, 65, 111-120.

Miyajima, H., Miyawaki, R., and Ito, K. (2002) Matsubaraite, $Sr_4Ti_5(Si_2O_7)_2O_8$, a new mineral, the Sr-Ti analogue of perrierite in jadeitite from the Itoigawa-Ohmi district, Niigata prefecture, Japan. European Journal of Mineralogy, 14, 1119-1128.

Miyawaki, R., Matsubara, S., and Miyajima, H. (2002) The crystal structure of rengeite, $Sr_4ZrTi_4(Si_2O_7)O_8$. Journal of Mineralogical and Petrological Sciences, 97, 7-12.

Miyawaki, R., Matsubara, S., Yokoyama, K., Momma, K., Sano, T., Tsutsumi, Y., Shigeoka, M. and Nishikubo, K. (2012) Chevkinite-(Ce) in tuff at Heguri, Boso Peninsula, Chiba Prefecture, Japan. Bulletin of the National Museum of Natural Sciences, Ser. C, 38, 7-13.

Miyazaki, T., and Santosh, M. (2005) Cooling history of the Putetti alkali syenite pluton, southern India. Gondwana Research, 8, 567-574.

Monchoux, P., Fontan, F., de Parseval, P., Martin, R.F., and Wang, R.C. (2006) Igneous albitite dikes in orogenic lherzolites, Western Pyrénées, France: a possible source for corundum and alkali feldspar xenocrysts in basaltic terranes. 1. Mineralogical Associations. The Canadian Mineralogist, 44, 817-842.

Montel, J.M. (1986) Experimental determination of the solubility of Ce-monazite in SiO_2-Al_2O_3-K_2O-Na_2O melts at 800°C, 2 kbar, under H_2O-saturated conditions. Geology, 14, 659-662.

Montel, J.M. (1993) A model for monazite/melt equilibrium and application to the generation of granitic magmas. Chemical Geology, 110, 127-146.

Muhling, J.R., Suvorova, A.A., and Rasmussen, B. (2014) The occurrence and composition of chevkinite-(Ce) and perrierite-(Ce) in tholeiitic intrusive rocks and

1316 lunar mare basalt. American Mineralogist, 99, 1911-1921.
1317 Mutanen, T. (1997) Geology and ore petrology of the Akanvaara and Koitelainen mafic
1318 layered intrusions and the Keivitsa-Satovaara layered complex, northern Finland.
1319 Geological Survey of Finland, Bulletin**,** 395, 233 pp.
1320 Nekrasov, I.Ya., Gorshkov, A.I., Doynikova, O.A., Nekrasova, R.A., Sivtsov, A.V., and
1321 Vlasova, Ye.Y. (1993) A new hydrated ytrrium-calcium carbonate from the Tommot
1322 Deposit in NE Yakutia. Doklady of the U.S.S.R. Academy of Sciences: Earth Science
1323 Section, 328, 148-151.
1324 Nespolo, M., Ferraris, G., and Ohasi, H. (1999) Charge distribution as a tool to
1325 investigate structural details: meaning and application to pyroxenes. Acta
1326 Crystallographica, Section B, Structural Science. 55, 902-916.
1327 Noble, D.C. (1965) Gold Flat Member of the Thirsty Canyon Tuff – a pantellerite ash-
1328 flow sheet in southern Nevada. U.S. Geological Survey Professional Paper 525-B,
1329 B85-B90.
1330 Novak, S.W. and Mahood, G.A. (1986) Rise and fall of a basalt-trachyte-rhyolite
1331 magma system at the Kane Springs Wash Caldera, Nevada. Contributions to
1332 Mineralogy and Petrology, 94, 352-373.
1333 Ontoyev, D. (1993) Ore-bearing metasomatites at the Bayan Obo rare earth deposit,
1334 Inner Mongolia, China. International Geology Review, 35, 271-278.
1335 Padilla, A.J., and Gualda, G.A.R. (2016) Crystal-melt elemental partitioning in silicic
1336 magmatic systems: An example from the Peach Spring Tuff high-silica rhyolite,
1337 Southwest USA. Chemical Geology, 2016, 440, 326-344.
1338 Papoutsa, A.D., and Pe-Piper, G. (2013) The relationship between REE-Y-Nb-Th
1339 minerals and the evolution of an A-type granite, Wentworth Pluton, Nova Scotia.

American Mineralogist, 98, 444-462.

Parodi, G.C., Della Ventura, G., Mottana, A., and Raudsepp, M. (1994) Zr-rich non metamict perrierite-(Ce) from holocrystalline ejecta in the Sabatini volcanic complex (Latium, Italy). Mineralogical Magazine, 58, 607-613.

Payette, C., and Martin, R.F. (1988) The Welsford anorogenic igneous complex, southern New Brunswick: rift-related Acadian magmatism. Geological Survey of Canada Open File 1727.

Peretyazhko, I.S., Savina, E.A., and Karmanov, N.S. (2015) Comendites and pantellerites of Nemrut volcano, Eastern Turkey: genesis and relations between the trachyte-comendite, comenditic, and pantelleritic melts. Petrology, 23, 576-622.

Pin, C., Monchoux, P., Paquette, J.-L., Azambre, B., Wang, R.C., and Martin, R.F. (2006) Igneous albitite dikes in orogenic lherzolites, western Pyrénées, France: a possible source for corundum and alkali feldspar xenocrysts in basaltic terranes. II. Geochemical and petrogenetic considerations. The Canadian Mineralogist, 44, 843-856.

Popov, V.A., Pautov, L.A., Sokolova, E., Hawthorne, F.C., McCammon, C., and Bazhenova, L.F. (2001) Polyakovite-(Ce), (*REE*,Ca)$_4$(Mg,Fe^{2+})(Cr^{3+},Fe^{3+})$_2$ (Ti,Nb)$_2$Si$_4$O$_{22}$, a new metamict mineral species from the Ilmen Mountains, southern Urals, Russia: mineral description and crystal chemistry. The Canadian Mineralogist, 39, 1095-1104.

Portnov, A.M. (1964) Strontium perrierite in the North Baikal region. Doklady of the Academy of Sciences USSR: Earth Science Section, 156, 118-120.

Povarennykh, O.S., and Ganzeeva, L.V. (1972) Manganous chevkinite from alkaline

metasomites of the Russian Platform. Dopodivi Akademiyi Nauk Ukrayins'koyi RSS Seriya B : Geologichni, Khimichni ta Biologichni Nauki, 9, 794-797 (in Russian).

Prol-Ledesma, R.-M., Melgarejo, J.C., and Martin, R.F. (2012) The El Muerto "NYF" granitic pegmatite, Oaxaca, Mexico, and its striking enrichment in allanite-(Ce) and monazite-(Ce). The Canadian Mineralogist, 50, 1055-1076.

Proshchenko, Ye.G. (1967) Rare earth minerals from albitites of eastern Siberia. Pp. 103-136 in: Mineralogiya pegmatitov i gidrotermalitov shchelochnykh massivov. Akademii Nauk SSSR, Institut Mineralogii, Geokhimii, Kristallokhimii Redk.Elementov, Moscow (in Russian).

Rajesh, H.M. (2003) Outcrop-scale silicate liquid immiscibility from an alkali syenite (A-type granitoid)-pyroxenite association near Puttetti, Trivandrum Block, South India. Contributions to Mineralogy and Petrology, 145, 612-627.

Rapp, R.P., Ryerson, F.J., and Miller, C.F. (1987) Experimental evidence bearing on the stability of monazite during crustal anatexis. Geophysical Research Letters, 14, 307-310.

Rasmussen, B., Fletcher, I.R., Gregory, C.J., and Muhling, J.R. (2014) Six chronometers in one rock: Dating mafic intrusive rocks by in situ SHRIMP U-Pb geochronology. Goldschmidt 2014 Abstracts, #2034.

Ridolfi, F., Renzulli, A., Santi, P., and Upton, B.G.J. (2003) Evolutionary stages of crystallization of weakly peralkaline syenites: evidence from ejecta in the plinian deposits of Agua de Pau volcano (São Miguel, Azores Islands). Mineralogical Magazine, 67, 749-767.

Robinson, D., and Miller, C. (1999) Record of magma chamber processes preserved in accessory mineral assemblages. American Mineralogist, 84, 1346-1353.

Rozanov, K.I., Flerova, L.B., Khomich, P.Z., and Zingerman, A.Ya. (1983) Fractionation and concentration of lanthanides and ytrrium in Precambrian complexes of the western part of the Russian platform. Doklady, Academy of Sciences of the USSR, Earth Sciences Section, 258, 177-181.

Savel'eva, V.B., and Karmanov, N.S. (2008) REE minerals of alkaline metasomatic rocks in the Main Sayan Fault. Geology of Ore Deposits, 50, 681-696.

Savel'eva, V.B., and Karmanov, N.S. (2010) Quartz-albite-microcline metasomatic rocks in the Main Sayan Fault Zone: Evolution of metasomatism and composition of accessory minerals. Geology of Ore Deposits, 52, 302-321.

Sawyer, D.A., and Sargent, K.A. (1989) Petrologic evolution of divergent peralkaline magmas from the Silent Canyon caldera complex, southwestern Nevada volcanic field. Journal of Geophysical Research**,** 94, 6021-6040.

Scaillet, B., and Macdonald, R. (2001) Phase relations of peralkaline silicic magmas and petrogenetic implications. Journal of Petrology, 42, 825-845.

Segelstad, T.V., and Larsen, A.O. (1978) Chevkinite and perrierite from the Oslo region, Norway. American Mineralogist, 63, 499-505.

Semenov, E.I., Kulakov, M.P., Kostynina, L.P., Kazakova, M.E., and Dudykina, A.S. (1966) Scandium content in the quartz-fluorite pegmatites of Kazakhstan. Geokhimiya, 2, 244-246.

Semenov, E.I., Upendran, R., and Subramanian, V. (1978) Rare earth minerals of carbonatites of Tamil Nadu. Journal of the Geological Society of India, 19, 550-557.

Shannon, R.D. (1976) Revised effective ionic radii and systematic studies of interatomic distances in halides and chalcogenides. Acta Crystallographica, A32, 751-767.

Shellnutt, J.G., and Iizuka, Y. (2013) Chevkinite-group minerals from the mantle-derived metaluminous Woshui syenite of the Emeishan large igneous province. European

1412 Journal of Mineralogy, 25, 671-682.
1413 Shen, G., Yang, G., and Xu, J. (2005) Maoniupingite-(Ce): A new rare-earth mineral
1414 from the Maoniuping rare-earth deposit in Mianning, Sichuan, China. Sedimentary
1415 Geology and Tethyan Geology, 25, 210-216 (in Chinese with English abstract).
1416 Shimazaki, H., Yang, Z., Miyawaki, R., and Shigeoka, M. (2008a) Scandium-bearing
1417 minerals in the Bayan Obo Nb-REE-Fe deposit, Inner Mongolia, China. Resource
1418 Geology, 58, 80-86.
1419 Shimazaki, H., Miyawaki, R., Yokoyama, K., Matsubara, S., Yang, Z., and Shigeoka,
1420 M. (2008b) A reconnaissance study on minerals from the Bayan Obo Nb-REE-Fe
1421 deposit, Inner Mongolia, China. Bulletin of the National Museum of Nature and
1422 Science, 34, 1-26.
1423 Smith, M.P., Moore, K., Kavecsánszki, D., Finch, A.A., Kynicky, J., and Wall, F. (2016)
1424 From mantle to critical zone: A review of large and giant sized deposits of the rare
1425 earth elements. Geoscience Frontiers. doi: 10.1016/j.gsf.2015.12.006.
1426 Sokolova, E., Hawthorne, F.C., Della Ventura, G., and Kartashov, P.M. (2004)
1427 Chevkinite-(Ce): crystal structure and the effect of moderate radiation-induced damage
1428 on site-occupancy refinement. The Canadian Mineralogist, 42, 1013-1025.
1429 Stachowicz, M., Bagiński, B., Macdonald, R., Kartashov, P.M., Oziębło, A., and
1430 Woźniak, K. (2014) Structure of Sr-Zr-bearing perrierite-(Ce) from the Burpala
1431 Massif, Russia. Mineralogical Magazine, 78, 1647-1659.
1432 Stachowicz, M., Bagiński, B., Welch, M.D., Kartashov, P.M., Macdonald, R.,
1433 Balcerzak, J., Tyczkowski, J., and Woźniak, K. (in revision, a) Cation ordering, valence states
1434 and symmetry breaking in the crystal-chemically complex mineral chevkinite-(Ce), Part I:
1435 X-ray diffraction and photoelectron spectroscopy studies, and mechanisms of Nb enrichment.

American Mineralogist.

Stachowicz, M., Welch, M.D., Bagiński, B., Kartashov, P.M., Macdonald, R. and Woźniak, K. (in revision, b) Cation ordering, valence states and symmetry breaking in the crystal-chemically complex mineral chevkinite-(Ce), Part II: Recrystallization, transformation and metamict states in chevkinite. American Mineralogist.

Troll, V.R., Sachs, P.M., Schmincke, H.-U., and Sumita, M. (2003) The REE-Ti mineral chevkinite in comenditic magmas from Gran Canaria, Spain: a SYXRF-probe study. Contributions to Mineralogy and Petrology, 145, 730-741.

Van Bergen, M.J. (1984) Perrierite in siliceous lavas from Mt Amiata, central Italy. Mineralogical Magazine, 48, 553-556.

Vasquez, J.A. (2008) Allanite and chevkinite as absolute chronometers of rhyolite differentiation. Geological Society of America Abstracts with Programs, 40, No. 1, 74.

Vasquez, J.A., Manning, C.E., and Reid, M.R. (2004) Experimental determination of allanite stability in high-silica rhyolite. American Geophysical Union, Fall Meeting 2004, abstract #V41C-1407.

Vasquez, J.A., Kyriazis, S.F., Reid, M.R., Sehler, R.C., and Ramos, F.C. (2009) Thermochemical evolution of young rhyolites at Yellowstone: Evidence for a cooling but periodically replenished postcaldera magma reservoir. Journal of Volcanology and Geothermal Research, 188, 186-196.

Vasquez, J.A., Velasco, N.O., Schmitt, A.K., Bleick, H.A., and Stelten, M.E. (2014) ^{238}U-^{230}Th dating of chevkinite in high-silica rhyolites from La Primavera and Yellowstone calderas. Chemical Geology, 390, 109-118.

Vasyukova, O., and Williams-Jones, A.E. (2016) The evolution of immiscible silicate and fluoride melts: Implications for REE ore-genesis. Geochimica et Cosmochimica

1460 Acta, 172, 205-224.

1461 Viladkar, S.G., Sorokhtina, N.V., and Senin, V.G. (2009) The Zr-Ti mineralization in
1462 carbonatites of the Samchampi alkaline carbonatite complex, Assam, India.
1463 http://geo.web.ru/conf/alkaline/2009/Viladkar.htm

1464 Vlach, S.R.F., and Gualda, G.A.R. (2007) Allanite and chevkinite in A-type granites and
1465 syenites of the Graciosa Province southern Brazil. Lithos, 97, 98-121.

1466 Wang, D., Yang, J., Yan, S., Xu, J., Chen, Y., Pu, G., and Luo, Y. (2001) A special
1467 orogenic-type rare earth element deposit in Maoniuping, Sichuan, China: geology
1468 and geochemistry. Resource Geology, 51, 177-188.

1469 Warren, G.R., Byers, F.M., Broxton, D.E., Freeman, S.H., and Hagan, R.C. (1989)
1470 Phenocryst abundance and glass and phenocryst compositions as indicators of
1471 magmatic environments of large-volume ash flow sheets in southwestern Nevada.
1472 Journal of Geophysical Research, 94, 5987-6020.

1473 Wu, B., Wang, R.-C., Yang, J.-H., Wu, F.-Y., Zhang, W.-L., Gu, X.-P.,, Zhang, A.-C.
1474 (2016) Zr and REE mineralization in sodic lujavrite from the Saima alkaline
1475 complex, northeastern China: A mineralogical study and comparison with potassic
1476 rocks. Lithos, 262, 232-246.

1477 Xu, Y., Yang, G., Li, G., Wu, Z., and Shen, G. (2008) Dingdaohengite-(Ce) from the
1478 Bayan Obo REE-Nb-Fe Mine, China: Both a true polymorph of perrierite-(Ce) and a
1479 titanic analog at the *C*1 site of chevkinite subgroup. American Mineralogist, 93, 740-
1480 744.

1481 Yakovenchuk, V.N., Ivanuyk, G.Yu., Pakhomovsky, Ya.A., and Menshikov, Yu.P.
1482 (2005) Khibiny. F. Wall (ed.). Laplandia Minerals, Apatity. Published in
1483 association with the Mineralogical Society of Great Britain and Ireland. 468 pp.

1484 Yang, Z., Fleck, M., Smith, M., Tao, K., Song, R., and Zhang, P. (2002) The crystal
1485 structure of natural Fe-rich chevkinite. European Journal of Mineralogy, 14, 969-975.
1486 Yang, Z., Li, H., Liu, M., and Franz, P. (2007) Crystal chemistry of iron in non-metamict
1487 chevkinite-(Ce): valence state and site occupation proportions. Journal of Rare Earths, 25,
1488 238–242.
1489 Yang, Z., Giester, G., Ding, K., and Tillmanns, E. (2012) Hezuolinite,
1490 $((Sr,REE)_4Zr(Ti,Fe^{3+},Fe^{2+})_2Ti_2O_8(Si_2O_7)_2$, a new mineral species of the chevkinite
1491 group from Saima alkaline complex, Liaoning Province, NE China. European
1492 Journal of Mineralogy, 24, 189-196.
1493 Yang, Z., Pertlik, F., and Fleck, M. (2008) Hydroxyl groups in nonmetamict
1494 chevkinite-(Ce): a crystal chemical discussion. Journal of Rare Earths, 26, 609-
1495 613.
1496 Zhang, R., and Long, Z. (1987) The discovery of chevkinite from the alkali-granites in
1497 southwestern Sichuan. Journal of Chengdu College of Geology, 14, 61-64.
1498 Zozulya, D., and Eby, G.N. (2010) Rare-metal ore occurrences, related to the late Archean A-
1499 type granites from the Keivy zone (NE Fennoscandian shield). In: Raino, O.T., Lukkari, S.R.,
1500 and Heinanen, A.P. (Eds.) International conference on A-type granites and related rocks
1501 through time (IOCP-510), Helsinki, Finland, August 18-20. Abstract volume, 113-115.
1502
1503
1504 **Figure captions**
1505 **Figure 1. (a)** The (CaO+SrO) - FeO* (all Fe as Fe^{2+}) plot used as an empirical discriminant
1506 between the chevkinite and perrierite subgroups by Macdonald and Belkin (2002) and modified
1507 by Macdonald et al. (2009). Data plotted are for crystals which have had the β angle determined,

updated with post-2009 data. The Cr- and Mn- analogues of chevkinite-(Ce), polyakovite and christofschäferite, respectively, are omitted. Data sources: Table 2, this paper; Jaffe et al. 1956; Gottardi 1960; Segelstad and Larsen 1978; Zhang and Long 1987; Čech et al. 1988; Imaoka and Nakashima 1994; Parodi et al. 1994; Della Ventura et al. 2001; Yang et al. 2002; Sokolova et al. 2004; Yang et al. 2008; Miyawaki et al. 2012; Stachowicz et al. 2014. **(b)** All analyses from the data compilation in Supplementary Table 2 to show the wide spread of compositions across the fields of the chevkinite and perrierite subgroups.

Figure 2. 010 projection of a 4x4 multiplied lattice cell of **(a)** perrierite-type structure and **(b)** chevkinite-type structure. Each projection contains bold black lines representing the real unit cell of the crystal structure and bold red lines representing the unit cell of the other subgroup type.

Figure 3. The unit cell contents of **(a)** perrierite and **(b)** chevkinite, with an additional (lowermost green) sheet of REE. This plane is displaced by the vector [0 ½ 0] when comparing the two structure types – see broken-off bond. It ends in the middle of an REE hexagon in perrierite (a) and between two REE atoms in chevkinite (b).

Figure 4. The main compositional variation in chevkinite and perrierite, using the scheme of Vlach and Gualda (2007). Sr-rich varieties of perrierite, polyakovite and christofschäferite omitted. The perrierites with values of Ca+Sr+(Ti,Zr) <1 are mainly Al-rich varieties. Data source: Supplementary Table 2.

Figure 5. Triangular plot to show that chevkinite and perrierite tend to occur in different igneous lithologies. The fields marked “evolved, undersaturated” and “evolved, oversaturated” are

occupied only by chevkinite. The field of mafic and intermediate igneous rocks includes only perrierite. Slightly simplified from Macdonald and Belkin (2002). Data gathered since 2002 have tended to blur the distinction between the two "evolved" fields.

Figure 6. CaO+SrO – FeO* plot showing various magmatic trends crossing the empirical boundary between the chevkinite and perrierite subgroups. The arrows point in the down-temperature direction. 1, tholeiitic dolerite, French Pyrenees (Azambre et al. 1987); 2 and 3, Woodie and Eel Creek tholeiitic intrusions, Western Australia (Muhling et al. 2014); 4, Little Chief porphyry stock, California (McDowell 1979); 5, Roseland, Virginia (Macdonald et al. 2009).

Figure 7. Cation distribution in the A site in CGM. Data source: Supplementary Table 2.

Figure 8. $[La/Nd]_{CN}$ (as a measure of fractionation within the LREE) vs. $[La/Y]_{CN}$ (as a measure of LREE v. HREE fractionation).

Figure 9. La vs.Y plot to show that the degree of LREE enrichment is not simply dependent on host rock composition. Fields: 1, Woshui syenite, China; 2, comendites (mildly peralkaline rhyolites); 3, tholeiitic intrusions, Western Australia; 4, perrierite in potassic volcanics; 5, Al-rich perrierite, Antarctica and India. Data from Supplementary Table 2 and references cited therein (Supplementary Material).

Figure 10. Relative proportions of Fe^{2+}-Ti-Al in the C site of minerals of the chevkinite and perrierite subgroups, excluding Sr-dominant phases, christofschäferite-(Ce) and polyakovite-

(Ce). All Fe taken as Fe^{2+}. GP marks the composition of perrierite-(Ce) crystallized from REE-enriched silicate liquid at 20 kbar, T 1050 °C, by Green and Pearson (1988, sample 948).

Figure 11. Graphical representation of possible substitution mechanisms in Sr-dominant perrierites (Table 1). Possible substitutions to Sr-bearing perrierite from the Bearpaw Mountains (Chakhmouradian and Mitchell 1999) and Sr-Zr perrierite, Burpala Massif (Macdonald et al. 2012) are also shown, as dashed lines.

Figure 12. BSE images of CGM occurrences in igneous rocks. **(a)** Subhedral phenocryst of chevkinite-(Ce) (Chv) in comendite obsidian (glass, Gl), Olkaria complex, Kenya Rift Valley. **(b)** Associated with primary quartz (Qz) and biotite (Bt), Lucerne Granite, Hancock County, Maine, USA. Associated accessories are zircon (Zrn), ilmenite (Ilm) and LREE-bearing apatite (Ap). The crystal is surrounded by a hydrated alteration zone (black arrows). **(c)** Late magmatic chevkinite-(Ce) growing along boundaries between alkali feldspar crystals (Afs), Ełk syenite, NE Poland. **(d)** Euhedral chevkinite-(Ce) in pegmatite, Haramosh, Pakistan. **(e)** Acicular perrierite (P), in vug in sanidinite (Sa), Anguillara, Latium, Italy (e-rocks.com). **(f)** Chevkinite-(Ce) in quartzolite, Rova occurrence, Keivy massif, coexisting with monazite-(Ce) (Mnz), zircon (Zrn) and fergusonite-(Y) (Fer) (Macdonald et al. 2017b).

Figure 13. BSE images of CGM in metamorphic rocks**. (a)** Perrierite (P) with inclusions of garnet (G) and sillimanite (S) in a quartz and garnet assemblage, quartzofeldspathic granulite from the Napier Complex, East Antarctica (from Belkin et al. 2009). **(b)** Acicular perrierite in mesoperthite, in migmatitic sapphirine granulite, Anakpalle, south India (from Belkin et al. 2009). **(c)** Matsubaraite (Mat) in jadeitite (Jd), Itoigawa-Ohmi district, Niigata prefecture, Japan

(from Miyajima et al. 2002). **(d)** CGM (Chv) along contact between carbonate crystals, metacarbonate, Golden Lake, Ontario.

Figure 14. BSE images of various examples of CGM alteration. **(a)** Chevkinite-(Ce) (Chv) crystal altered along its rim and along internal cracks (Alt.Chv), in quartzolite, Keivy massif (from Bagiński et al. 2015**). (b)** Chevkinite-(Ce) partially replaced by ferriallanite-allanite-(Ce) (Aln), davidite (Dav) and aeschynite (Aes); in metasomatite, Keivy massif, Kola massif (from Macdonald et al. 2015c). **(c)** Chevkinite-(Ce) (Zone A) replaced first by altered chevkinite (Zone B) and then by a bastnäsite (Bst) –ilmenite (Ilm)- thorite (Thr) assemblage (C1), veins of which have penetrated into the chevkinite; metasomatite, Keivy massif, Kola Peninsula (from Macdonald et al., 2015b). **(d)** Chevkinite-(Ce) (A) replaced first by minerals of the epidote supergroup (B) and then by titanite-rutile-cerite-REE carbonate assemblages (C). From Macdonald et al. (2015d).

Figure 15. Ca plotted against Ti* (total Ti–2 apfu) for various suites carrying altered CGM. Data sources: samples numbered 160b are from the El'ozero occurrence, Keivy (Bagiński et al. 2015); K4 –syenitic pegmatite, Vishnevye Mountains (Macdonald et al. 2015b); 1-93 – quartzolite, Rova occurrence, Keivy (Macdonald et al. 2012; Bagiński et al. 2015); Ardnamurchan – Paleogene granite, Scotland (Macdonald et al. 2013); Shuiquangou syenite, China (Jiang 2006); Wentworth granite, Nova Scotia (Papoutsa and Pe-Piper 2013); Main Sayan Fault, southern Baikal, Russia (Savel'eva and Karmanov (2008). The inset shows a generalised trend from unaltered to strongly altered phases, based on the solid dashed trend in the main figure. The thin dashed line is for the Graciosa Province (Vlach and Gualda 2007). From Bagiński et al. (2015), except the Welsford trend, drawn from data for sample AGP-1 in Payette and Martin (1988).

Figure 16. (CaO+SrO) – FeO* plot to show how hydrothermal alteration can drive CGM across the empirical boundary between the chevkinite and perrierite subgroups (Macdonald et al. 2009). The trends are opposite to those formed by magmatic crystallization (Fig. 5). 1, A-type syenites and granites, Corupá, Brazil (Vlach and Gualda 2007); 2, syenitic pegmatite, Vishnevye Mountains (Macdonald et al. 2015b); 3, Shuiquangou syenite (Jiang 2006); 4, quartzolite, Rova occurrence, West Keivy massif (Bagiński et al. 2015); 5, carbonate veins, Vishnevogorsky complex (Makagonov and Muftakhov 2016).

Figure 17. Apparent chevkinite/melt partition coefficients for REE in mildly peralkaline (1 to 4) and metaluminous (5) rhyolites. 1, ignimbrite X, Gran Canaria (Troll et al. 2003); 2, 4, samples SMN49 and ND002, Olkaria complex, Kenya Rift Valley (Macdonald et al. 2002); 3, sample BL210b, Olkaria (Marshall et al. 2009); 5, Peach Springs Tuff, Arizona (Padilla and Gualda 2016).

Figure 18. Slightly reversely zoned hedenbergite from the Devine Canyon Tuff, Juntura, Oregon, USA, sample DCT_B. The crystal is filled with silicate melt inclusions (MI) and various solid inclusions, such as ilmenite (Ilm), REE-Si-rich apatite (Ap), zircon (Zrn), and chevkinite-(Ce) (CGM). The hedenbergite is surrounded by glass (Gl), with phenocrysts of alkali feldspar.

Figure 19. (a) A chevkinite-(Ce) (CGM) crystal that has partially reacted to form allanite-(Ce) (Aln), Lucerne Granite, Hancock County, Maine, USA. Later alteration, marked a, around the periphery of the allanite-(Ce) has removed most of the REE. Note the bottom middle two arrows indicating a scalloped reaction front. Other phases are biotite (Bt), apatite (Ap), ilmenite (Ilm),

and plagioclase (Pl). **(b)** Chevkinite-(Ce) and monazite-(Ce) apparently growing in equilibrium, in association with zircon and fergusonite-(Y), in quartzolite, Keivy massif (from Macdonald et al. 2017b). **(c)** Chevkinite (Chv) and monazite (Mnz) mantled by allanite, Sin Quyen (Li and Zhou 2018). An irregular layer of fluorapatite (Ap) lies between the monazite and allanite. Image courtesy of Dr X.-C. Li. **(d)** Chevkinite-(Ce) (Chv) in plagioclase, with late monazite-(Ce) (Mnz) on rims. Cañada Pinabete granite, Questa complex, New Mexico.

Table 1. Members of the chevkinite group accepted by the CNMNC-IMA .

Mineral	Formula	Reference
Chevkinite subgroup		
Chevkinite-(Ce)	$(REE,Ca)_4Fe^{2+}(Ti,Fe^{3+},Fe^{2+},Al)_2Ti_2Si_4O_{22}$	Ito and Arem 1971
Polyakovite-(Ce)	$(REE,Ca)_4(Mg,Fe^{2+})(Cr,Fe^{3+})_2(Ti,Nb)_2Si_4O_{22}$	Popov et al. 2001
Maoniupingite-(Ce)	$(REE,Ca)_4(Fe^{3+},Ti,Fe^{2+},\square)(Fe^{3+},Fe^{2+},Nb,Ti)_2Ti_2Si_4O_2$	Shen et al. 2005
Dingdaohengite-(Ce)	$Ce_4Fe^{2+}Ti_2Ti_2(Si_2O_7)_2O_8$	Xu et al. 2008
Christofschäferite-(Ce)	$(Ce.La,Ca)_4Mn(Ti,Fe^{3+})_3(Fe^{3+},Fe^{2+},Ti)(Si_2O_7)_2O_8$	Chukanov et al. 2012b
Delhuyarite-(Ce)	$Ce_4Mg(Fe^{3+}{}_2W)\square(Si_2O_7)_2O_6(OH)_2$	Holtstam et al. 2017
Perrierite subgroup		
Perrierite-(Ce)	$(REE,Ca)_4Fe^{2+}(Ti,Fe^{3+},Fe^{2+},Al)_2Ti_2Si_4O_{22}$	Ito and Arem 1971
Strontiochevkinite	$(Sr_2[La,Ce]_{1.5}Ca_{0.5})_4Fe^{2+}{}_{0.5}Fe^{3+}{}_{0.5}(Ti.Zr)_4Si_4O_{22}$	Haggerty and Mariano 1983
Rengeite	$Sr_4ZrTi_4Si_4O_{22}$	Miyajima et al. 2001
Matsubaraite	$Sr_4Ti_5(Si_2O_7)_2O_8$	Miyajima et al. 2002
Hezuolinite	$(Sr,REE)_4Zr(Ti,Fe^{3+},Fe^{2+})_2Ti_2O_8(Si_2O_7)_2$	Yang et al. 2012
Perrierite-(La)	$(La,Ce,Ca)_4(Fe^{2+},Mn)(Ti,Fe^{3+},Al)_4(Si_2O_7)_2O_8$	Chukanov et al. 2012a

Table 2. Compositions of type minerals in the chevkinite group.

	Chevkinite subgroup						Perrierite subgroup					
Sample	1	2	3	4	5	6	7	8	9	10	11	12
wt%												
WO_3	-	-	-	-	-	15.53	-	-	-	-	-	-
Nb_2O_5	1.90	3.98	0.47	2.79	0.96	-	0.08	<0.01	0.24	0.00	0.28	0.75
Ta_2O_5	-	-	0.00	-	-	-	-	-	0.07	0.00	-	-
SiO_2	20.62	19.08	19.29	20.03	19.38	18.16	20.43	19.71	22.58	22.60	21.90	20.06
TiO_2	15.16	9.49	18.26	16.05	19.02	0.09	18.81	22.78	29.88	39.06	24.42	16.13
ZrO_2	0.31	-	-	-	-	-	0.62	10.60	9.49	0.00	9.18	bd
HfO_2	-	-	-	-	-	-	-	-	-	-	0.39	-
ThO_2	3.48	2.79	0.16	0.41	-	-	2.87	<0.01	-	0.00	0.80	bd
UO_2	-	0.03	-	-	-	-	-	<0.01	-	-	0.01	bd
Al_2O_3	0.50	-	0.04	0.17	0.08	0.73	3.93	0.11	0.20	0.00	0.16	2.59
Cr_2O_3	-	7.42	-	-	-	-	-	0.46	-	-	-	bd
Y_2O_3	0.13	0.38	0.00	0.02	-	0.22	0.35	<0.01	-	0.00	-	-
La_2O_3	15.19	15.94	19.53	12.73	19.60	14.58	11.01	8.79	0.00	0.00	7.12	22.92
Ce_2O_3	20.52	24.24	28.08	23.03	22.95	23.29	21.53	8.33	0.38	0.00	8.16	19.64
Pr_2O_3	1.32	2.01	-	1.58	0.56	1.89	1.95	-	0.10	0.00	0.45	0.83
Nd_2O_3	3.37	4.76	-	5.64	2.28	6.15	6.22	-	0.29	0.00	1.34	2.09
Sm_2O_3	-	0.38	-	0.37	-	0.74	0.58	-	0.04	0.00	0.10	bd
Eu_2O_3	-	-	-	0.46	-	-	-	-	-	-	0.16	bd
Gd_2O_3	-	-	-	0.07	-	0.37	0.27	-	-	-	0.06	bd
Tb_2O_3	-	-	-	0.01	-	-	-	-	-	0.00	-	bd
Dy_2O_3	-	-	-	0.01	-	0.03	bd	-	-	-	-	bd
Ho_2O_3	-	-	-	0.03	-	-	-	-	-	-	-	bd
Er_2O_3	-	-	-	0.02	-	0.04	-	-	-	-	-	bd
Yb_2O_3	-	-	-	0.02	-	0.12	0.01	-	-	0.00	-	bd
Lu_2O_3	-	-	-	0.19	-	-	-	-	-	-	-	bd
FeO*	11.55	4.96	10.00	11.78	6.98	11.57	5.41	5.70	0.10	0.00	4.19	7.91
MnO	0.73	0.05	-	0.32	4.39	-	0.04	0.11	-	0.00	0.07	2.25
MgO	0.24	2.61	1.32	0.17	0.08	2.43	0.87	<0.01	0.00	0.00	0.01	0.25
CaO	3.62	1.06	2.17	3.39	2.61	0.76	4.26	1.78	0.43	0.00	2.46	3.26
SrO	0.17	-	-	-	-	-	0.03	20.48	34.32	38.84	20.12	-
BaO	0.07	-	-	-	-	-	-	0.31	0.13	0.00	-	-
Na_2O	0.05	-	0.00	-	-	-	bd	0.05	-	0.00	0.35	bd
F	0.20	-	-	-	-	0.05	-	-	-	-	-	bd
Cl		-	-	-	-	0.03	-	-	-	-	-	bd
H_2O+		0.14	-	-	-	1.33	-	-	-	-	-	-
Sum	100.13	101.18	99.32	99.29	98.89	98.11	99.27	99.21	98.25	100.50	101.73	98.68
O ≡ F, Cl	0.08	-	-	-	-	0.03	-	-	-	-	-	-
Total	100.05	101.18	99.32	99.29	98.89	98.08	99.27	99.21	98.25	100.50	101.73	98.68

bd, below detection. -, not reported. FeO*, total Fe as Fe^{2+}. * total includes other REE = 1.16 wt.%.

Samples: 1, chevkinite, near Miass, Urals, Russia (Macdonald and Belkin 2002); 2, polyakovite, Ilmen Mts, Urals, Russia (Popov et al. 2001); 3, dingdaohengite, Bayan Obo, China (Xu et al. 2008); 4, maoniupingite, Mianning, Sichuan, China (Shen et al. 2005); 5, christofschäferite-(Ce), Eifel, Germany (Chukanov et al. 2012b): 6, delhuyarite-(Ce), Nya Bastnäs, Sweden (Holstam et al. 2017); 7, perrierite-(Ce), Nettuno, Italy (Macdonald et al. 2009); 8, strontiochevkinite, Sarambi, Paraguay (Haggerty and Mariano 1984); 9, rengeite, Itoigawa-Ohmi district, Japan (Miyajima et al. 2001); 10, matsubaraite, Itoigawa-Ohmi district, Japan (Miyajima et al. 2002); 11, hezuolinite, Saima complex, China (Yang et al. 2012); 12, perrierite-(La), Eifel, Germany (Chukanov et al. 2012a).

All analyses are as given in original publications except that all Fe is presented as Fe^{2+}.

Table 3. Summary of site allocations in the CGM.

Ref.	Mineral	unit cell	A1	ssv (epfu)	A2	ssv (epfu)	B(M1)	ssv (epfu)	C (M2)	ssv (epfu)	D1 (M3)	ssv (epfu)	D2 (M4)	ssv (epfu)
	Chevkinite subgroup													
1	**Chevkinite-(Ce) 2an**	*C*2/*m*	REE, Ca	58	REE, Ca	58	Fe^{2+}	26.5	Fe, Ti, Nb	25.0	Ti	22	Ti	22
2	**Polyakovite-(Ce)**	*C*2/*m*	REE, Ca	56.4	REE, Ca	56.4	Mg, Fe^{2+}	14.8	Ti, Nb, □	23.3	Cr, Fe^{3+}	24.7	Cr, Fe^{3+}	24.7
3	**Strontiochevkinite**	$P2_1/a$[a]	Sr, REE, Ca	42.2	Sr, REE, Ca	42.2	Fe^{2+}, Fe^{3+}	26	Ti, Zr	27.8	Ti, Zr	25.0	Ti, Zr	25.5
4	**Fe-rich chevkinite-(Ce)**	*C*2/*m*[a]	REE, Ca, □	54.6	REE, Ca, □	53.7	Fe^{3+}, Ti, Fe^{2+}, Mn,□, Mg	21.1	Ti,Fe^{3+}, Fe^{2+}, Nb, Al, □	23.5	Ti,Fe^{3+}, Fe^{2+}, Nb, Al, □	22.9	Ti,Fe^{3+}, Fe^{2+}, Nb, Al, □	23.2
5	**Christofschäferite-(Ce)**	$P2_1/m$[a]	REE, Ca	51.7	REE, Ca	51.7	Mn, Fe^{+2}	25.8	Ti, Fe3+	22.8	Fe^{3+}, Ti	24.7	Ti, Fe^{3+}	22.8
6	**Chevkinite-(Nd)**	$P2_1/a$	Nd	60	Nd	60	Co	27	Ti, Co	23.6	Ti, Co	22.9	Ti, Co	22.9
7	**Chevkinite-(Nd)**	$P2_1/a$	Nd	60	Nd	60	Mg	12	Ti, Mg	18.8	Ti, Mg	20.3	Ti, Mg	20.1
8	**Delhuyarite-(Ce)**	*C*2/*m*	REE, Ca	55.6	REE, Ca	55.5	Mg, W, Fe^{3+}	22.0	□, Fe^{3+}, W	21.9	Fe^{3+}, Al, W	33.9	Fe^{3+},W	41.1
9	**Dingdaohengite-(Ce)**	$P2_1/a$[a,b]	REE, Ca	52.8	REE, Ca	51.6	Ti / (Fe, Mg)[c]	21.3	Ti, Fe, Mg /(Ti, Fe)[c]	23.2	Ti	21.8	Fe / (Ti)[c]	21.8
	Perrierite subgroup													
10	**Perrierite-(Ce)**	*C*2/*m*	REE, Ca, Na	50.0	REE, Ca, Na	50.0	Fe, Ca	23.2	Ti	22	Ti, Mg, Fe	20.8		
11	**Perrierite-(Ce)**	*C*2/*m*	REE, Ca	48.5	REE, Ca	48.5	Fe	26	Ti	22	Al, Ti	17.5		
12	**Perrierite-(La)**	$P2_1/a$	La	57	La	57	Mg	12	Ti, Mg	18.2	Ti, Mg	20.8		
13	**Perrierite-(La)**	$P2_1/a$	REE, Ca	45.9	REE, Ca	57	Fe, Mn, Mg	25.5	Ti	22	Ti,Fe^{3+}, Al Nb	25.5		
14	**Matsubaraite**	*C*2/*m*	Sr	38	Sr	38	Ti	22	Ti	22	Ti	22		
15	**Hezuolinite**	*C*2/*m*	Sr, REE	41.5	Sr, REE	40.5	Zr, Fe^{2+}	38.7	Ti, Fe^{3+}, Fe^{2+}	22.6	Ti	22		
16	**Rengeite (REE poor)**	$P2_1/a$[b]	Sr, Ca	39.1	Sr,Ca	38.5	Zr, Ti	40	Ti	21.6	Ti	22.4		
17	**Rengeite (REE rich)**	$P2_1/a$[b]	Sr, REE, Ca	39.1	Sr, REE, Ca	38.5	Zr	40	Ti, Al, Fe, Nb	21.6	Ti, Al, Fe, Nb	22.4		
18	**Sr-Zr-bearing perrierite-(Ce)**	*C*2/*m*	Ce, La, Sr, Ca, Nd, Na	43.2	Ce, La, Sr, Ca, Nd, Na	42.6	Zr, Fe, Mn	33.2	Ti, Fe	21.5	Ti	22		

[1] (Sokolova et al. 2004) crystal 2an; [2] (Popov et al. 2001); [3] (Haggerty and Mariano 1983); [4] (Yang et al. 2002); [5] (Chukanov et al. 2012a); [6,7, 12] (Calvo and Faggiani 1974); [8] (Holtstam et al. 2017); [9] (Xu et al. 2008), from Inorganic Crystal Structure Database; [10, 11] (Gottardi 1960); [13] (Chukanov et al. 2012b); [14] (Miyajima et al. 2002); [15] (Yang et al. 2012); [16] (Miyawaki et al. 2002); a – the origin of the unit cell shifted; b – pseudo *C*2/*m*; c- site assignment in brackets, proposed by the authors of this review. ssv = site scattering values

Table 4. Compositional ranges and averages of chevkinite and perrierite

	Chevkinite					Perrierite				
	n	minimum	maximum	average	s.d. (2σ)	*n*	minimum	maximum	average	s.d. (2σ)
wt%										
P_2O_5	38	bd	0.16	0.07	0.04	23	bd	0.38	0.13	0.09
Nb_2O_5	136	bd	7.40	1.39	1.24	63	bd	3.81	0.50	0.59
Ta_2O_5	48	bd	0.50	0.11	0.10	16	bd	0.43	0.13	0.11
SiO_2	164	17.26	23.20	19.70	0.89	89	18.34	24.12	20.88	0.93
TiO_2	164	8.54	25.96	17.00	2,14	89	9.52	22.19	17.88	2.16
ZrO_2	102	bd	2.71	0.59	0.51	71	bd	7.20	1.78	1.79
HfO_2	21	bd	0.25	0.07	0.06	21	bd	0.44	0.13	0.09
ThO_2	156	bd	4.87	1.15	0.99	78	bd	4.60	1.25	1.03
UO_2	36	bd	2.53	0.16	0.42	20	bd	0.23	0.08	0.07
Al_2O_3	142	bd	8.12	0.64	0.93	84	0.18	9.04	3.25	2.07
Sc_2O_3	1	bd	0.02	0.02	-	5	bd	3.26	0.80	1.38
V_2O_3	1	0.09	0.09	0.09	-	2	0.41	0.49	0.45	0.06
Cr_2O_3	8	bd	11.54	4.79	5.25	0	bd	-	-	-
Y_2O_3	133	bd	3.01	0.63	0.52	71	bd	8.47	0.91	1.25
La_2O_3	164	9.08	33.22	13.06	3.32	89	2.17	22.92	11.60	3.54
Ce_2O_3	164	12.28	28.33	21.89	1.96	89	8.11	26.69	19.73	2.87
Pr_2O_3	150	0.37	3.56	1.98	0.44	85	0.64	4.07	1.90	0.64
Nd_2O_3	159	1.52	11.40	6.28	1.71	87	1.45	12.97	5.65	2.57
Sm_2O_3	136	bd	3.00	0.75	0.55	68	bd	5.40	0.71	0.71
Eu_2O_3	30	0.01	1.15	0.25	0.28	5	bd	0.49	0.27	0.14
Gd_2O_3	111	bd	2.49	0.45	0.36	54	bd	5.79	0.69	0.92
Tb_2O_3	19	bd	0.21	0.06	0.06	13	bd	0.60	0.15	0.15
Dy_2O_3	67	bd	0.62	0.17	0.15	40	bd	2.76	0.31	0.46
Ho_2O_3	16	bd	0.30	0.07	0.07	3	bd	0.23	0.13	0.10
Er_2O_3	32	bd	0.61	0.11	0.13	24	bd	0.42	0.13	0.10
Tm_2O_3	9	bd	0.13	0.04	0.05	2	bd	0.14	0.09	0.08
Yb_2O_3	56	bd	0.91	0.11	0.18	39	bd	0.56	0.09	0.10
Lu_2O_3	12	bd	0.74	0.15	0.22	3	bd	0.15	0.13	0.02
MgO	111	bd	2.61	0.36	0.49	84	bd	3.02	0.84	0.72
CaO	164	0.26	5.50	2.72	1.02	89	0.03	10.83	4.70	2.11
MnO	125	bd	5.00	0.54	0.67	61	bd	2.25	0.32	0.45
FeO*	164	1.04	13.66	10.65	1.73	89	0.31	9.85	6.84	1.78
SrO	50	bd	2.38	0.23	0.41	19	bd	9.96	2.30	3.07
BaO	29	bd	0.54	0.16	0.14	6	bd	0.55	0.21	0.19
PbO	12	bd	1.03	0.14	0.29	7	bd	0.55	0.26	0.19
Na_2O	23	bd	0.35	0.09	0.09	5	bd	0.72	0.32	0.29
K_2O	20	bd	0.15	0.04	0.04	8	bd	0.14	0.07	0.05
F	33	bd	1.00	0.31	0.15	9	0.17	0.47	0.30	0.12
Cl	4	0.02	0.03	0.03	0.01	1	0	0.63	0.09	-
H_2O	12	0.06	0.90	0.33	0.26	1	0.08	0.08	0.08	-

s.d. = standard deviation. *n* = number of analyses used in averaging.

Analyses given as bd (below detection) not used in averaging. FeO*, all Fe as Fe^{2+}.

Table 5. Apparent chevkinite-melt partition coefficients.

	1	2	3	4	5	6
La	1062	1472	1039	988	1536	3484
Ce	854	1293	842	806	1528	3310
Pr	791	1147	718	626	-	2025
Nd	733	1075	595	615	1239	2326
Sm	421	569	265	392	996	1607
Eu	134	129	152	225	-	1028
Gd	260	250	115	142	530	829
Tb	152	169	59	-	-	523
Dy	102	118	37	72	-	352
Ho	70	74	21	-	-	186
Er	54	64	19	-	-	157
Tm	52	46		-	-	120
Yb	53	49	10	-	-	158
Lu	63	47	9	-	-	200
Y	51	54	11	74	-	140
Ba	-	-	1.6	-	-	133
Sr	2.6	6	27	84	-	8.62
Nb	79	56	26	15	-	21
Ta	42	-	-	-	-	13
Zr	6.5	6	-	3.55	-	57
Hf	12	5	-	-	-	104
Th	280	158	87	>50	-	271
U	22	11	7	-	-	6.82
Sc	68	-	-	-	-	964
PI glass	1.05	1.05	1.34	1.11	0.99	0.94

Explanation: 1, 2 and 3, peralkaline rhyolites, Olkaria Volcanic Complex, Kenya samples BL210b (Marshall et al. 2009) and ND002, SMN49 (Macdonald et al. 2002)
4, peralkaline rhyolite, ignimbrite X, Gran Canaria (Troll et al. 2003);
5, metaluminous rhyolite, Chinati, Texas (Cameron and Cameron 1986); 6, Peach Spring Tuff, metaluminous rhyolite, Arizona (Padilla and Gualda 2016).
PI, peralkalinity index [mol. $(Na_2O+K_2O)/Al_2O_3$].

Fig 1

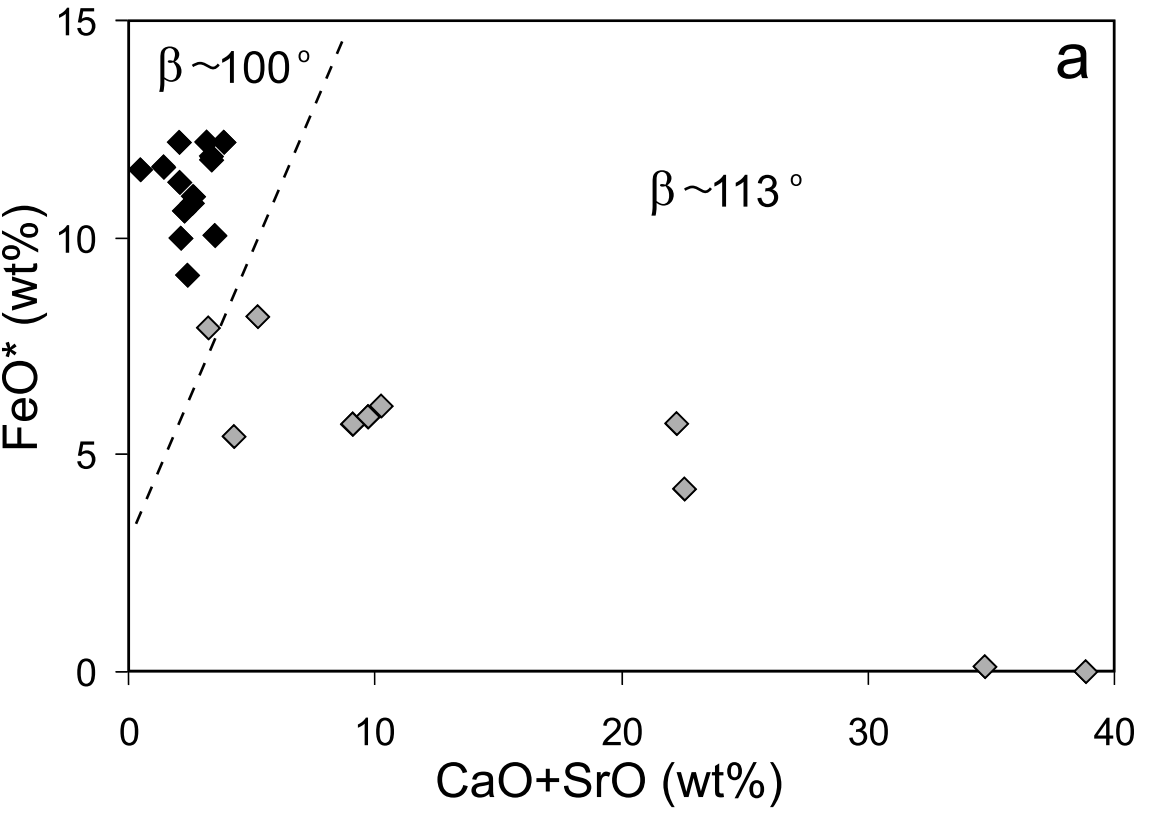
a
β ~100°
β ~113°
FeO* (wt%)
CaO+SrO (wt%)
0
5
10
15
0
10
20
30
40

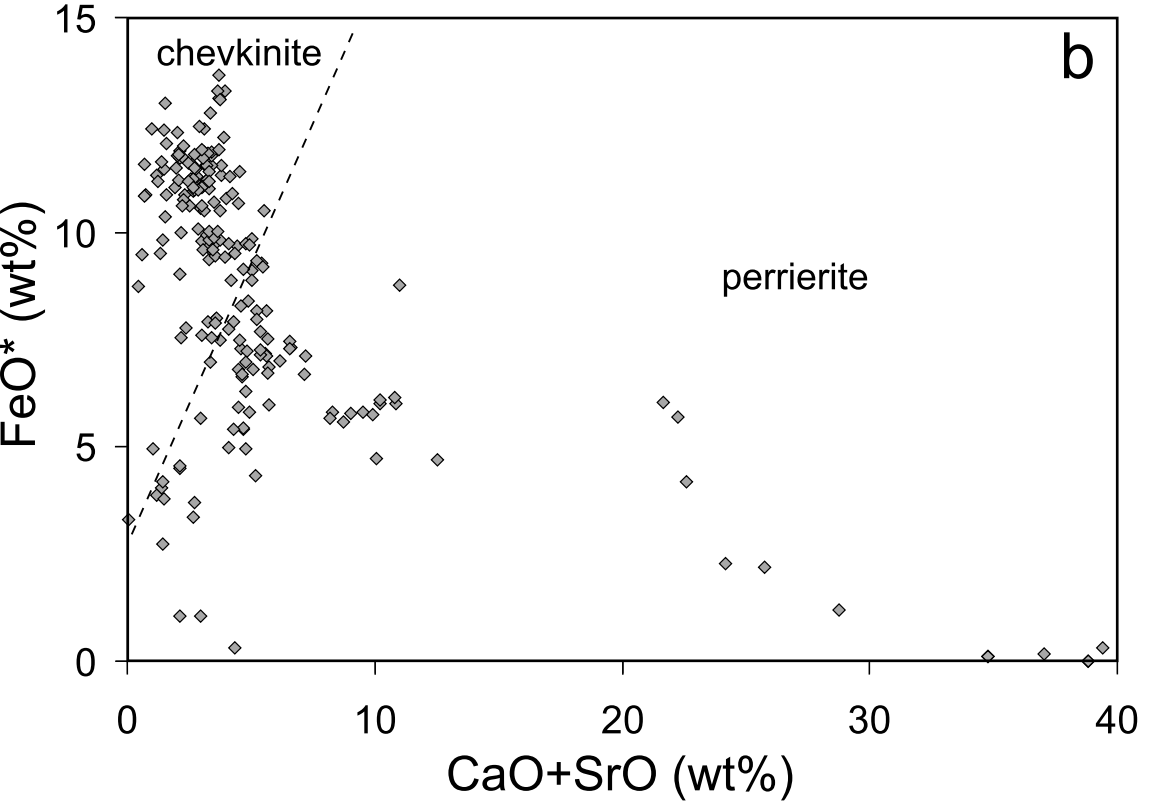
b
chevkinite
perrierite
FeO* (wt%)
CaO+SrO (wt%)
0
5
10
15
0
10
20
30
40

Fig 2

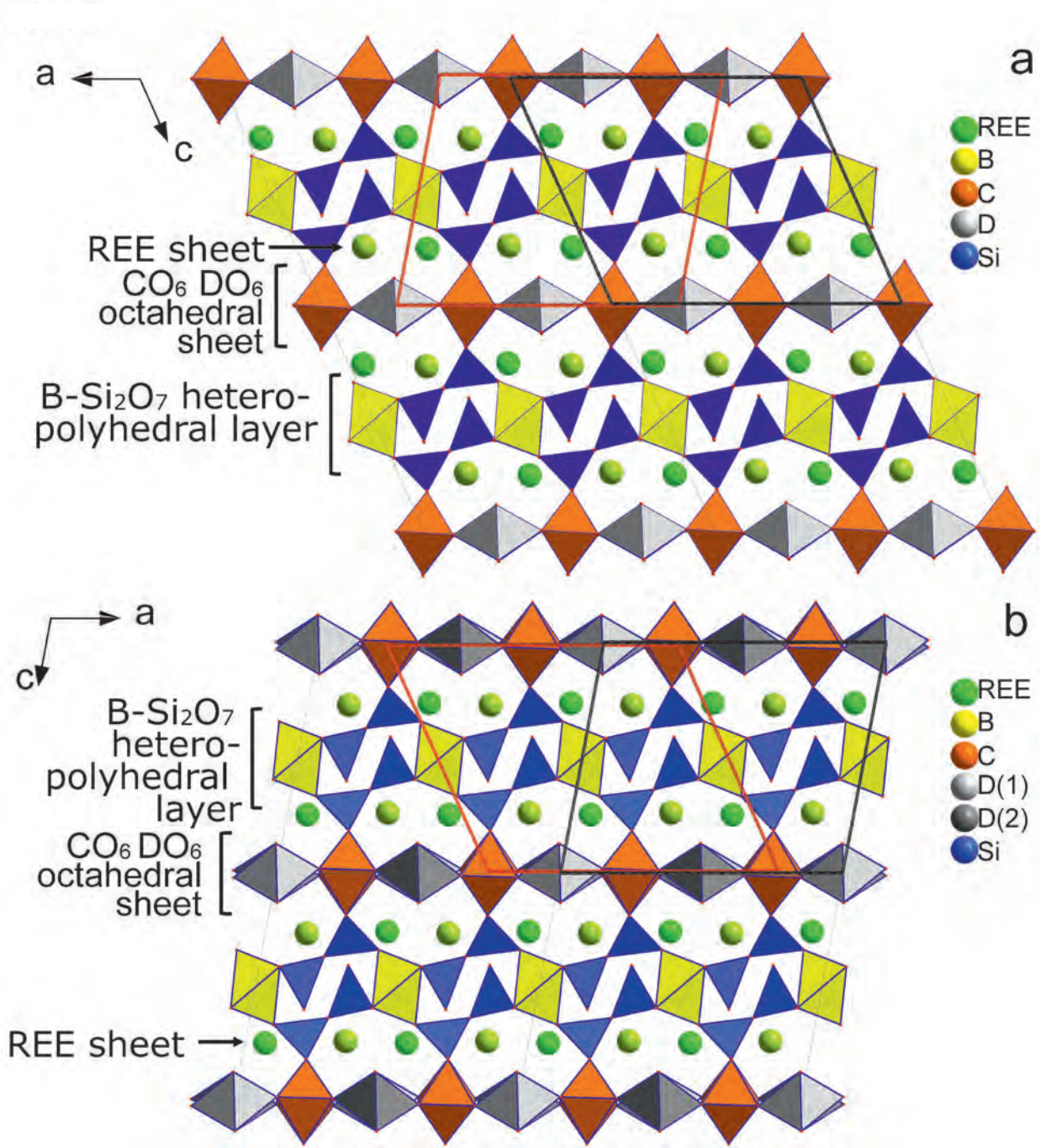
a
a
c
REE
B
C
D
Si
REE sheet
CO6 DO6
octahedral
sheet
B-Si2O7 hetero-
polyhedral layer
a
b
c
REE
B
C
D(1)
D(2)
Si
B-Si2O7
hetero-
polyhedral
layer
CO6 DO6
octahedral
sheet
REE sheet

Fig 3

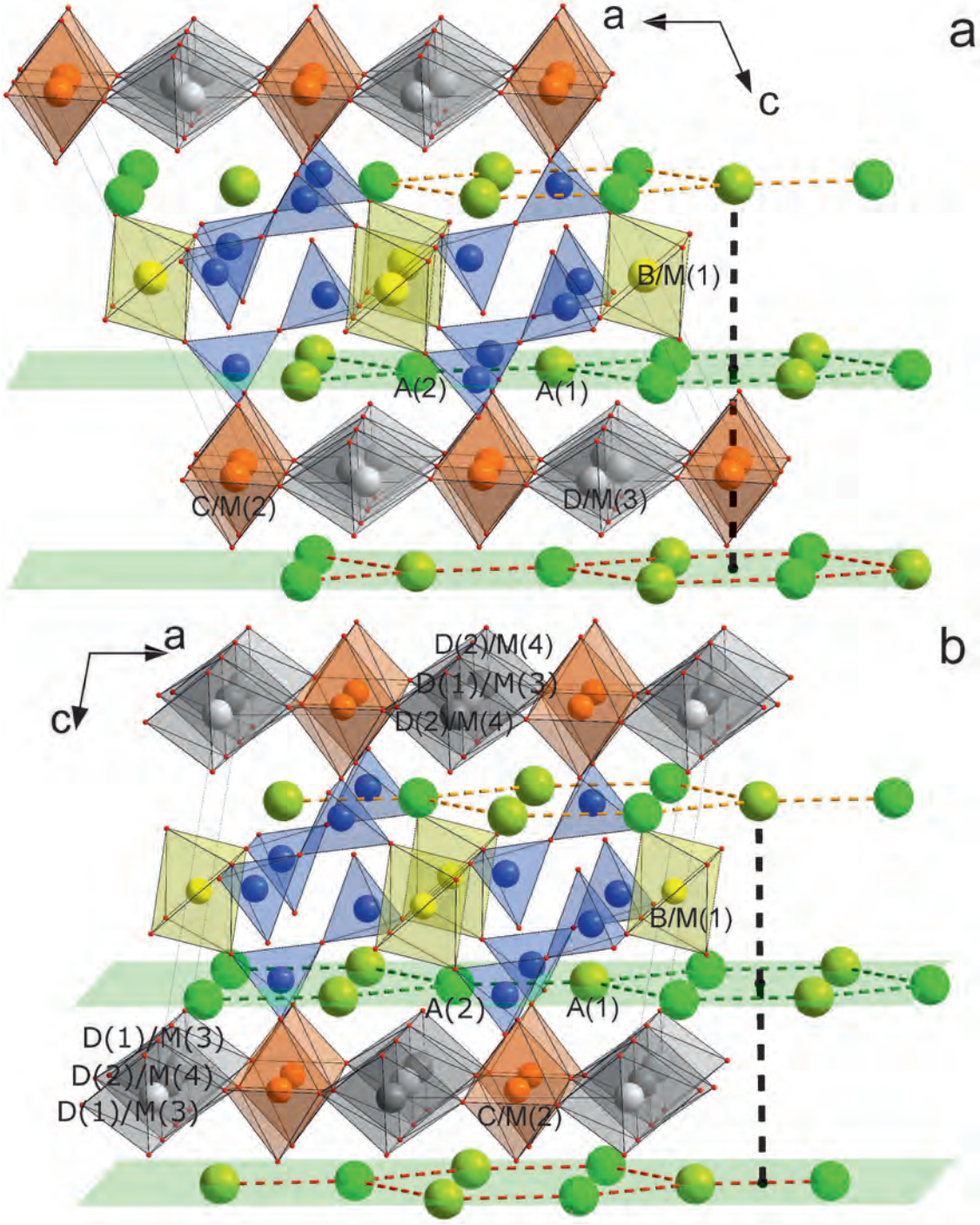
a
a
c
B/M(1)
A(2)
A(1)
C/M(2)
D/M(3)
b
a
c
D(2)/M(4)
D(1)/M(3)
D(2)/M(4)
B/M(1)
A(2)
A(1)
D(1)/M(3)
D(2)/M(4)
D(1)/M(3)
C/M(2)

Fig 4

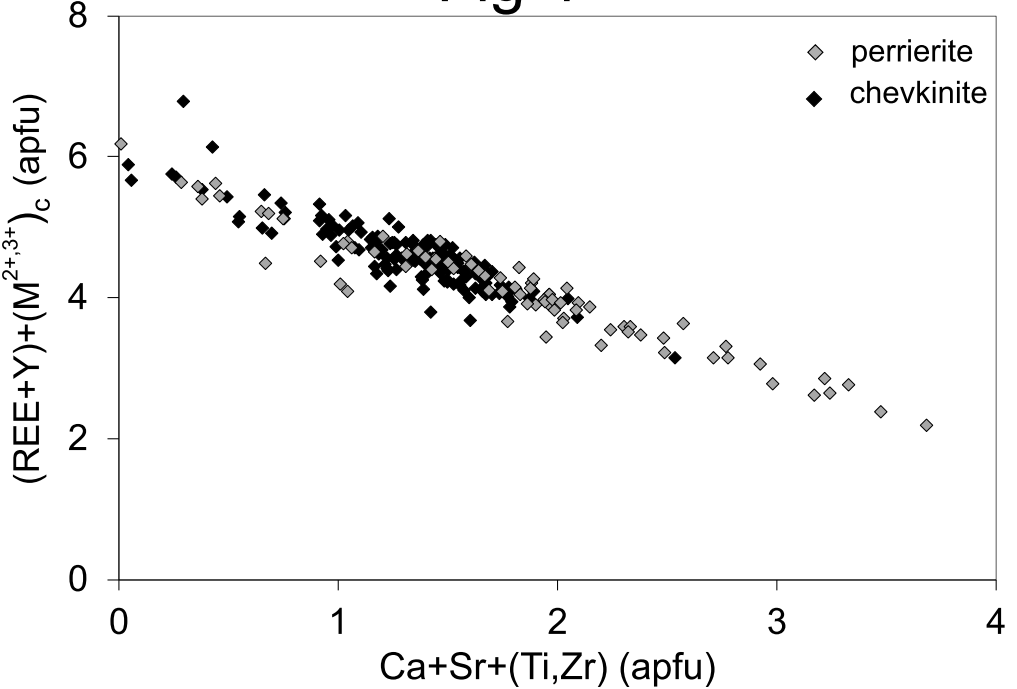
perrierite
chevkinite
(REE+Y)+(M2+,3+)c (apfu)
Ca+Sr+(Ti,Zr) (apfu)
0
2
4
6
8
0
1
2
3
4

Fig 5

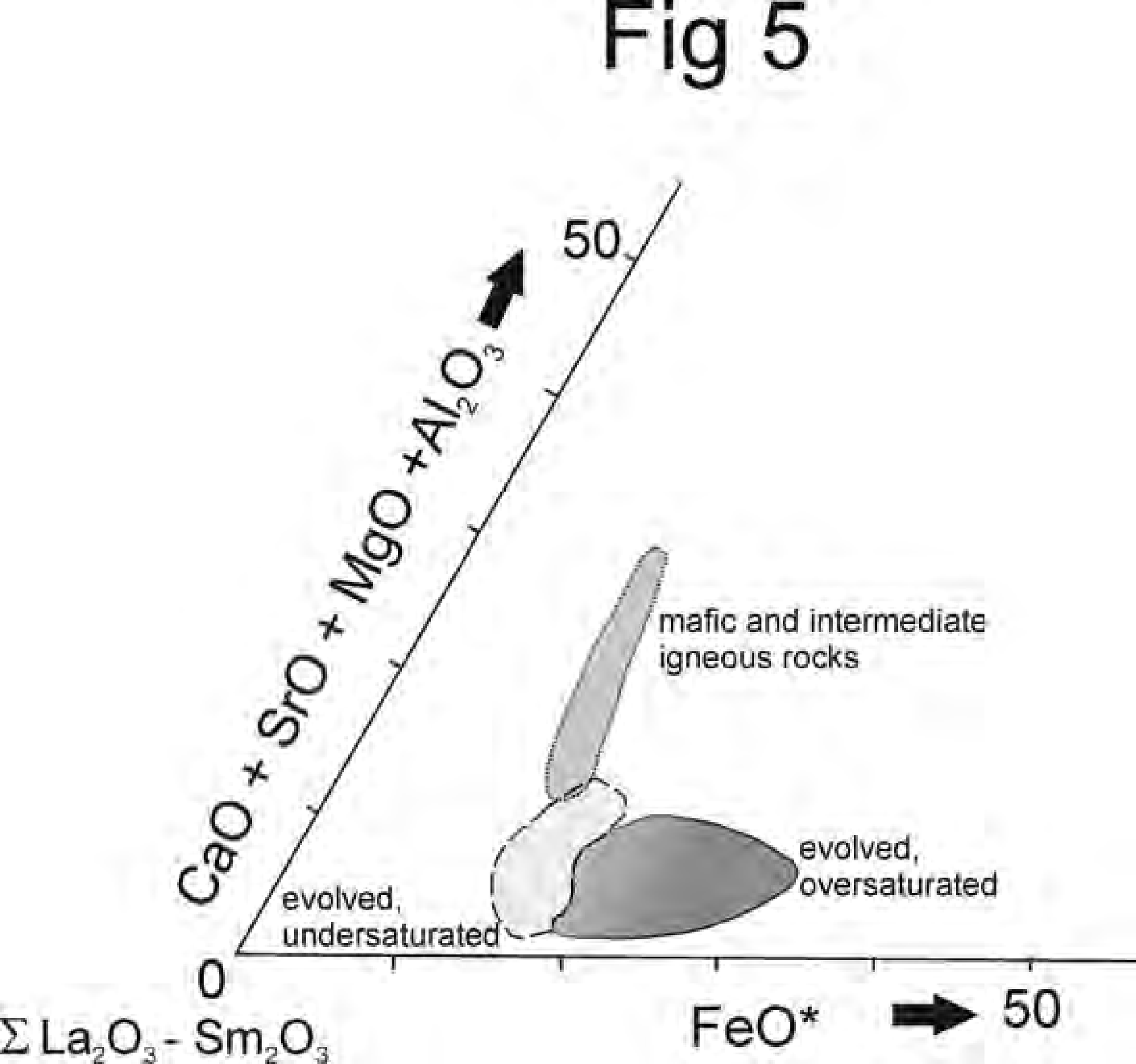
50
CaO + SrO + MgO +Al2O3
mafic and intermediate
igneous rocks
evolved,
oversaturated
evolved,
undersaturated
0
ΣLa2O3 - Sm2O3
FeO*
50

Fig 6

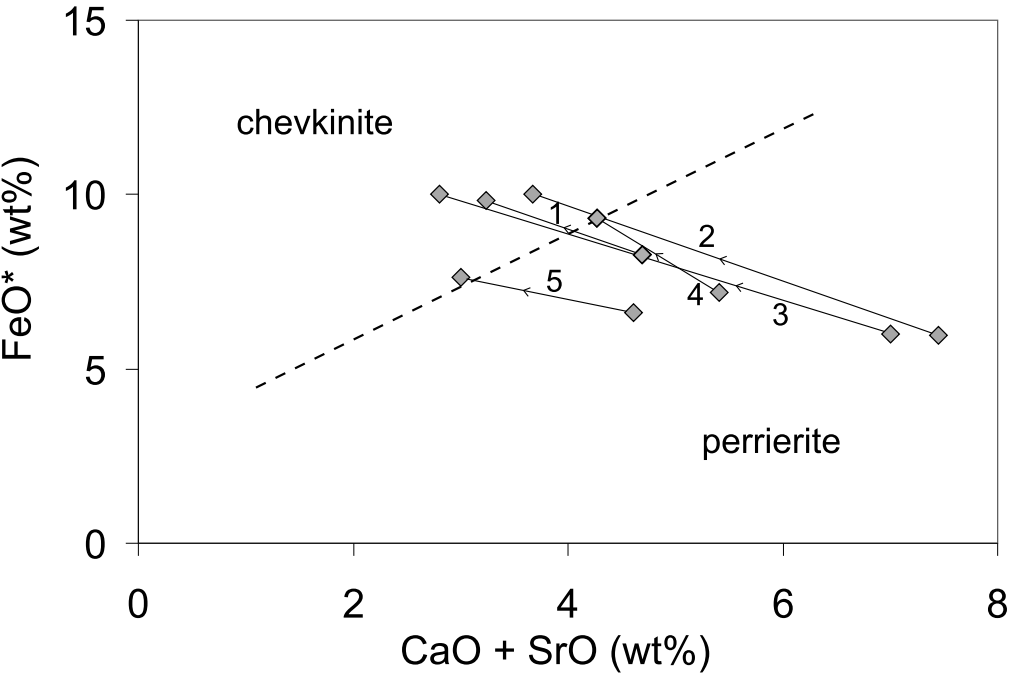

Fig 7

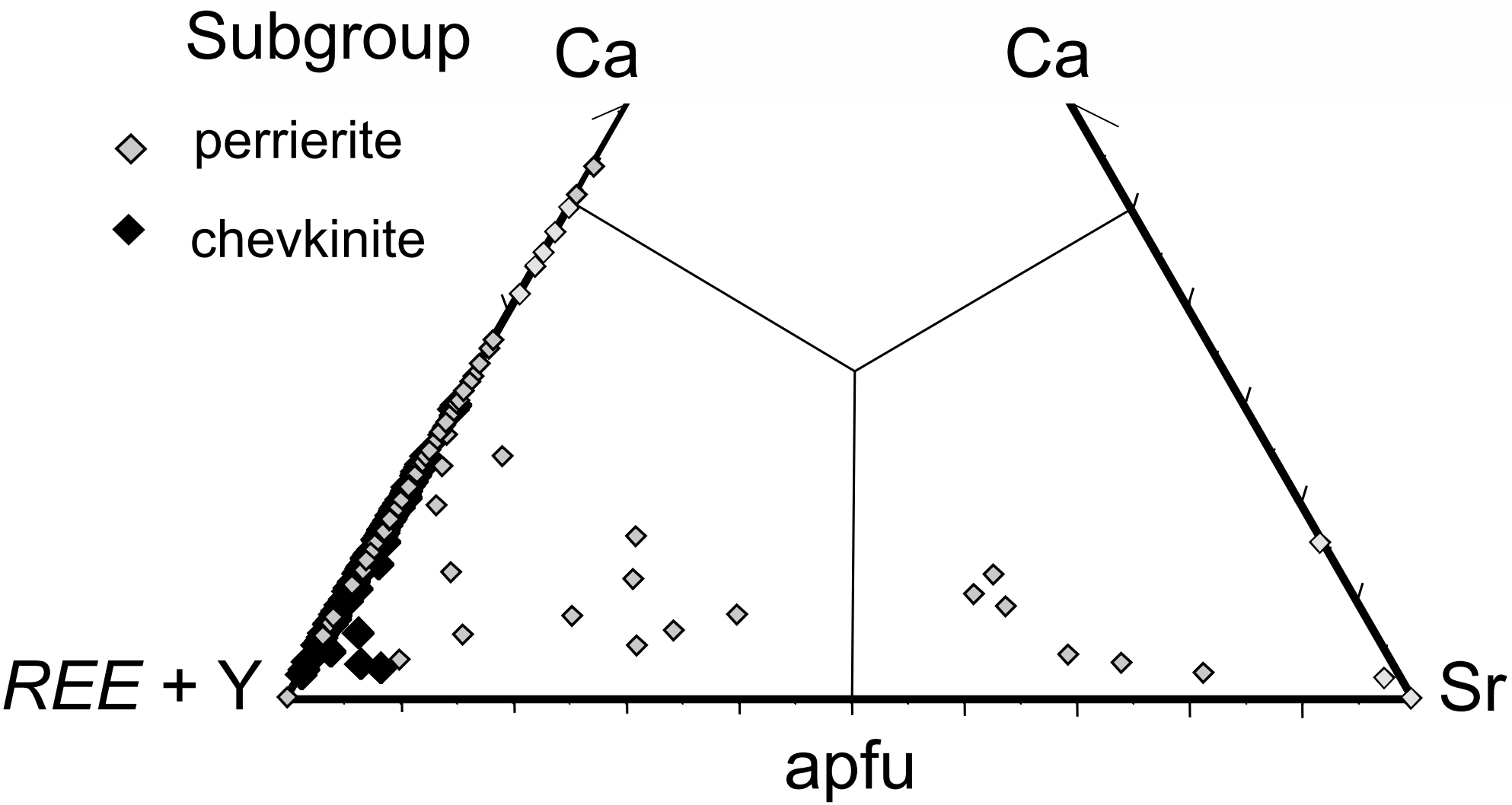

Fig 8

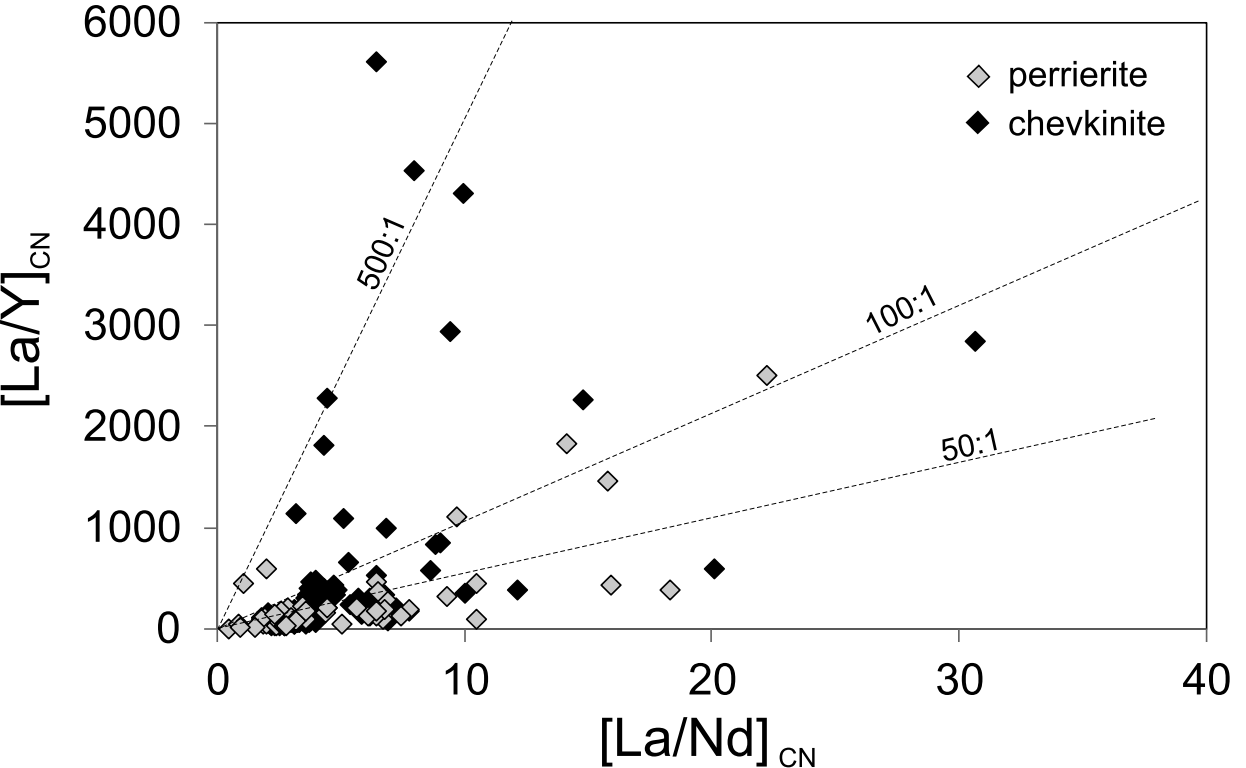
6000
5000
4000
3000
2000
1000
0
0
10
20
30
40
[La/Y]CN
[La/Nd] CN
perrierite
chevkinite
500:1
100:1
50:1

Fig 9

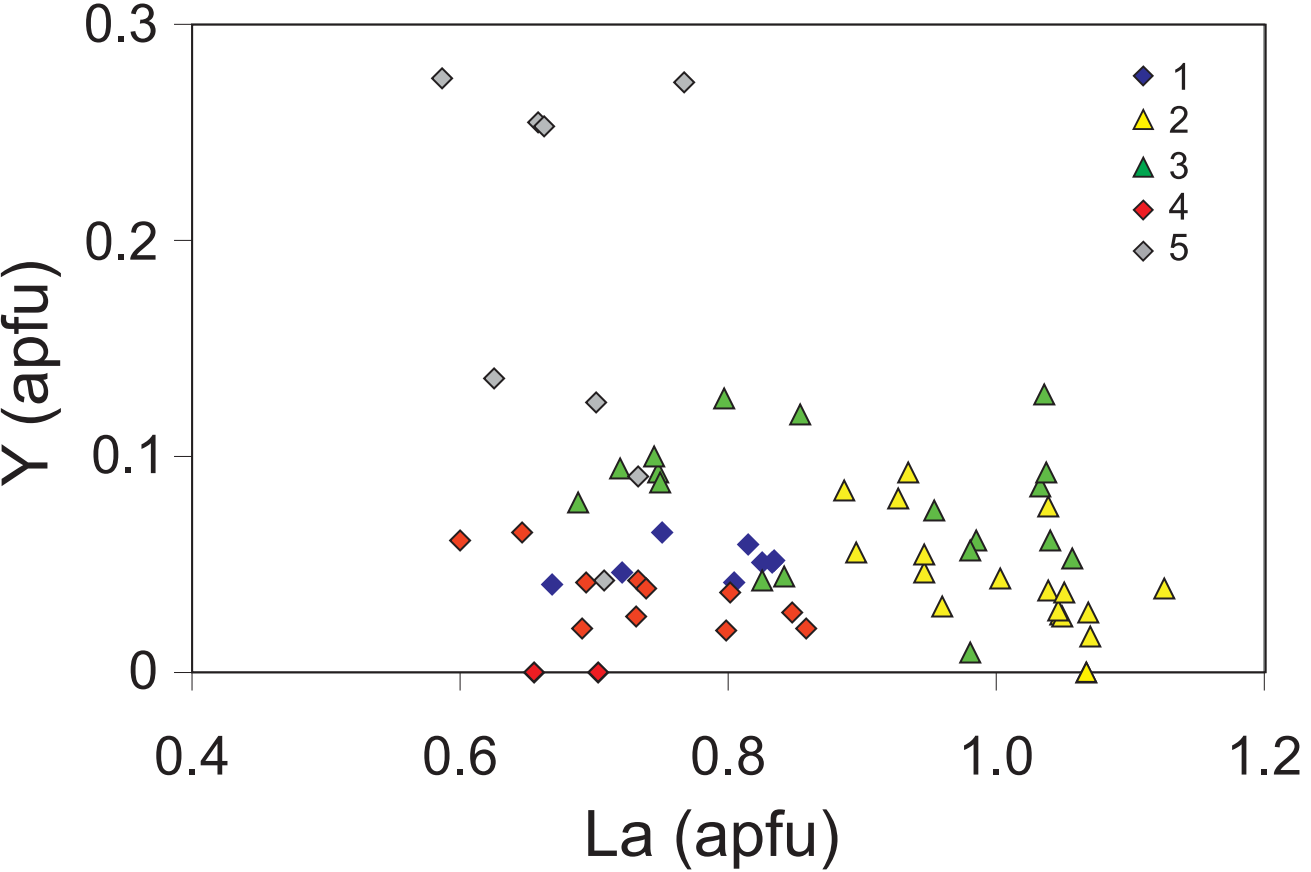

Fig 10

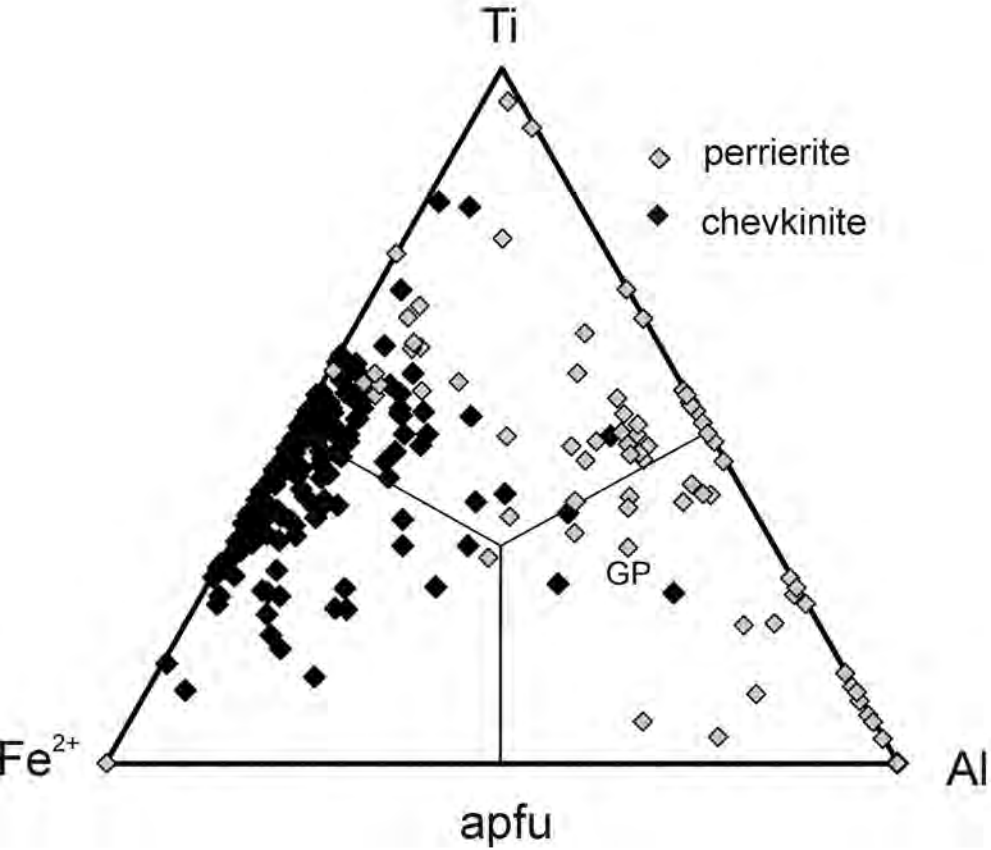

Fig 11

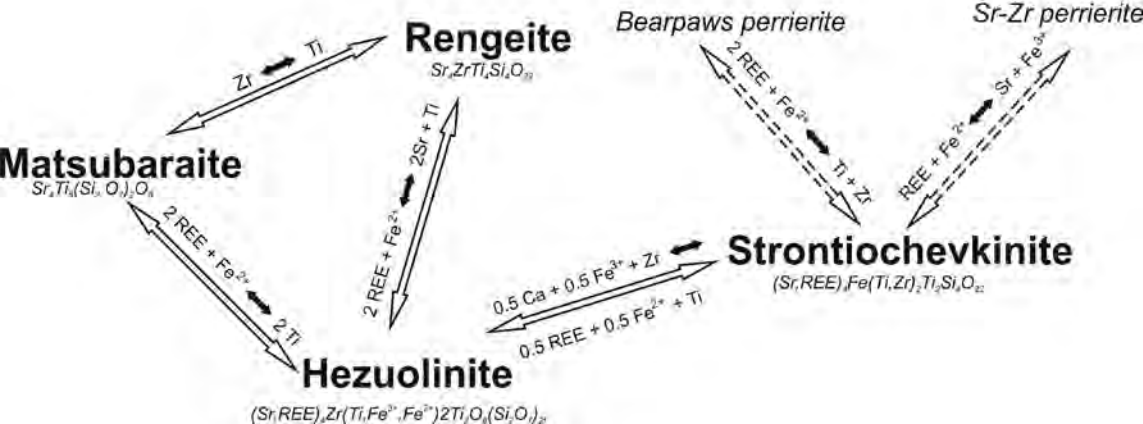
Rengeite
Sr2ZrTi4Si4O22
Matsubaraite
Sr4Ti8(Si4O14)2O8
Hezuolinite
(Sr,REE)4Zr(Ti,Fe3+,Fe2+)2Ti2O8(Si2O7)2
Strontiochevkinite
(Sr,REE)3Fe(Ti,Zr)2Ti2Si4O22
Bearpaws perrierite
Sr-Zr perrierite
Zr ⇌ Ti
2Sr + Ti
2 REE + Fe2+
2 REE + Fe2+ ⇌ 2 Ti
0.5 Ca + 0.5 Fe3+ + Zr
0.5 REE + 0.5 Fe2+ + Ti
2 REE + Fe2+ ⇌ Ti + Zr
REE + Fe2+ ⇌ Sr + Fe3+

Fig 12

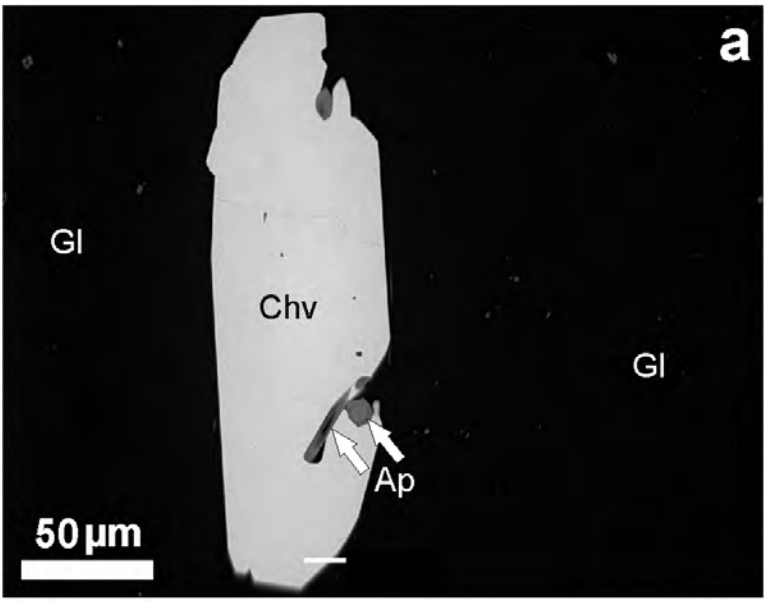
a
Gl
Chv
Gl
Ap
50 µm

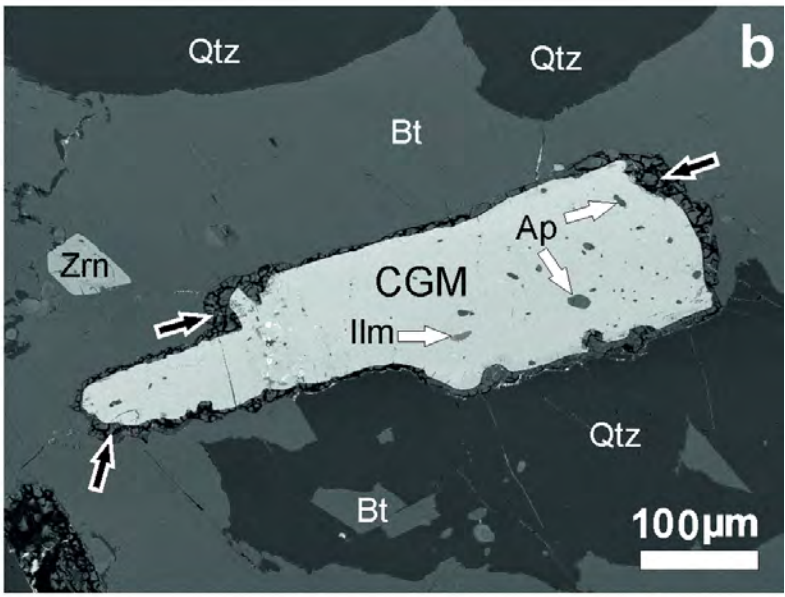
b
Qtz
Qtz
Bt
Ap
Zrn
CGM
Ilm
Qtz
Bt
100µm

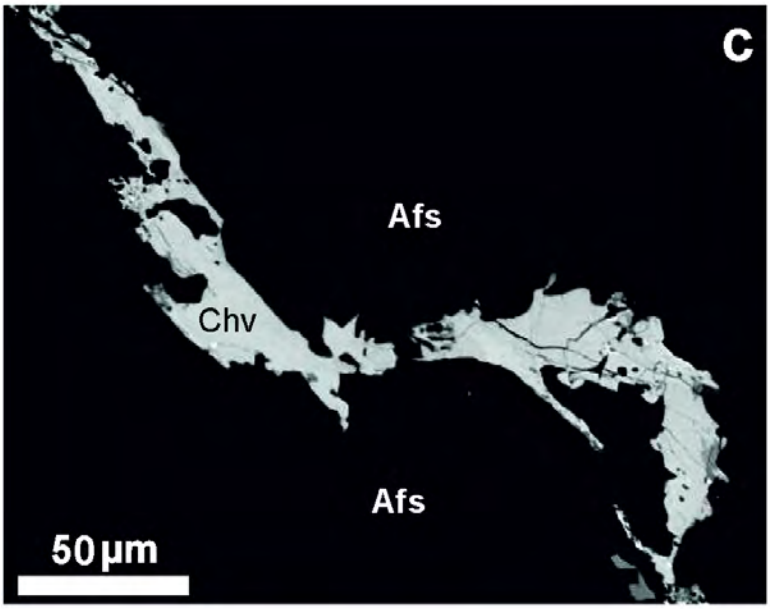
c
Afs
Chv
Afs
50 µm

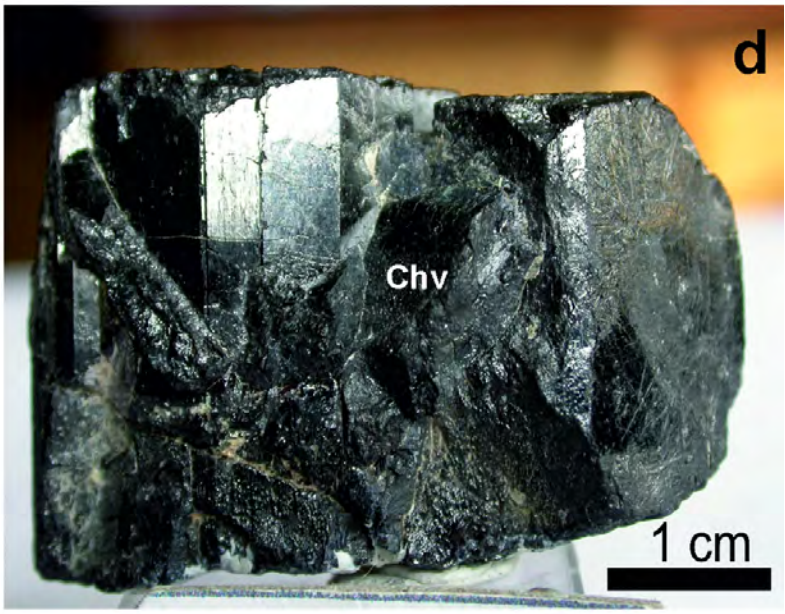
d
Chv
1 cm

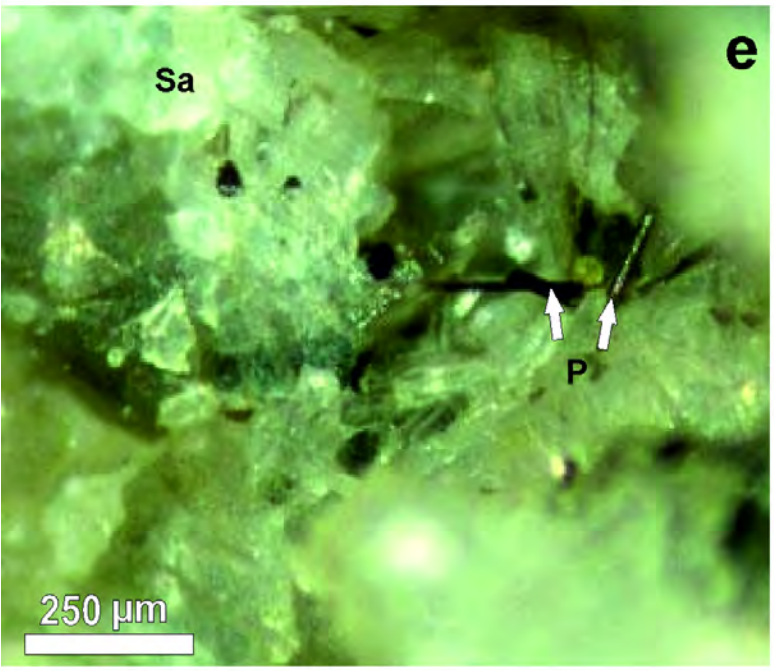
e
Sa
P
250 µm

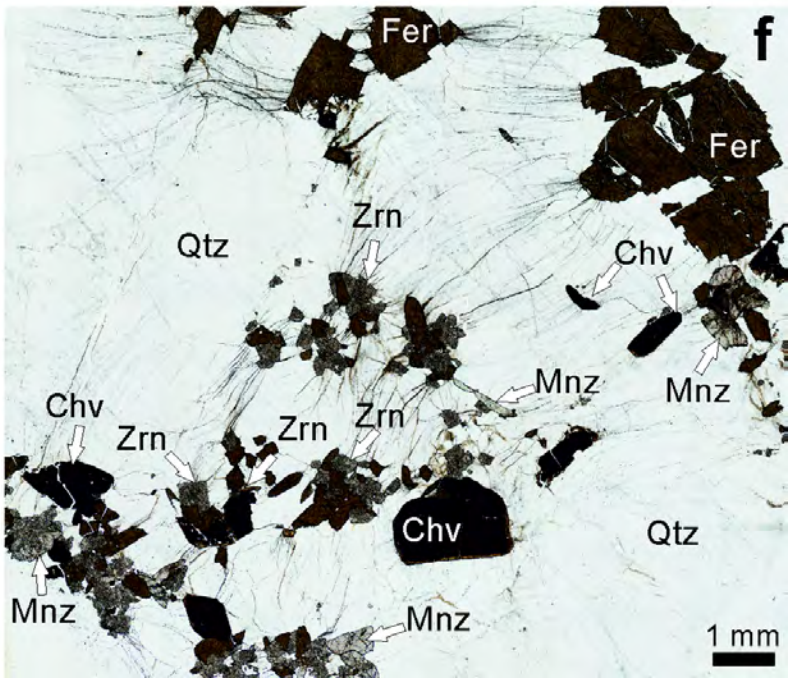
f
Fer
Fer
Zrn
Qtz
Chv
Mnz
Mnz
Chv
Zrn
Zrn
Zrn
Chv
Qtz
Mnz
Mnz
1 mm

Fig 13

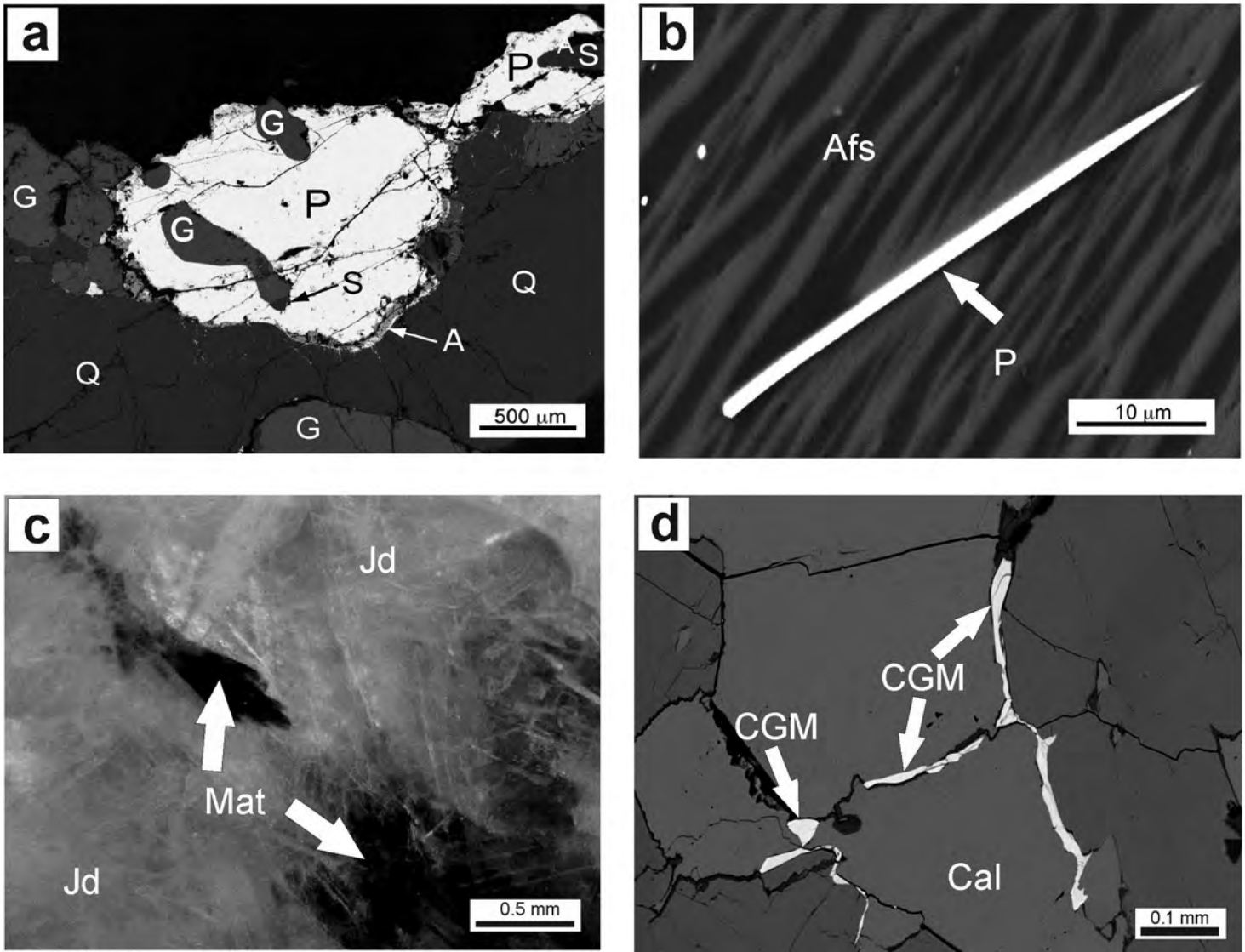
a
P
S
G
G
P
G
S
Q
A
Q
G
500 μm
b
Afs
P
10 μm
c
Jd
Mat
Jd
0.5 mm
d
CGM
CGM
Cal
0.1 mm

Fig 14

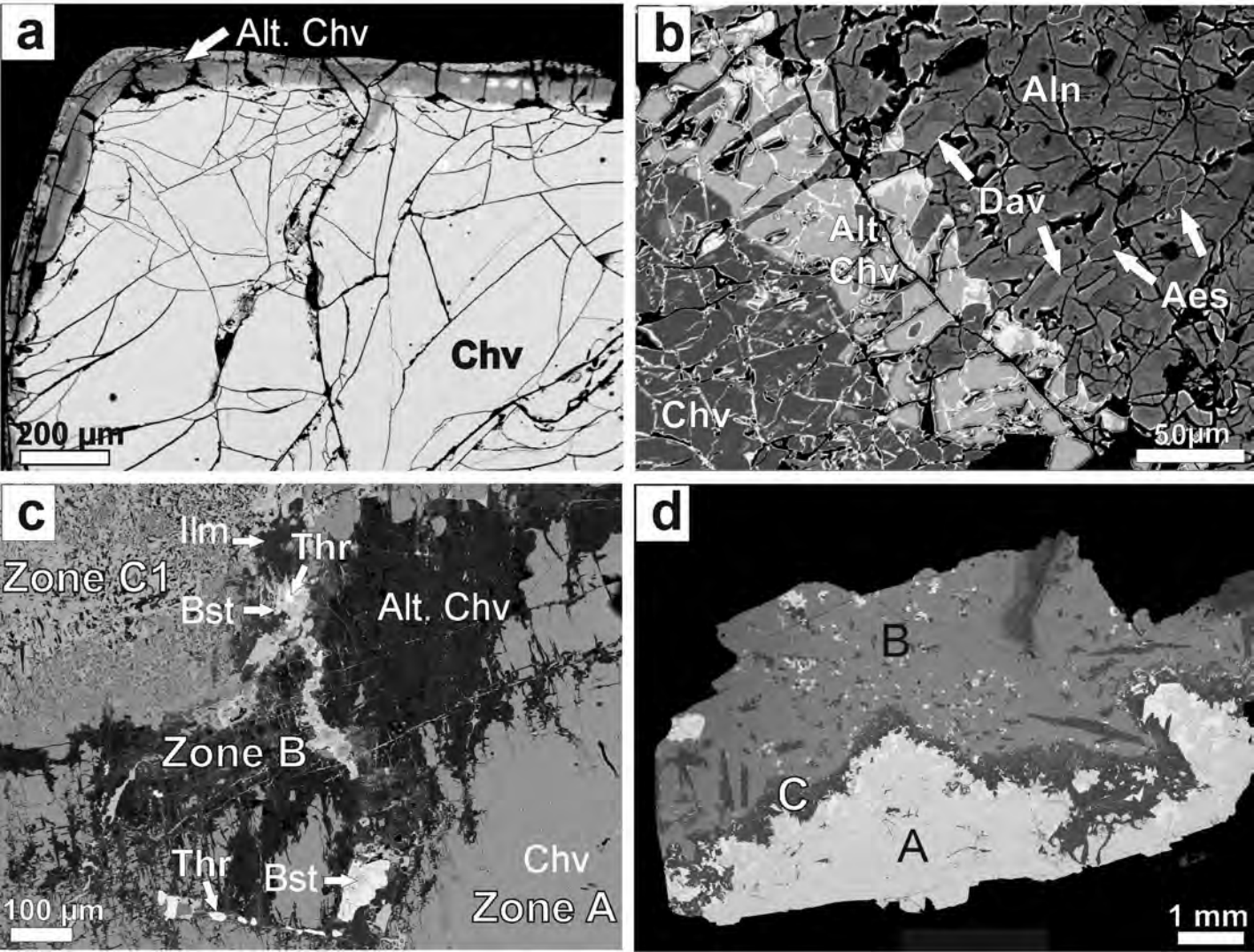
a
Alt. Chv
Chv
200 µm
b
Aln
Dav
Alt
Chv
Aes
Chv
50µm
c
Ilm
Thr
Zone C1
Bst
Alt. Chv
Zone B
Thr
Bst
Chv
Zone A
100 µm
d
B
C
A
1 mm

Fig 15

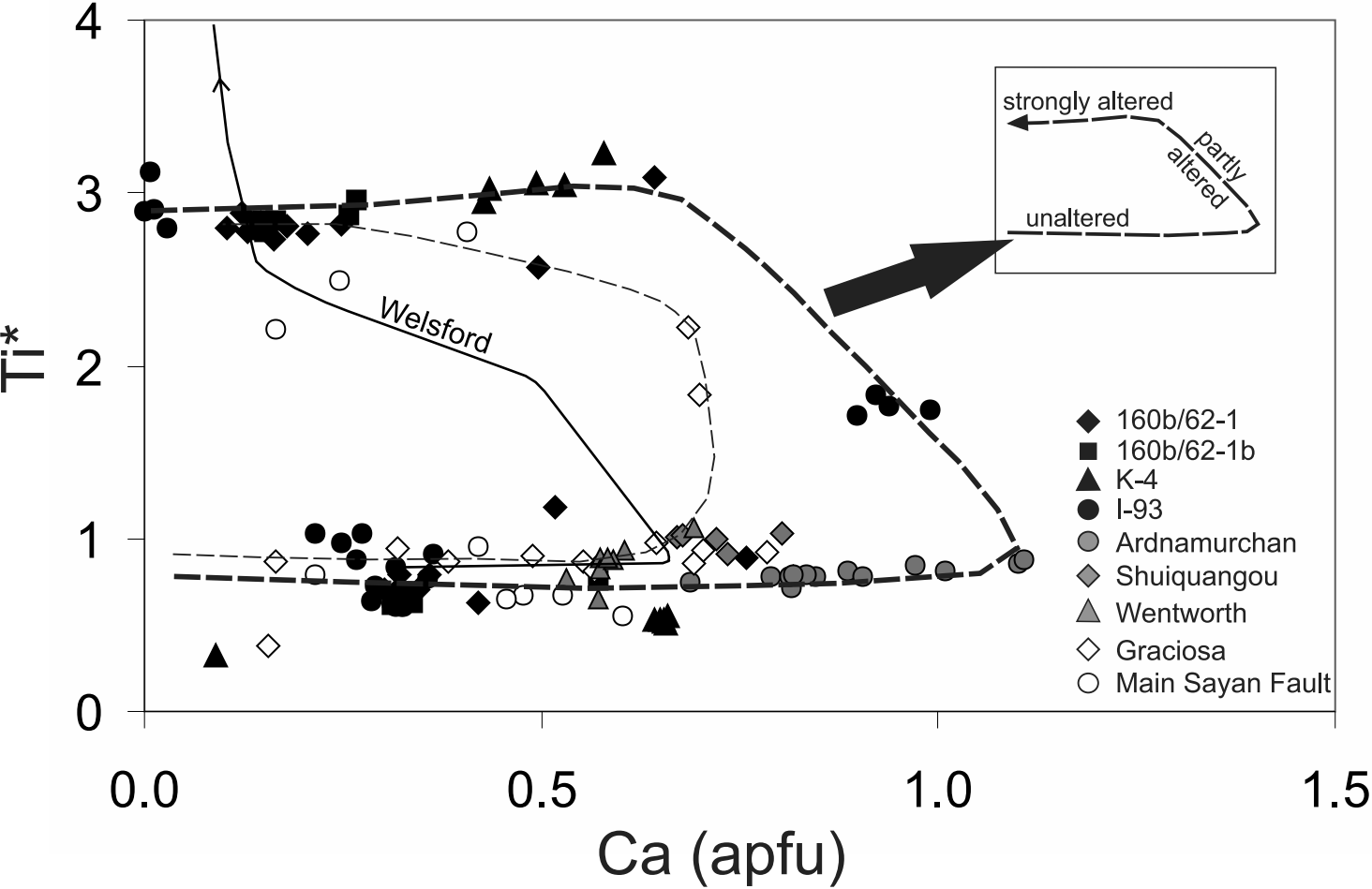
4
3
2
1
0
Ti*
0.0
0.5
1.0
1.5
Ca (apfu)
strongly altered
partly altered
unaltered
Welsford
160b/62-1
160b/62-1b
K-4
I-93
Ardnamurchan
Shuiquangou
Wentworth
Graciosa
Main Sayan Fault

Fig 16

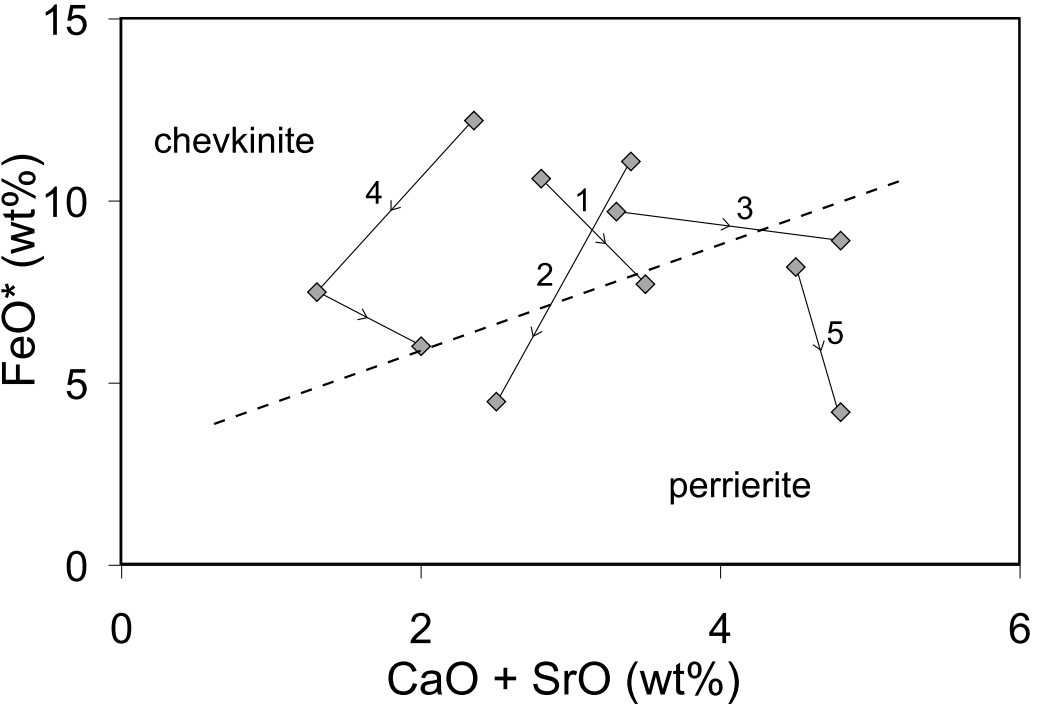

Fig 17

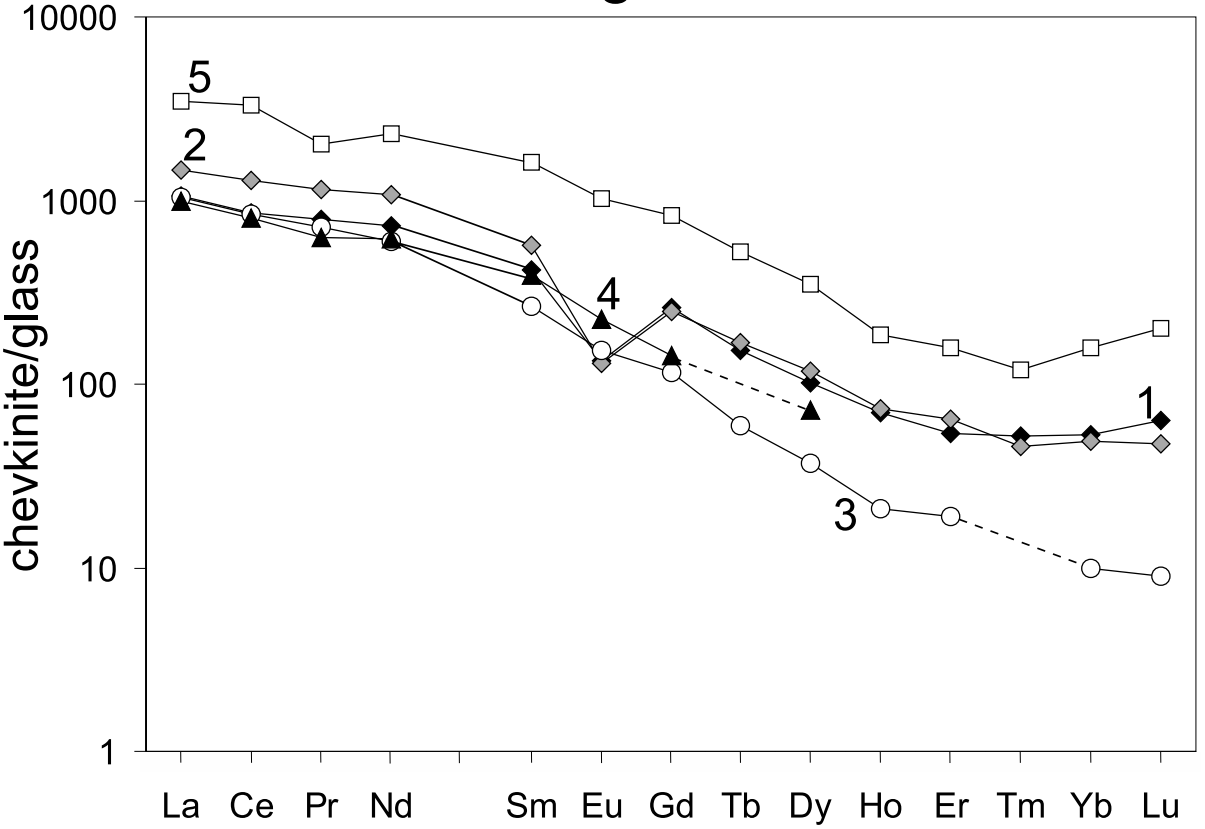
10000
1000
100
10
1
chevkinite/glass
5
2
4
1
3
La
Ce
Pr
Nd
Sm
Eu
Gd
Tb
Dy
Ho
Er
Tm
Yb
Lu

Fig 18

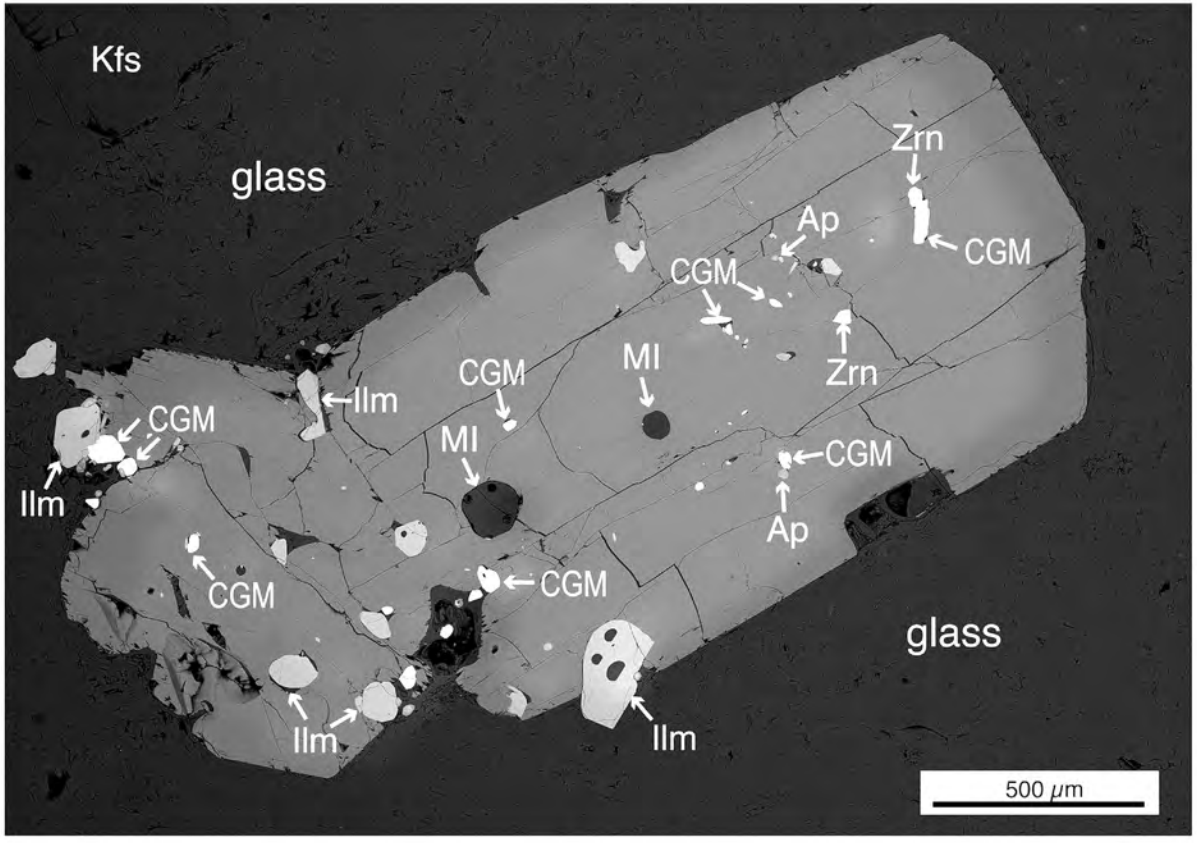
Kfs
glass
Zrn
Ap
CGM
CGM
CGM
MI
Zrn
Ilm
CGM
MI
CGM
CGM
Ilm
Ap
CGM
CGM
glass
Ilm
Ilm
500 μm

Fig 19

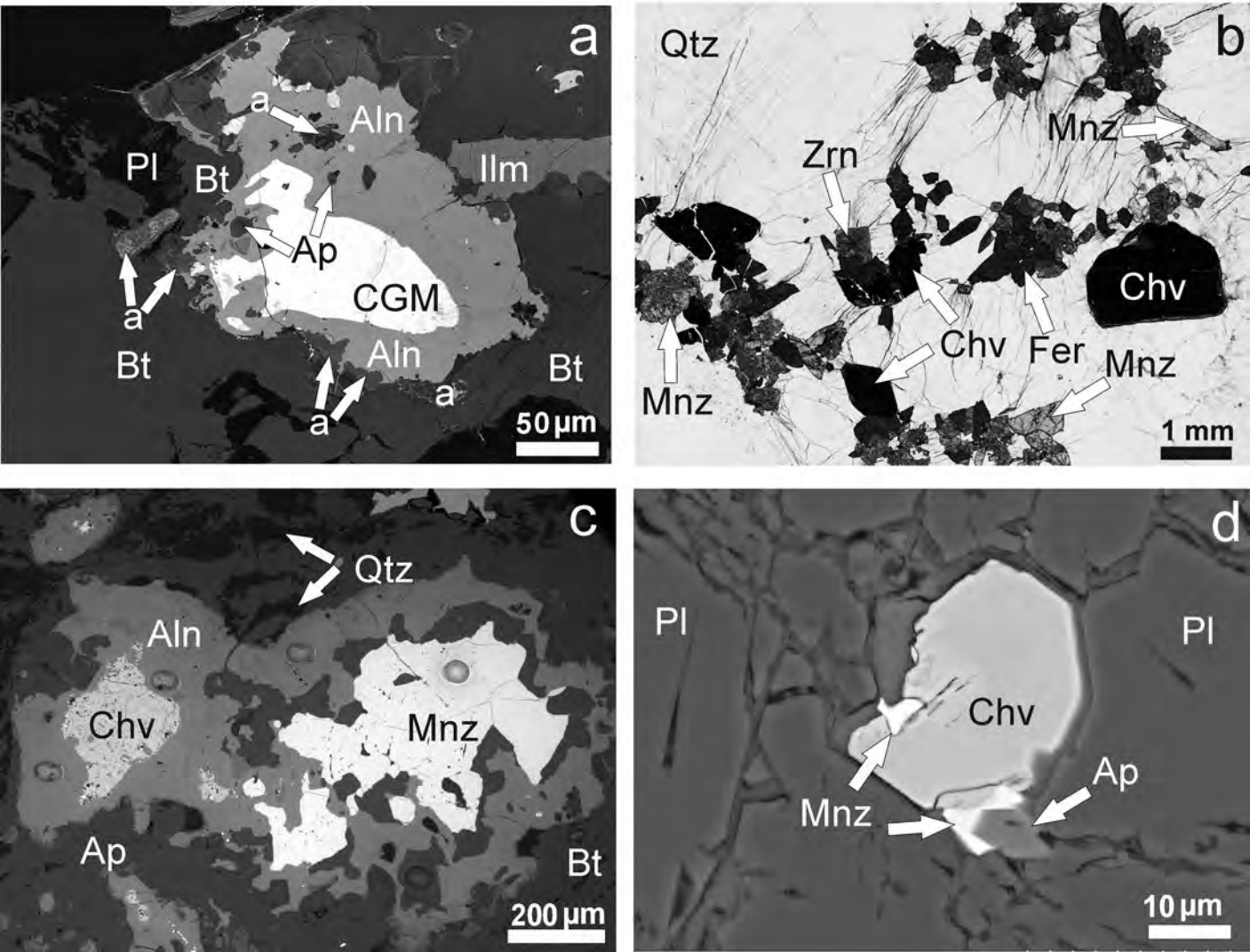
a
a
Aln
Pl
Bt
Ilm
Ap
CGM
a
Bt
Aln
Bt
a
a
50 µm
b
Qtz
Mnz
Zrn
Chv
Chv
Fer
Mnz
Mnz
1 mm
c
Qtz
Aln
Chv
Mnz
Ap
Bt
200 µm
d
Pl
Pl
Chv
Ap
Mnz
10 µm